Micro- and Nano-Transport of Biomolecules
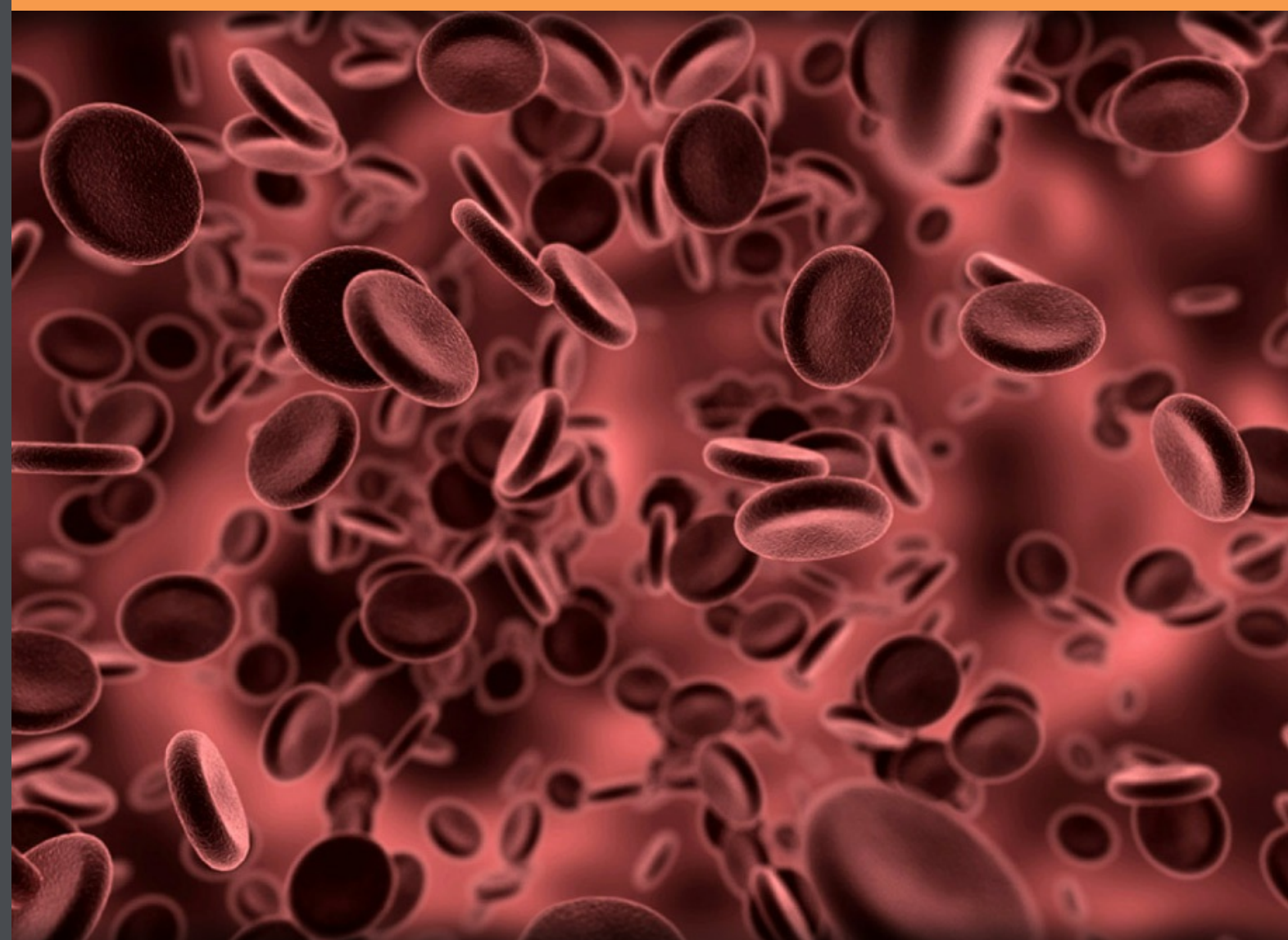
David Bakewell

David Bakewell

Micro- and Nano-Transport of Biomolecules

Contents

Preface

The micro- and nano- transport of biomolecules is of interest to a wide range of scientific and engineering communities. Application areas include miniaturized technology that will support and advance key sectors, including healthcare, food provisioning, environment services, etc. This e-book is generally intended for undergraduate students from chemical, life and physical sciences wanting to find out about the basic properties of biomolecules and how they can be transported in liquids on the micro- to nano-scale. The e-book tends to be oriented towards engineering aspects, especially with the transport of biomolecules in micro-devices powered electrically. It is hoped it will also be useful for interdisciplinary researchers surveying the field of biomolecule transport.

Much of the book can be read with no more than high school level of science and mathematics and selected areas that require engineering mathematics can be omitted if need be. Vector notation for example has been deliberately omitted until Chapter 4. At the same time the more mathematical sections in Chapter 4 are expected to be useful for researchers entering this area of science.

1 Introduction

This chapter introduces biomolecules in a general context in which they are studied scientifically and applied to real-world problems.

1.1 Motivation: biomolecules in scientific context

Biomolecules are organic molecules that are biologically important. Examples of biomolecules include nucleic acids - deoxyribonucleic acid (DNA) and ribonucleic acid (RNA), proteins – filamentous (e.g. actin filaments and microtubules) and globular (e.g. haemoglobin that transports oxygen in our bodies), carbohydrates and lipids. The transport of biomolecules on the nano- and micro-length scale is of interest to a number of scientific and engineering communities – ranging from life and chemical sciences, to engineering and mathematics.

Scientific enquiry and engineering application is supported by, and contributes to, a wider public society. Fig. 1-1 is a general sketch of the relationship between knowledge disciplines embedded within a wider public arena. It is a simple sketch, in so far as a more complete web- or map-of-knowledge should be rendered in several dimensions, illustrate more elaborate interconnections, etc. Nonetheless, it represents the basic idea and the above disciplines are listed in three quadrants: Biology and Biomedical Science, Physics and Engineering, and Chemistry.

Broadly speaking, as a community, life scientists seek to understand the minute biological processes that occur inside living organisms. Their discoveries inform about transport processes and it is important to integrate their observations within frameworks of established physical and chemical laws. In recent years this has become more apparent when the community has used tools made available from micro- and nano-technology in their investigations, e.g. nano-bioparticles.

Another community, engineering scientists, seek to find applications of naturally evolved biological processes to create novel components, devices and systems. During the past decade there has been increasing interest in miniaturising biotechnical processes – and methods developed by highly successful semiconductor manufacturing have been borrowed to achieve this. Knowledge about biomolecule transport is needed for choosing controllable forces that drive movement and for ensuing micro-device design.

Practical scientific enquiry and development on the nano- to micro-scale is largely performed by, or at least is underpinned by, chemistry - and its related wide ranging sub-disciplines. Much is owed to the chemistry community for the development of polymers, photolithographic resists, nano-bioparticles, microarrays, etc. Again, the importance of transport processes is evident.

The fourth quadrant in Fig. 1-1 lists mathematical, computing and statistical sciences. These quantitative disciplines play a pivotal role with their experimental-oriented (biological, chemical and engineering) disciplines in numerous ways. To describe a couple: first, assuming a given set of laws, boundary conditions, and parameter values, they enable quantitative prediction of the motion
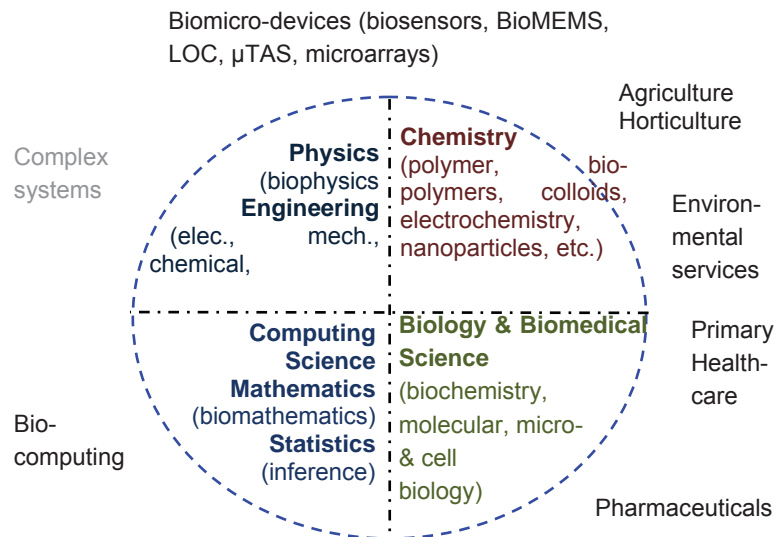

Fig. 1-1 Discipline-based knowledge and related industries, services and wider public arena.

of biomolecules; second, they enable experimental data to infer the most likely models applicable (or parameter values of selected models). These attributes of *prediction* and *inference* are cornerstones for supporting and nourishing a successful emerging science.

The involvement of experimental-oriented biological, chemical, and engineering disciplines is evident in scientific meetings, international conferences and journals that discuss biomolecular and cellular transport on small scales. Examples include micro Total Analysis Systems (µTAS) conference, and Lab-On-Chip (LOC) journal. Consequently, the acronyms µTAS and LOC, listed at the top of Fig. 1-1, are often associated with micro-devices – along with BioMEMS (Bio-MicroElectroMechanical Systems), biosensors and microarrays.

Bioinformatics and systems biology journals and conferences are venues that attract biological, medical and life scientists along with computing, mathematical and statistical scientists. They have tended to attract less hardware and 'wet-lab' engineers and chemists.

1.2 Length scale of transport

Transport is the movement of an object from one point to another and is often integral to a particular process, such as, a biochemical reaction. Transport takes time. In biological environments and manufactured structures, spaces are compartmentalised so that shorter length scales reduce processing time. Processing time reduction is one of the key reasons for motivating miniaturisation or scale-down biotechnology. Other reasons include savings in amount of biochemical reagents needed, reduction in energy consumption and mass (or weight) of devices, thus creating opportunities for portability. To further imagine the possible impact on our future lives, it is helpful to glimpse back to the historical past.

Drawing on analogies with computing, one remembers the large size of computers early last century and time duration it took to do calculations compared with today. Science museum displays and old films remind us of mechanical or early electronic valve computers that occupied entire rooms. Computers were comparatively slow so that programs were run in batches – sometimes overnight or for weeks on end. Nowadays, computing has become so ubiquitous that computing devices such as microprocessors are part of many home and workplace appliances, making them 'smart' and improving user-friendliness. Integrating a camera, music player, radio, telephone and clunky computer would have been almost unthinkable a century ago; today they're packaged and work together in a standard cell phone. The point is that smaller and faster technology has many follow-on ramifications in terms of weight, cost, availability, functionality, pervasiveness and influence on our lives.

It is possible that scaled-down biotechnology in the form of chip-like micro-devices will also give rise to new ways of doing new things almost unimaginable at present. As in the past, it will in-part be shaped by scientific and societal challenges and opportunities. At present, most countries aim to improve healthcare, food provisioning, energy and water recycling and resourcing, and confront global problems, such as, climate-change. Recognition of these current challenges is enough to motivate considerable scientific and engineering effort in discovering, understanding and utilising micro- and nano-scale transport of biomolecules. The future could even be more fictive.

1.3 Biomolecule transport example: engineered microdevices

This e-book focuses on the transport of biomolecules in water driven by electric fields. The suspensions are assumed to be enclosed in microstructures with feature lengths on the scale of tens to thousands of nanometers (nm). These laboratory microstructures represent micro-devices that are being developed for applications ranging from diagnostics to security. It is important that the micro-devices are communicable with each other and generally the most convenient medium that is capable of conveying both information and power simultaneously, is electrical signalling. Other signal media include microfluidic and optical radiation. Even using molecular motors, extracted from naturally evolved biological systems, could form a long distance communication link deploying similar motility systems to nerve fibers in our bodies.

An example schematic of three micro-devices connected to an electronic communication and power controller is illustrated in Fig. 1-2. Device A is a sketch of nucleic acid (DNA or RNA) fragments that are being drawn out their suspension in water into the region between two planar electrodes. The inert metal electrodes have been micro-fabricated on glass, such as a microscope slide, using standard photolithographic methods. The electrodes are being supplied with electrical signals from the communication and power controller via multiplexed cable, as shown. The electrode edges are very close to each other - on the order of microns (μm). They are energised with voltage differences between them of no more than, say, 20 volts at radio frequencies (MHz).

Strong non-uniform electric fields generated between electrodes attract the nucleic acid fragments so that they position at right angles (orthogonal) to the edges, as shown. The fragments are not normally visible so they have fluorescence dyes attached, or labeled, to them. This enables their movement to be detected and monitored using optical equipment, such as, a fluorescence microscope, as shown. Information about the biomolecule movement is then sent back to the
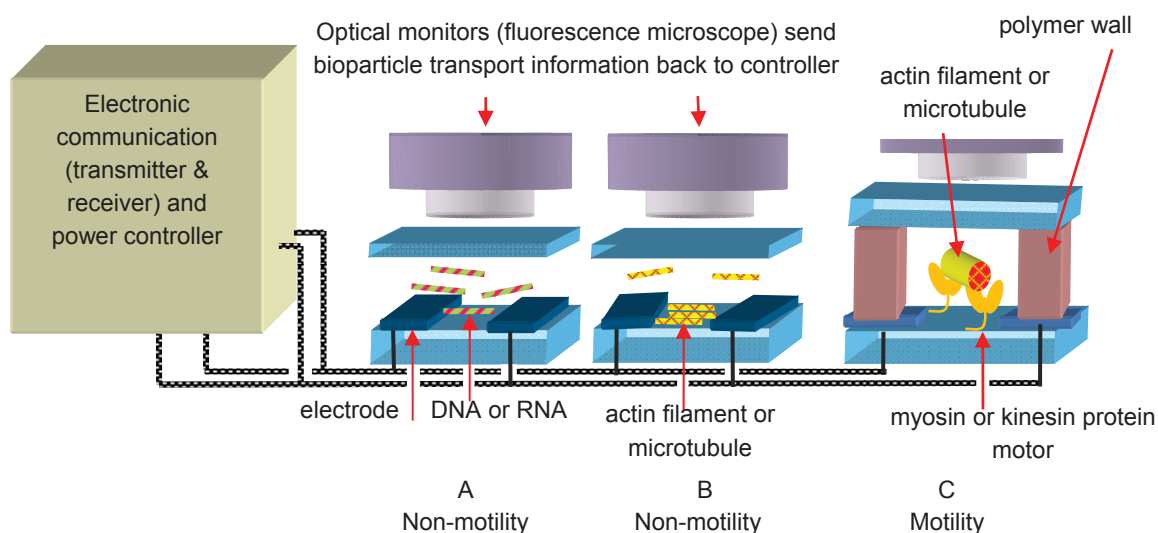
Fig. 1-2 Electronic remote control & monitoring of a micro-device platform (not to scale).

controller. Other methods of non-optical sensing of biomolecules between electrodes include differences in electrical impedance (not shown).

Details of the electrokinetic mechanism for moving the fragments is not important for the moment, and are elaborated later in this book. The key point is that the strength of the electric field driven movement can between the monitored and controlled 'remotely' (away from the micro-electrodes) to yield a biomolecular transport device.

Device B is similar to A but the biomolecules are protein filaments, such as, actin filaments (AFs) or microtubules (MTs) rather than nucleic acids. The gap between the electrodes is made variable, rather than constant as in device A, so as the filaments electro-kinetically concentrate. The details how the electrokinetic mechanism works will become evident later in this chapter. In living (*in vivo*) biological systems, such as cells, these motility filaments are involved in a wide of processes, such as, muscle contraction, linear transport of metabolites, and movement of chromosomes during cell division. AFs and MTs are the 'tracks' the corresponding linear protein motors, myosin and kinesin, practically 'step' on as they transport cellular material. As with Device A, AFs or MTs in Device B are fluorescently labelled, and can be controlled and monitored remotely.

Device C shows the protein motors, adsorbed to chemically modified glass substrate, and associated in some way to an AF or MT. The size of the motors are in terms of tens of nanometres and they use adenosine triphosphate (ATP) as fuel with high efficiency. In this 'glass' (*in vitro*) role, they are operating in reverse to *in vivo* where they move and transport cargo. Instead, they are

stationary and their 'stepping' motion moves their respective AF or MT filament, with 5 nm and 8 nm step-lengths. AFs and MTs are made of asymmetrical monomers that fit into each other so as to provide stable structures with directionality. Even so, they need mechanical guidance and this is provided by the polymer walls, as shown. Electric fields are used to govern the direction of AFs and MTs and bias their movement, rather than propel them which mechanically powered from ATP.

The scale of the myosin and kinesin motors and step sizes is on the order of tens of nanometres and they are a very good example of 'bottom up' assembled machines. This is important because making nano-sized mechanisms or machines that will operate inside microdevices is difficult in terms of today's available 'top-down' methods. This is due to resolution and cost limitations of photo- or electron- lithographic processes. Motivated by molecularly assembled 'bottom up' motor construction and high energy efficiency, researchers have developed *in vitro* biochemical procedures or *motility gliding assays* where these nanosized linear protein motors operate on chemically modified glass or polymer surfaces; the platforms are termed 'hybrid-devices'. Therefore, in Fig. 1-2 Device C is labelled as motility, whereas devices A and B are non-motility. As with A and B, Device C is also monitored. All three micro-devices can communicate with each other thus enabling coordinated biomolecular transport.

1.4 Structure of this e-book

This e-book focuses on devices non-motility devices A and B, leaving C for further work as recently reviewed (Bakewell and Nicolau, 2007; Conceição *et al*., 2008).   The structure and function of biomolecules and their electrical properties is described in Chapter 2. The emphasis on DNA since it is an important biomolecule and because its properties are often referred to in subsequent chapters. The concept of a bioparticle is introduced as a biomolecule with a rigid shape, typically spherical, for several reasons. These include the increasing use of model bioparticles, such as, latex nanospheres (beads) in bioscience and bioengineering research, that many biomolecules have well defined shapes in water suspensions, and that their transport can be mathematically modeled using Newton's laws of motion.

An account of the way in which biomolecules are moved by electric fields and mechanisms of dielectric polarization are described in Chapter 3, complemented with calculation examples. The primary transport driving forces are introduced in Chapter 4 with emphasis on motion arising from non-uniform electric fields (*dielectrophoresis*). The forces are categorised as *deterministic* - that are known, and *stochastic* – that arise from thermal random motion and give rise to diffusion. The single bioparticle motion is described by the Langevin equation that combines both deterministic and stochastic forces. The motion of a population (or suspended solute) can be derived from the Langevin equation and is described by the Fokker Planck equation or modified diffusion equation.

The final chapter in the book describes example experiments and computer simulations of bioparticle and biomolecule (DNA) transport under the action of nonuniform electric fields in a microdevice context.   The experiments and simulations draw together concepts and theoretical models presented in the in the previous chapters.

2 Biomolecules and their electrical properties

In this chapter the biologically important organic molecules (biomolecules) mentioned briefly in the previous are introduced in their natural - cellular context - since the cell is the smallest living unit in nature. The biomolecules are then discussed including their chemical structure and function in a natural environment, e.g. *in vivo* (within living organism). Students needing to understand more biology can refer to highly informative science textbooks including, for example, Alberts *et al*. (2008), Nelson and Cox (2008), and Pollard and Earnshaw (2008).

2.1 Biomolecules in cells

A very simple sketch of a cross-section of a typical animal cell is shown Fig. 2-1.

Legend
actin filaments (AFs)
chromatin
cytoplasm
nucleus
nucleus wall
nucleolus
centrosome
endoplasmic reticulum (ER)
Golgi apparatus
Microtubule (MT)
mitochondrion
plasma membrane
ribosomes
vesicles
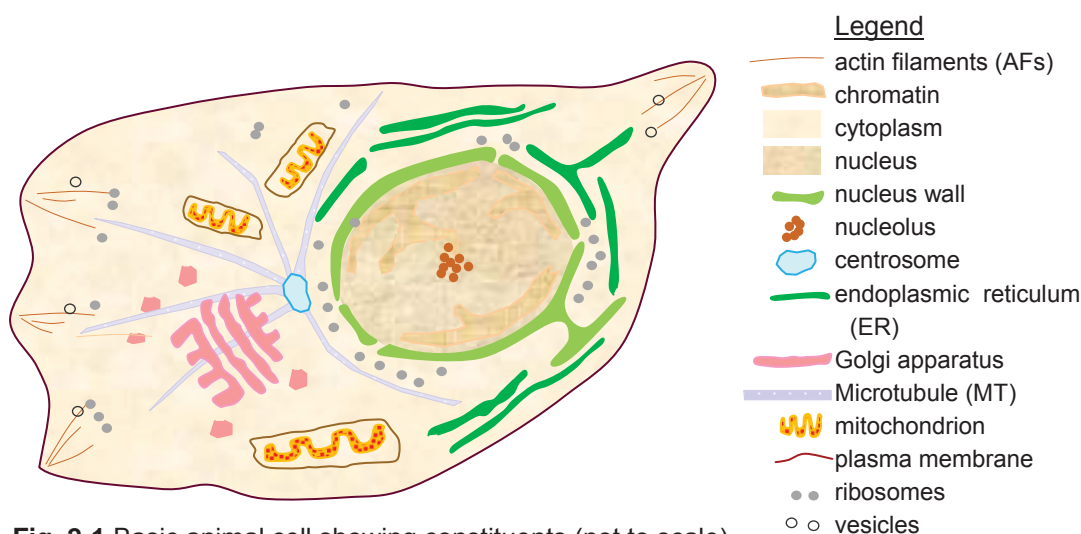
Fig. 2-1 Basic animal cell showing constituents (not to scale). Other cells, such as, plant cells have similar characteristics.

It is a eukaryote, i.e. contains nucleus – as shown that in enclosed by a wall (green). This is in contrast to prokaryote that do not have a nucleus. Cells are *dynamic* in the sense that they need to reproduce (divide into two copies of the original cell), move and search for nutrients to feed on, exhaust waste products, defend themselves from invaders, etc. The nucleus contains genetic information in the form of coiled DNA that is arranged into *chromatin* fibers. DNA essentially stores information in the form of a genetic code that describes the constituents for assembling other biomolecules both within the cell and outside, for example, the extracellular matrix. Hence, it is often referred to as the genetic 'blueprint' or 'instruction manual' or for a particular organism.

The remaining portion of the cell that is exterior to the nucleus and within the cell plasma membrane is the *cytoplasm*. Surrounding the nucleus within the cytoplasm are *ribosomes* that are responsible for translating the genetic code into proteins – discussed further in the next section. The illustration shows other key parts of the cell. Many of these are called *organelles* that are biochemically functioning entities enclosed by a membrane. Examples include the centrosome, endoplasmic reticulum (ER), mitochrondria (plural of mitochondrion), and Golgi complex:

14

- the centrosome is centrally located and is responsible for organizing the network of MTs associated with it, as illustrated. It is the pole (or spindle pole) during cell division for reproduction (mitosis).

- the ER is involved with the synthesis of lipids and proteins; not shown are ribosomes attached to the ER, called rough ER

- the mitochrondria are known as the 'power-house' of the cell and produce most of a key molecule called adenosine triphosphate (ATP) which is an energy supply or 'currency' for cells, organisms, etc. It also where important biochemical reaction pathways occur, for example, tricarboxylic (or citric) acid cycle.

- the Golgi complex is involved with protein and lipid modifications and sorting - including preparation for their integration into membranes.

Other entities in Fig. 2-1 include AFs and vesicles that carry various biochemical cargoes, etc. MTs and AFs filaments have dual roles acting as mechanical scaffolding and as 'rail tracks' for molecular motors to step along as they actively transport metabolites.

2.2 Biomolecules: structure and function

The structure of biomolecules is related to their chemical properties and their biological function, and is also influenced by the natural, or artificial, environment that surrounds them.

2.2.1 Nucleic acids

Nucleic acids are divided into deoxyribonucleic acid (DNA) and ribonucleic acid (RNA). The basic chemical building blocks of nucleic acids are nucleotides that consist of three characteristic components

- a nitrogen containing base that is either a
    - purine, there are two possibilities: Adenine (A) or Guanine (G) or a
    - pyramidine, there are three possibilities: Cytosine (C), Thymine (T) or Uracil (U)

- a pentose sugar ring (denoted S_R)
    - for DNA it is a 2'-deoxy-D-ribose
    - for RNA the ring is a D-ribose

- a phosphate (P_O)

In DNA and RNA, the nucleotides are covalently linked together with the phosphates acting as 'bridges' between the pentoses. Chemically, the 5´ - phosphate group of one nucleotide is linked to the 3´ - hydroxyl group of the next nucleotide; the linkages are often referred to as the 'sugar phosphate backbone'. The three constituents of the four nucleotides for DNA is shown in Fig. 2-2. A key property of nucleic acids is that a single strand of linked nucleotides can form complementary pairs with another strand. That is, each base of a nucleotide on one strand can form hydrogen (H) bonds with the base of a nucleotide on the opposite strand. This occurs for all bases on each strand and purines pair with pyramidins. Generally the following rules apply:

- DNA contains A, C, G, and T
- DNA bases usually pair as A with T (double H-bond) , C with G (triple H-bond)

- RNA contains A, C, G, and U
- RNA bases, when they pair, do so as A with U (double H-bond), C with G (triple H-bond)

DNA and RNA are distinguished by their pentoses, i.e. DNA entails 2′-deoxy-D-ribose; RNA entails D-ribose. They also differ by one of the bases (T rather than U) and only on very rare occasions do exceptions to these rules occur.

There are a number of different structures of DNA, two of the most common are single-stranded DNA (ssDNA) and double-stranded DNA (dsDNA). Fig. 2-2 shows base pairing where A and C on the left ssDNA strand forms H-bonds with T and G on the right strand. The complementary pairing of ssDNA strands into dsDNA and subsequent natural formation into double helix

16

underpins the powerful replication capabilities of this biomolecule. There are also different forms of dsDNA, namely A, B, and Z. The standard double helical DNA usually referred to is (Crick and Watson) B-form.
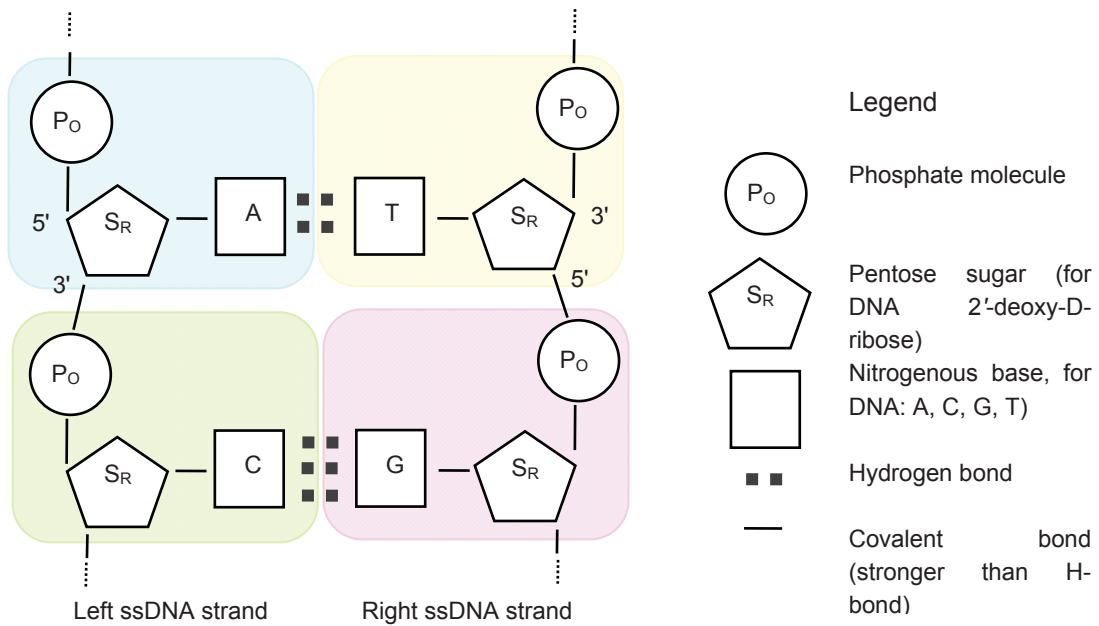

Fig. 2-2 Sketch of dsDNA nucleic acid showing the constituents of each nucleotide (base, S_R, P_O – other chemical details not shown) and pairing of left and right strands.

Fig. 2-3 shows a very short length of dsDNA as it occurs in aqueous (or water) solution, that is, in the energetically favorable state as a double helix. The sugar-phosphate double helical backbones are shown as thick lines - though structurally 'backbone' is a somewhat of a misnomer in the sense that it provides little stiffness. These are hydrophilic (water loving) and lie on the exterior of the biomolecule. The hydrophobic nucleotide base-pairs (bp) lie within the biomolecule, away from the polar water molecules. They are represented symbolically (A – T, C – G pairs) with respective double and triple H-bonds, as in the previous figure. The displacement along the major helical axis between base pairs is shown as 0.34 nm, so that the length between repetitive positions of the double helix is about 3.4 nm (10 bp). The diameter is the biomolecule is about 2 nm.

RNA is mainly involved with reading of DNA, called *transcription*, and its *translation* into proteins and other biomolecules associated with cellular information. There are a number of different types of RNA that perform different functions inside a cell:
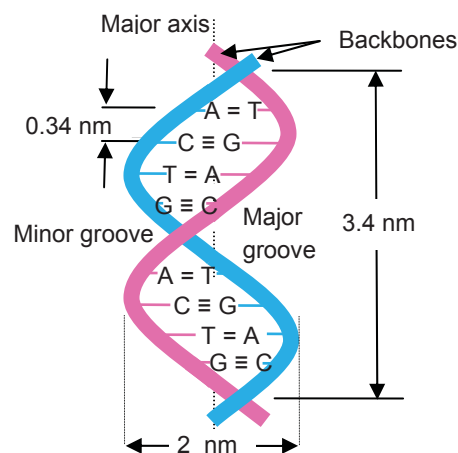
Fig. 2-3 A very short fragment of dsDNA as it appears in aqueous solution, double helical B-form. See text for details.

-   messenger RNA (mRNA) is concerned with transfer of genetic 'blueprint' information that codes for proteins. There are 20 different amino acids found in Nature, and DNA codes for them using the A, C, G, T bases available or 'quaternary alphabet'. This means that it requires a triplet of bases to sufficiently code for 20 AAs. That is, 4 bases to choose independently for first (base) position, then 4 bases to choose independently for the second position, then another 4 for the third position, yields total of 4×4×4 = 64 combinations or possible AAs. This is more than enough to code for the actual 20 AAs needed to make proteins so the genetic code is said to have redundancy. The triplet of bases that codes for each AA (and also some DNA reading instructions) is called a *codon*.

-   transfer RNA (tRNA): reads (decodes) the mRNA and transfers an appropriate AA onto a polypeptide chain that is being synthesized during production of a particular protein. tRNAs are small RNAs (about 80 nucleotides) with a characteristic clover leaf shape and act as adapters.

- ribosomal RNA (rRNA): ribosomal RNA constitutes part of the ribosome. These are located in the cytoplasm of a cell and are responsible for the synthesis of AA peptides and hence, protein, by decoding mRNA.

- noncoding RNA is that RNA that is *not* mRNA (does not code for protein) or rRNA or tRNA; and are short ~ 22 nucleotides single strands. These perform a whole variety of functions that are being currently discovered. These include, for example, small interfering RNA (siRNA) that can silence reading (gene expression) of DNA code, micro RNA (miRNA) that has been linked with cell cycle regulation, cardiac pathology, cancer, etc.

If one extracts RNA from cells, say fish liver cells, the dominant amount of RNA is rRNA with the amounts other RNA's being much smaller. This means that mRNA needed for understanding the protein production has to be carefully separated from the total amount of RNA.

Referring back to the illustration of a cell, a close-up of Fig. 2-1 is shown in Fig. 2-4 and outlines the process of making the protein according to genetic instructions. In eukaryote cells the reading of DNA, or transcription, occurs inside the cell nucleus. Since the DNA is packaged as chromatin, it needs to be unwound before its base sequence can be read. After unwinding, the DNA (dsDNA) is separated into two ssDNA strands, as shown on the left, in Fig. 2-4. Aided by RNA polymerase, unpaired bases on one of the ssDNA strands code for complementary bases thus forming a mRNA sequence. The mRNA is processed, packaged and exported through the nuclear pore, as shown.

The mRNA is translated in the cytoplasm at a ribosome; each one is made of about 50 different proteins and several rRNAs. The matching of the triple-base mRNA codon to AA is performed by a set of tRNA adaptor molecules. Reading the mRNA 5′ to 3′, the codon 'ACU', for example, pairs with the anti-codon tRNA adapter thus adding the AA Threonine (Thr) to the polypeptide chain.
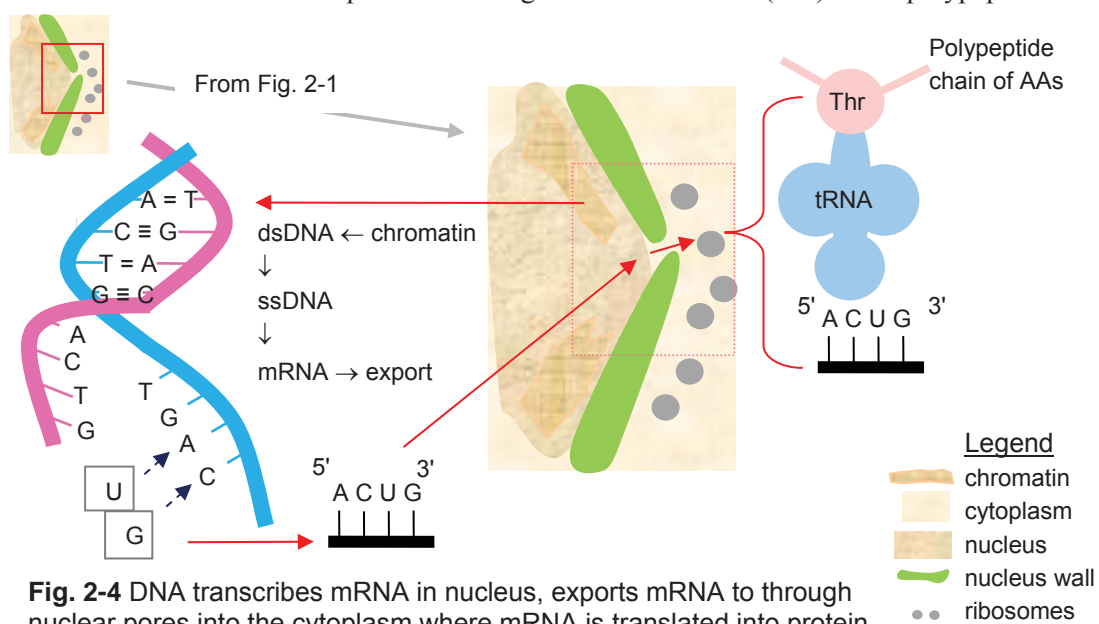

Fig. 2-4 DNA transcribes mRNA in nucleus, exports mRNA to through nuclear pores into the cytoplasm where mRNA is translated into protein.

19

2.2.2 Proteins

Proteins are made of peptides of amino acids (AAs) and may also contain some residues of uncommon AAs. The linear sequence of monomer units in a polymer is called a *primary structure*; the AAs in peptides fit this definition, so AA sequence is referred to as the primary structure. The twenty possible AAs are classified according to their electrical charge and as to whether parts of the AA have charge imbalance, i.e. parts have more positive charge and other parts more negative, that is, if they are *polar*. A water molecule itself is polar - with the oxygen atom carrying positive charge, and the two H-atoms carrying the balance of negative charge. Therefore, polar AAs near water tend to form H-bonds and are therefore energetically stable and consequently observed to be hydrophilic or water soluble (at biological pH that is about 7.0). Conversely, nonpolar AAs tend to be hydrophobic and tend to aggregate together in water. The 20 AAs are classified according to their R groups (or side chains); there are five classes:

- aliphatic, nonpolar R groups: the seven hydrophobic AAs are Glycine (Gly), Alanine (Ala), Proline (Pro), Valine (Val), Leucine (Leu), Isoleucine (Ile) and Methionine (Met)

- aromatic R groups: the three AAs are Phenylalanine (Phe), Tyrosine (Tyr) and Tryptophan (Trp)

- polar, uncharged R groups: the five AAs that are more soluble in water than the nonpolar AAs are Serine (Ser), Threonine (Thr), Cysteine (Cys), Asparagine (Asn) and Glutamine (Gln)

- positively charged R groups: the three AAs soluble in water are Lysine (Lys), Histidine (His) and Arginine (Arg)

- negatively charged R groups: the two AAs soluble in water are Aspartate (Asp) and Glutamate (Glu)

In solution the primary sequence of AAs forms bonds so that the polypeptide forms a defined structure. The term *secondary* structure refers to regular folding pattern in a localized vicinity, such as, α-helices and β-sheets. *Tertiary* structure refers to the three dimensional (3D) folding of a polypeptide chain into a protein unit, e.g. globin. Quaternary structure refers to the spatial relationship of protein subunits that form a complex, e.g. haemoglobin that carries in oxygen in our blood and is made up of two α-globin and two β-globin chains.

Proteins that can be positively or negatively charged depending on the concentration of anions and cations in solution (or pH). They can be classified in many ways, for example, according to their structural properties. Filamentous proteins, for example, include AFs and MTs that perform important functions, such as, the active transport of cargoes within cells, as mentioned earlier in section 2.1. Globular proteins are another example – as described above.

2.2.3 Carbohydrates

Carbohydrates are generally known as food sources and certain kinds, such as, sugar and starch, form a large part of peoples' diet in many parts of the world. Carbohydrates are not only involved with energy storage and use, they also perform numerous other roles, such as, signal messengers for cells.

Carbohydrates can be classified according to their size

- monosaccharides are simple sugars and example include sugar D-glucose, or dextrose - as is labeled sometimes in the laboratory.

- oligosaccharides are monosaccharides linked by glycosidic bonds into short chains. The most frequently encountered in daily life are disaccharides (two monosaccharides), such as, sucrose or cane sugar.

- polysaccharides are sugar polymers with tens to thousands of units, some as linear chains, others are branched. Two of the most important polysaccharides for storing energy are starch in plants and glycogen in animal cells. Cellulose is another polysaccharide that is found in cell walls of plants and constitutes much of wood and cotton.

2.2.4 Lipids

Lipids are insoluble in water and soluble in organic solvents, such as, benzene. They are chemically diverse and perform a range of biological functions, for example

-   energy storage : triacylglycerol droplets are the simplest of fatty acid fats and are found in the cytoplasm of many cells. Derivatives of fatty acids we are familiar with include fats (e.g. animal fats in cream or meat) and oils (e.g. corn and olive oils). Fatty acids are often classified as being saturated or unsaturated.

-   membrane structures: phospholipids are one class of membrane lipids and each molecule with a hydrophilic, polar head and two hydrophobic fatty acid tails, is capable of assembling with others to form a stable bi-layer in an aqueous environment. They are the basis for cell membranes.

-   signaling: lipids can act as hormones for cell communication including prostaglandins and steroids, for example, derived from cholesterol - testosterone, estradiol, cortisol, aldosterone, etc.

-   other: lipids are also known for their pigment properties, for example, vitamin A is both a hormone as well as a pigment for vertebrate eyes.

2.3 Biomolecules: electrical properties

One of the most potent forces for moving biomolecules is the electromagnetic (EM) field, one of the four fundamental forces of Nature – the remaining three being gravity, strong nuclear, and weak nuclear forces. Biomolecules are generally responsive to the electric component of the EM field and electric fields are fairly easily generated – especially in today's world of electronic devices and gadgets that supply electrical power. For this reason, and the fact that electrons play a fundamental role in chemical bonds, the electrical (or dielectric) properties are detailed.

2.3.1 Polyelectrolytes

Polyelectrolytes are molecules with a large number of charged chemical groups. Example biomolecules typically referred to in scientific literature are DNA and collagen. As introduced in the previous section, biomolecules, such as DNA and RNA possess a net *negative* charge. Proteins are made of amino acids that can be positively or negatively charged in varying amounts – and also dependent on pH or concentrations of anions and cations in solution.

An electrolyte or aqueous environment with salts acts as a supply for dissociated ions for example, Na^+, Mg^{2+}, OH^-, Cl^-. Consequently, if the biomolecule is electrically charged, it will attract ions of the opposite charge (or *counterions*) by Coulombic forces in order to restore charge neutrality. These counterions form a cloud around the biomolecule and act to electrically screen in the biomolecule by a certain amount. Further away from the biomolecule, the charge of the

counterions themselves in turn attracts ions of the opposite charge that have the same charge as the biomolecule and are termed *co-ions*.

This polyelectrolyte phenomenon is illustrated in Fig. 2-5, i.e. the same dsDNA as Fig. 2-3 including the solvent. The double-helical structure is shown to be straight in Fig. 2-5 but this only applies for relatively short lengths. The mechanical properties of DNA are partly determined by its chemical composition. As before, the sugar-phosphate 'backbone' is a misnomer and instead it is the stacking of the nitrogen bases that gives the molecule its backbone (Calladine & Drew, 1997).
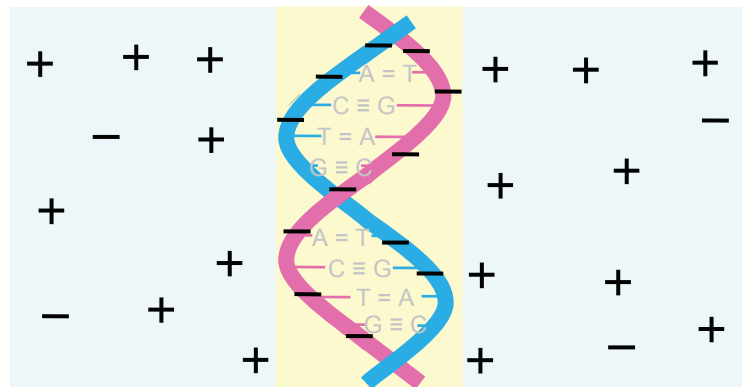

Fig. 2-5 dsDNA (or DNA) as a negatively charged polyelectrolyte in solution attracts positive counterions. These form around the polyelectrolyte to electrostatically screen the charge.

The flexibility of DNA also depends on the ionic composition of the solvent. In the situation of low concentration of counterions there is little electrostatic screening of the polyelectrolyte with itself. That is, the biomolecule electrostatically repels itself, so to be energetically favorable it tends to be straight. Conversely, in solvents with high molar counterion concentrations, screening occurs to the extent the biomolecule repels itself less, so it is more flexible.

2.3.2 DNA can be modeled as wormlike chain

A measure of straightness is known as the persistence length L_p, as sketched in Fig. 2-6. Typically for standard biological conditions for dsDNA, L_p = 50 nm (Hagerman, 1998). In this way the behavior of dsDNA in water is modeled as a worm-like chain with each straight link equal to the Kuhn length that is twice the persistence length, $L_K = 2L_p$ long (Bloomfield *et al*., 1974; Viovy and Duke, 1993). In this chain the next link is randomly oriented and independent from the previous link; randomness arises from thermal motion. This means that each link is about 100 nm or roughly 30 double helical turns or 300 bp.
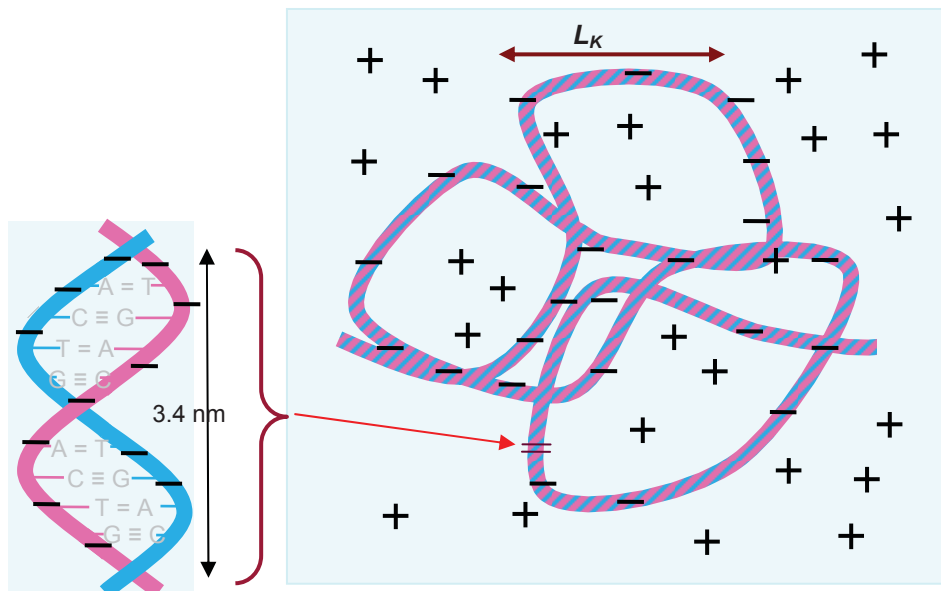
Fig. 2-6 Worm-like chain model of dSDNA with close-up, in aqueous suspension, showing relatively straight segments of Kuhn length L_K. Not to scale.

A biomolecule moving in a solvent (e.g. DNA in water) can behave hydrodynamically as if it is a rigid body, such as, a sphere. This is due to the worm-like chain retaining a roughly spherical (or ellipsoidal) shape due to ions and water molecules being attracted and dragged along with it. The mass of DNA, ions and water exerts a hydrodynamic drag equivalent to a sphere with a radius, r_h. This is the hydrodynamic radius and is an important parameter that can be inferred and estimated from experimental measurements (Newman, *et al*., 1974; Smith *et al*., 1996)

24

2.3.3 Biomolecules and bioparticles

The electrical and hydrodynamic properties of the biomolecules may enable them to be approximated as a body or point-particle. That is, the biomolecule is assumed to behave like a fairly rigid body with known properties or parameters, for example, centre of mass, electrical charge, size (or volume), solid-solution interface, etc. Appropriate circumstances for biomolecules to be modeled as bioparticles include, for example, instances where the biological or minute chemical activity is not being questioned; rather physical and broader questions are asked about the motion of the biomolecule for length scales much larger than the biomolecule itself. There are a number of reasons for introducing and justifying the notion of a bioparticle:

- the transport of bioparticles is more convenient to mathematically model compared with flexible biomolecules, such as, DNA. This applies to either approximate 'back-of-the-envelope' calculations or with more sophisticated computer models.

- the transport of bioparticles is often measured using fluorescence microscopy where the biomolecule itself is often not larger than the limit of optical resolution for recording; hence, a particle model is sufficient.

- globular proteins and filaments with well defined shapes can be modeled as rigid bodies or bioparticles to a first approximation when applying Newton's laws of motion.

- the use of latex (polystyrene) and metal nano- and micro-spheres (or *beads*) in biological are increasingly being used in investigations for many purposes such as functionalizing biomolecules. This means that it is not only the transport of biomolecules themselves that is of interest, but also the beads. The beads themselves can be used as a diagnostic and as 'ideal biomolecule' for researching and developing transport processes.

- modeling flexible biomolecules (e.g. DNA) as bioparticles is less straightforward than, for example, with beads but with care can be performed using parameters, such as, the hydrodynamic radius.

Biomolecules that are modeled as bodies or particles are collectively called 'bioparticles'. Micro- and nano-beads capable of being biologically functionalized are also included. Importantly, the dielectric properties of bioparticles are critical for the main transport process discussed in this e-book.

2.3.4 Electrical double layer

Investigations on the behavior of polyelectrolytes and colloids that mimic bioparticles have indicated the presence of an electrical double layer, shown in Fig. 2-7. Counterions adjacent and close to the bioparticle form the Stern layer. Counterions further away from the bioparticle and Stern layer are more diffuse and screen the bioparticle charge in such a way as to attract co-ions.

This diffuse layer has characteristic length, λ_D, as shown and is referred to as the Debye screening length.
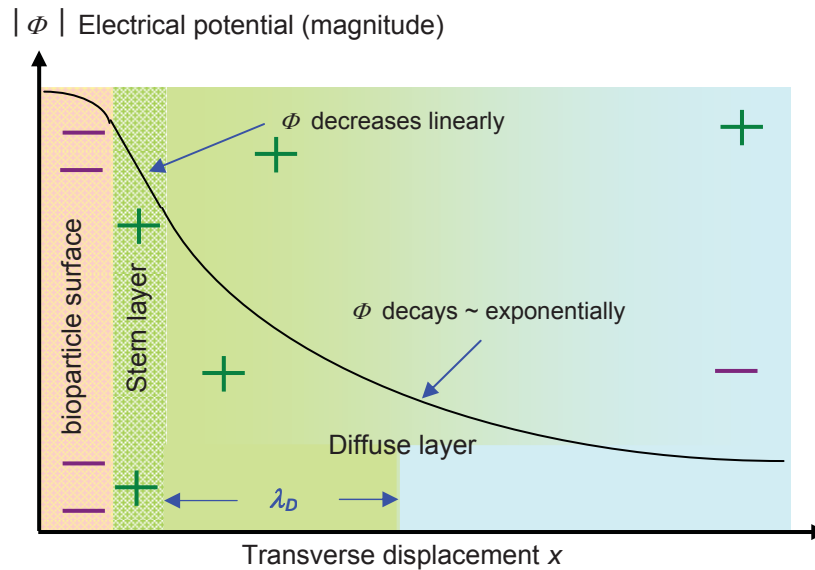

Fig. 2-7 The electrical double-layer scheme with potential magnitude Φ superposed: a layer of negative charges at the particle surface is surrounded by a positively charged counterion layer. This consists of a thin Stern layer and diffuse layer with characteristic length, λ_D (not to scale).

In conjunction with the Coulombic and diffusive forces, the diffuse layer is subjected to hydrodynamic forces. The 'slip plane' designates where part of the diffuse layer that moves with the body, in comparison with the remainder that tends to be dragged away by the surrounding medium. The zeta potential Φ_ζ (not shown in Fig. 2-7) is the electrical potential at the slip plane (Pethig, 1979; Russel *et al.*, 1999).

2.3.5 Introduction to dielectric polarization

Polarisation is a term that describes how charges, within a dielectric, respond to an externally applied electric field. Charges that are free to move reveal their movement on a macroscopic scale as conduction. If the movement of the charges is blocked they are said to be 'polarised'. In this respect, polarisation is the 'intention' of the charges to move in response to an applied electric field.

There are many of kinds of polarisation: electronic, atomic, molecular, interfacial (or space-charge), and counterion polarisation. The first three are attributed to the displacement, or orientation, of bound charges; the latter two concern movement on a larger scale. *Electronic* polarisation arises from a slight asymmetric displacement of electrons (with respect to the positive nuclei of atoms) caused by an externally applied electric field.

Atoms constituting a molecule, such as sodium chloride, have different net charges due to an unequal sharing of electrons. Consequently, when an external electric field is applied, the atoms behave differently. This causes a displacement of the atoms, from their equilibrium positions, resulting in *atomic* polarisation. An example of a molecule that exhibits atomic polarisation is sodium chloride. Both electronic and atomic polarisations are *induced*, and contribute only modestly to the total polarisability.

The asymmetric distribution of electrons in molecules also gives rise to *permanent* dipoles. The interaction of such a dipole with an externally applied electric field causes a torque that attempts to orient the molecule in the field direction. The polarisation is appropriately called *orientation*, or *dipole*, polarisation (Von Hippel, 1954). Water is an example of a molecule with a permanent dipole, and is responsible for manifesting a significant permittivity for frequencies up to 17 GHz. In summary, of the first three types of polarisation, only molecular dipole polarisation, tends to feature in the literature concerning dielectric properties of bioparticles and DNA.

The last two kinds of polarisation, interfacial and counterion, involve large-scale charge movement. Currently, there is no universal consensus in the literature on the high frequency polarisation mechanisms for biomolecules, such as, DNA. At present, the emphasis tends to favour Maxwell-Wagner interfacial polarisation for bioparticles with well defined interfaces between AAs and water molecules, and counterion fluctuation polarisation, along the longitudinal axis, for DNA and probably for RNA.

Interfacial, or *space-charge*, polarisation arises from free charge accumulation across the interfaces, between different dielectric materials, when they are juxtaposed. The interfacial charge

accumulation, or polarisation, results in dielectric dispersions when the aggregate of dissimilar materials is exposed to AC electric fields (Pethig, 1979; Takashima, 1989). The simplest form of interfacial polarisation is a Maxwell-Wagner type, and is detailed in the following chapter.

Counterions are ions in solution that are attracted to bodies of the opposite charge. They form 'clouds' around the bodies that become distorted when an external electric field is applied. *Counterion* polarisation arises when the movement of these counterions is restricted. Counterion movement around the surface of bioparticles, and along the double helical axis of DNA, is also detailed further in the next chapter.

2.3.6 Polarisation parameters: a brief view

The free movement of charges can be expressed, in terms of electrical circuit parameters, as the in-phase conductivity; and the restricted movement, or polarisation, as the out-of-phase conductivity, (Pohl, 1978). An equivalent, and frequently used alternative, is to parameterise the free movement of charges as the out-of phase permittivity ε'', and polarisation as the in-phase permittivity ε'. The complex permittivity ε is the combination of these,

$$\varepsilon(\omega) = \varepsilon' - j\varepsilon''$$

(2.1)

Usually ε' is referred to as the real (in-phase) part of ε, or simply *permittivity*, ε'' is called the imaginary (out-of-phase) part of ε or *dielectric loss*, and $j = \sqrt{-1}$. Polarisability is a measure of response of a body to an external electric field. It is represented quantitatively by the constant, α. A highly polarisable body, for example, features many charges that are responsive to an electric field, but their movement is in some way restricted.

The literature on dielectric properties of bioparticles and DNA suspended in solution, motivates an extension of equation (2.1) to include the conductivity (or low frequency Ohmic loss) of the ionic solution, σ (Grant *et al.,* 1978; Jones, 1995). In addition, the frequency dependency is also made explicit, hence the relation for the complex permittivity becomes

$$\varepsilon(\omega) = \varepsilon'(\omega) - j(\varepsilon''(\omega) + \sigma/\omega)$$

(2.2)

An alternative expression used in the literature for the frequency dependent dielectric complex permittivity ignores the dielectric loss ε'' since it is often small compared with Ohmic loss σ/ω. The superscript $'$ notation is omitted,

$$\underline{\varepsilon}^* = \varepsilon - j\sigma/\omega$$

(2.3)

where ε is the permittivity (real part of $\underline{\varepsilon}^*$) or "dielectric constant" (Takashima, 1989). The form for the complex permittivity given by (2.3) is useful for describing polarisation mechanisms in the next chapter.

2.3.7 Measurement of biomolecule polarisation parameters

An important parameter for determining the value of the polarisability of a particle, is the dielectric increment (Takashima, 1989), or decrement,

$$\Delta\varepsilon' = \varepsilon'_{rl} - \varepsilon'_{rh}$$

<div align="right">(2.4)</div>

where ε_{rl} and ε_{rh} are the low and high frequency relative permittivities, or limiting dielectric constants. Another parameter is the relaxation time constant, τ associated charges 'relaxing' after being perturbed by an electric field. The charges resonate at a dispersion frequency f_R (Hz) or angular frequency ω_R (rad s^{-1})

$$\tau_R = \frac{1}{f_R} = \frac{2\pi}{\omega_R}$$

<div align="right">(2.5)</div>

Dispersions arise when the oscillating cloud of charges can no longer follow the alternating electric field and this effect is observed in both real and imaginary parts of the complex permittivity. Biomolecules can have more than one dielectric dispersion characterized by a decrement and associated time constant. The decrement, $\Delta\varepsilon'$, is used for experimentally characterising the frequency dependent polarisability of macromolecules and polyelectrolytes, such as, DNA.

Commercial time-domain dielectric spectrometers (Feldman *et al.*, 1996; Kamyshny *et al.*, 2000) can be used to estimate the dispersion decrement $\Delta\varepsilon'$ and time constant τ_R using a sample, e.g. say 150 microlitres (μl), of macromolecules suspended in an appropriate solvent, such as, water.

The polarisability corresponding to a suspension of n_p bioparticles each with volume, V, or macromolecule (or part of it), can be determined from the polarisability for the total volume V_T

$$\alpha = \frac{\alpha_\Sigma}{v_f}$$

(2.6)

where v_f is the volume fraction, $v_f = n_p V / V_T$. The result is from dielectric mixture theory (Asami *et al.*, 1980; Hilfer *et al.*, 1994) and is illustrated in Fig. 2-8.

Bioarticle with permittivity ε_p^* and volume, V.

Region with volume V_T

Equivalent body with effective permittivity ε_{eff}^* and volume V_T.

Medium with permittivity ε_m^*

(a)   (b)
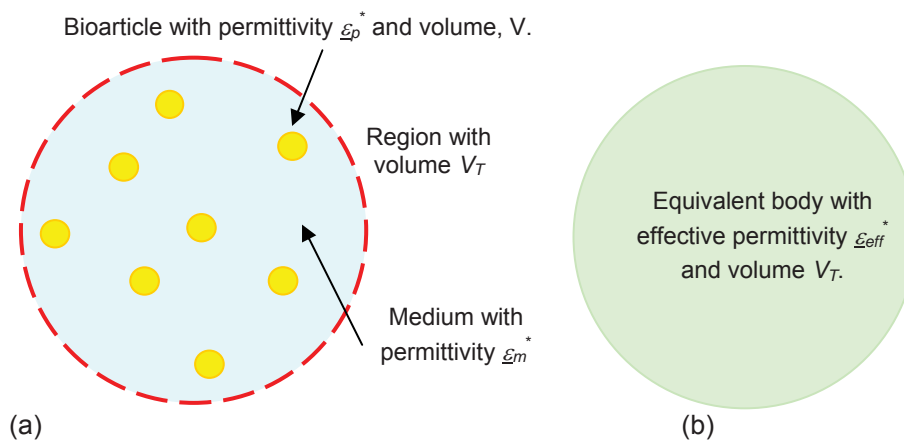
Fig. 2-8 Suspension of spherical particles. (a) n_p particles with permittivity ε_p^* and spherical volume, V enclosed in volume, V_T (b) Equivalent sphere with effective permittivity ε_{eff}^* and volume V_T.

2.4 Concluding remarks

This chapter has described the structure and biological function of biomolecules and introduced their electrical properties as they behave in aqueous solution. Concepts, such as double-layer, dielectric polarization, and bioparticle will be important for subsequent chapters that focus on biomolecule transport, particularly using electric fields.

3 Moving biomolecules using electric fields

It is often thought biomolecules that are electrically *neutral* do not move when an electric field is applied across, or external, to the suspension. This is true if the biomolecules are lying within in a *uniform* electric field – they remain stationary. However, it is not necessarily true if the electric field is *nonuniform* – the biomolecules may move in accordance with their dielectric properties relative to the medium they are suspended within. *Electrophoresis* is the movement of a charged biomolecule under the action of a uniform electric field; *dielectrophoresis* refers to the movement of under the action of a nonuniform electric field that depends on the dielectric properties. The biomolecule may be electrically neutral or charged. This chapter explains basics of biomolecule response to both uniform and nonuniform electric fields that forms a potent force underpinning current and emerging technologies.

3.1 Electrophoresis

When an electric field is applied, by energising a pair of submerged electrodes, to a charged biomolecule suspended in salt water electrolyte the surrounding double layer counter-ion cloud is disturbed. The biomolecule itself is not entirely electrically screened - and 'feels' the presence of the field and moves under the action of Coulombic force. Suppose for example the biomolecule is negatively charged (e.g. DNA); from Coulomb's law, the biomolecule moves towards the positive electrode. The counter-ions, that are positive by definition, will move towards the negative electrode.

Since the counterions are moving in the opposite direction to the biomolecule and remain attracted to it, then the net force on the biomolecule cannot be simply described by Coulomb's law. In addition, as the biomolecule moves, the effects of hydrodynamic viscous drag have an effect so that a 'comet-tail' shape tends to form behind the behind the biomolecule, O'Brien and White (1978) and DeLacey and White (1981). Taking these effects into account, the *electrophoretic* force (denoted by the subscript 'EP') is described by the relation,

$$F_{EP} = \mu \, \zeta \, E \tag{3.1}$$

where ζ is the fluid drag coefficient with units (kg s^{-1}), E is the electric field (V/m) and μ is Smoluchowski's mobility relation. It is $\mu = \varepsilon_m \Phi_\zeta / \eta$ where Φ_ζ is the zeta potential of the electrical double layer surrounding the biomolecule, and η is the dynamic viscosity of the medium (kg m^{-1} s^{-1}) (Ohshima, 1997; Grattarola and Massobrio, 1998; Arnold *et al*., 1993; Reese, 1994).

Biomolecules have charge proportional to length and mass. In suspensions of long biomolecules with thicknesses or width much less than their length, the viscous friction in water or liquid medium is also proportional to mass. Therefore, the electrophoretic and viscous forces often negate each other and there is no net charge advantage. Attempting to separate biomolecules based

on length or mass is unsuccessful. Instead, biomolecules can be separated using a porous medium, such as, a gel where the electrophoretic and friction forces do not cancel each other.

3.2 Dielectrophoresis (DEP)

If a biomolecule is electrically neutral so that electrophoresis does not occur, it can be moved by applying a non-uniform field. To understand this phenomenon and its application, consider Fig. 3-1 where a neutral bioparticle lies in a uniform field established by a electric potential difference being applied across two parallel plates. The field causes elementary charge movement, within the dielectric material, that opposes the (original) field. The movement of these charges resulting from the external electric field, results in *induced dipoles*, as shown schematically.   The charge movement is the same throughout the bioparticle. Consequently, the interaction of the uniform external field with the charges means the sum of the forces is zero and the neutral bioparticle (yellow) does not move. In contrast the small positively charged test bioparticle (blue) experiences a Coulombic force, and moves to the left.

The movement of charges within a neutral dielectric bioparticle, to establish equilibrium, also occurs when a *non-uniform* electric field is imposed, Fig. 3-2. The charged regions have equivalent amounts of charge, as shown. However, the strength of the electric field with which they interact, varies between local regions throughout the bioparticle. Consequently, the total force on the bioparticle, equaling the sum of the Coulombic forces of each *local* region, is no longer zero and neutral bioparticle moves in accordance with the spatial distribution of field strength.

Assuming the bioparticle is more polarisable than the surrounding medium, it moves towards the region of highest field non-uniformity. The phenomenon is called dielectrophoresis (DEP).
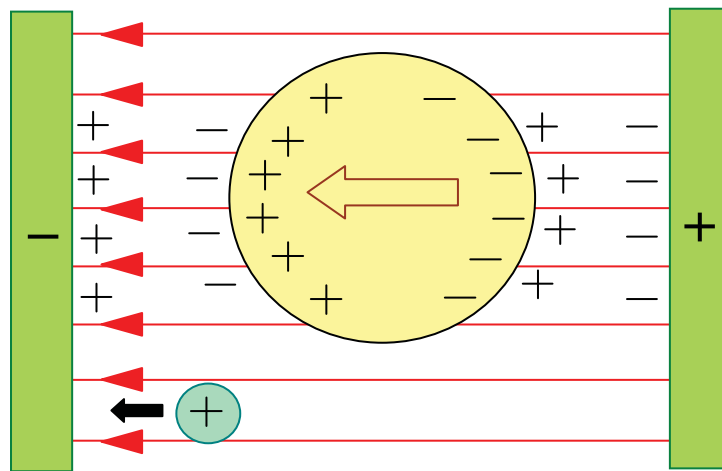

Fig. 3-1 Charge movement in a neutral bioparticle (yellow) in a uniform electric field (red arrows) results in induced dipoles (the sum of the induced dipoles represented by the brown, unfilled, arrow). The sum of the forces is zero so the neutral bioparticle does not move. In contrast, a positive test charge (aqua), acting under a Coulombic force, moves to the left. In this example, the polarisability of the bioparticle is greater than the surrounding medium.

The imbalance of forces on the neutral bioparticle can be explained by considering two elementary charges $+q$ and $-q$ at A and B, distance d apart, Fig. 3-3. The electric field at B is stronger than at
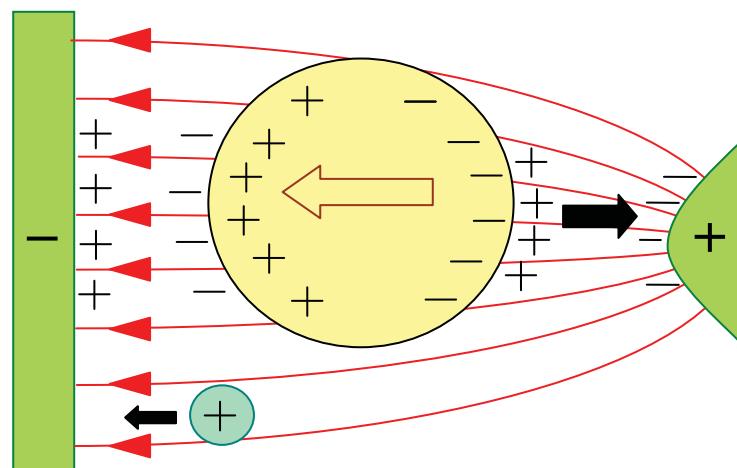
Fig. 3-2 Dielectrophoresis: the neutral body (yellow) in a nonuniform electric field (red arrows) experiences a net force depending on spatial distribution of electric field strength. In this example, where the polarisability of the body is greater than the surrounding medium, it moves to the right (black arrow).

A, $E_B > E_A$. Assuming the forces are acting in the horizontal direction and using a standard convention where forces acting to the right are positive, and those to the left are negative, the sum of the two Coulombic forces is

Fig. 3-3 The displaced charges at A and B interact with the electric field, E_A and E_B, generating Coulombic forces, F_A and F_B acting in the opposite directions, as shown. The force at B is greater than at A, $F_B > F_A$, so the neutral bioparticle moves to the right.

$$F_{total} = F_A + F_B = qE_B - qE_A = q(E_B - E_A) \tag{3.2}$$

and is positive, (i.e. acting towards the right). Note that the extra negative sign arise from the electric field acting towards the left.

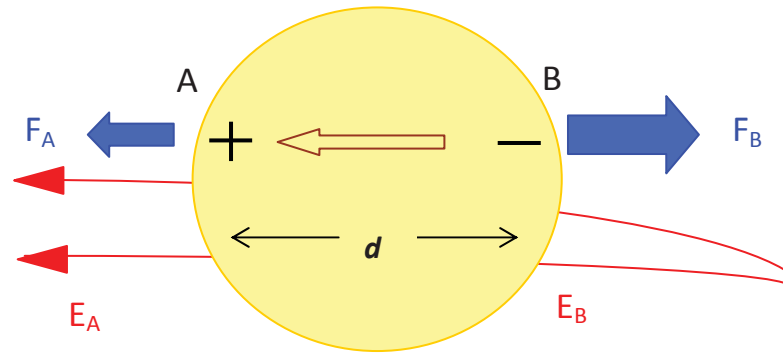Expressions for the net force acting on a neutral bioparticle in a nonuniform electric field have been developed using the energy variation principle, effective moment method, and Maxwell stress tensor approach. The effective moment method is the most straightforward, and includes situations where there is dielectric loss.

Equation (3.2) can be evaluated using a Taylor series approximation,

$$F_{DEP} = q\left(E_B - E_A\right) = q\left(E(x+d) - E(x)\right) \cong qd\frac{dE}{dx} \cong p\frac{dE}{dx} \tag{3.3}$$

where $p = qd$ (C m) is the induced (or effective) dipole moment. This parameter can be expressed as

$$p = \alpha VE \tag{3.4}$$

where α is the induced polarisability, or effective dipole moment, per unit volume in unit electric field and has dimensions Farad per metre (Fm^{-1}). The physical-chemical origin of the polarisability was introduced in the previous chapter and will be discussed further in this chapter. It is assumed, for the force to be proportional to the derivative of E in (3.3), that the dimension of the dipole p is small compared with the characteristic length of the electric field non-uniformity. Any spatial electric field phase variation is considered to be negligible.

To keep the argument simple, our interest lies solely in the in-phase component of the DEP force and it is usual for experimental arrangements to supply electrodes with potentials of 180° phase difference. Combining (3.3) and (3.4) and using the differential calculus product rule,

$$F_{DEP}\big|_{DC} = \alpha V E \frac{dE}{dx} = \frac{1}{2}\alpha V \frac{dE^2}{dx} \tag{3.5}$$

where the subscript signifies that this equation is applicable for a constant (DC) signal applied to electrodes.

Equation (3.5) underlines an important property of dielectrophoresis; the direction of the force is *invariant* to the electric field direction (or sign of the electrode potentials). This fundamental and important property means that the neutral bioparticle continues to moves in the same direction – *independent* of the sign of electrode potentials, as shown in Fig. 3-4. Therefore, alternating current (AC) signals can be used rather than direct current (DC) signals that tend to cause hydrolysis reactions between the electrode surface and electrolyte. Using AC radio frequencies above 1 kHz avoids hydrolysis for most water solutions that are not too salty. This enables microelectrodes with micron to sub-micron features to drive bioparticle or biomolecule transport for LOC-type applications.

Fig. 3-4. The DEP movement of a neutral body is invariant to the sign of the electrode potentials and direction of the electric field.

3.2.1 Polarisation and DEP biomolecule transport

Assuming AC signals that are more useful, the small-time averaged DEP force is just half the DC value

$$\langle F_{DEP} \rangle_t = \frac{1}{4} \alpha V \frac{dE^2}{dx} = \frac{1}{2} \alpha V \frac{dE_{rms}^2}{dx} \tag{3.6}$$

where 'small-time' average, denoted by $\langle \ \rangle_t$, over an oscillation period and can be expressed in terms of the electric field root-mean-square (rms), E_{rms}. The DEP force is understood to be 'almost instantaneous'.

The proof for (3.6) is given in the next chapter that entails a higher level of mathematics needed for the more general three dimensional (3D) case. In terms of understanding and computing the DEP force, the electric field gradient for realistic geometric electrode designs can be determined, analytically for simple cases, or by appropriate electromagnetic simulation software. The volume of the bioparticle V is usually known or can be estimated. The remaining parameter is the polarizability, α, and it is important to discuss it in the following sections for at least three reasons:

- the polarisability turns out to be frequency dependent so that its magnitude and sign will influence the direction and magnitude of the DEP force

- the polarisability may be not be straightforward to calculate or estimate, and may need to be to be determined by experimental means, such as, by dielectric measurements

- the dielectric polarisability of biomolecules is not covered in usual biology textbooks at present, and engineering texts tend not to cover biology at the molecular level – it is interdisciplinary and somewhat specialist

3.2.2 Maxwell-Wagner interfacial polarisation

A schematic diagram of Maxwell-Wagner (MW) interfacial polarisation for an electrically neutral bioparticle (latex yellow) suspended in aqueous solution, is shown in Fig. 3-5. The bioparticle lies in a uniform electric field established by an electric potential difference being applied between two parallel plates. The charges have moved to their interfaces in accordance with Coulomb's Law and their movement is the same throughout the bioparticle. Consequently, the interaction of the uniform external field with the charges means the sum of the forces is zero and the neutral bioparticle does not move. A comparison with the setup shown for DNA in Fig. 2-5 shows some similarities and also differences that are instructive to point out:

- the bioparticle is electrically neutral, compared with the DNA that had a net (negative) charge.

- the bioparticle lies in an externally applied electric field, compared with the DNA that did not have an electric field imposed on it.
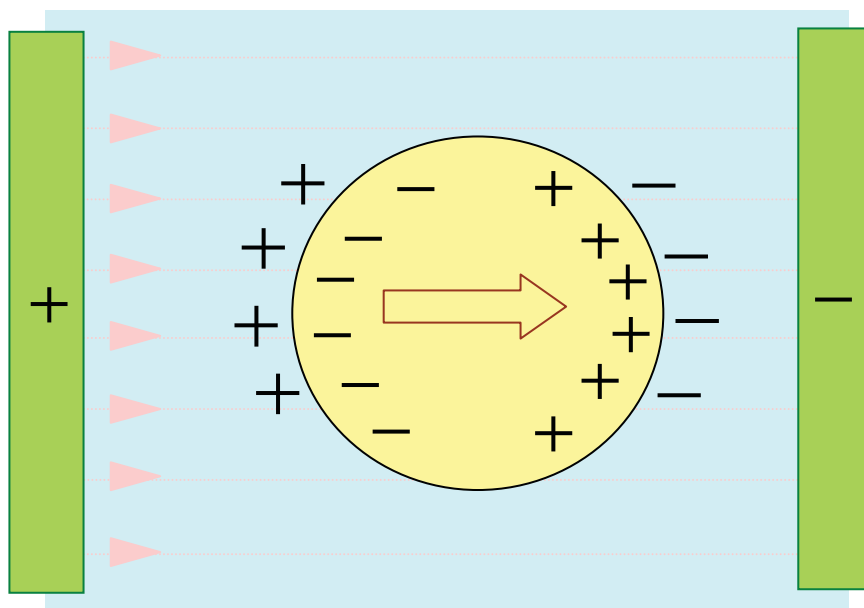
Fig. 3-5 Maxwell-Wagner (M-W) interfacial polarisation of a neutral dielectric body in a uniform field. Charges accumulate at the interface between the dielectric sphere and the aqueous medium.

Suppose the potential on the electrodes is suddenly reversed to that they are opposite to the values shown in Fig. 3-5. There will be time delay before the charges redistribute themselves, inside the body, to the imposed electric field. There will also be a delay for the counterions to re-cluster around the polarised body. The time taken for the charges to redistribute, or 'relax', is called the

37

relaxation time. The movement of the charges, restricted by interfaces between layers, manifests itself as polarisation. The delay also occurs when the electrode potentials are reversed, again, back to the original state. Thus, applying an AC electric potential across the electrodes causes the charges within the bioparticle to be attempting to respond to temporal changes in the electric field.

3.2.3 Maxwell-Wagner interfacial polarisation for bioparticles

The polarisation mechanisms applicable to bioparticles or ideal biomolecules (Sasaki *et al.*, 1981) have been characterised by similar investigations on bioparticles and polyelectrolytes with spherical geometry, (O'Konski, 1960; Schwartz *et al.*, 1962; Schwan *et al.*, 1962; Lyklema *et al.*, 1983; Springer *et al.*, 1983; Lyklema *et al.*, 1986). The expression for the effective polarisability, α, or dipole moment per unit volume per unit electric field, for interfacial polarisation of a spherical particle immersed in a medium is (Von Hippel, 1954; Jones, 1995)

$$\alpha = 3\varepsilon_m \, \mathrm{Re}\{f_{CM}(\omega)\} = 3\varepsilon_m \, \mathrm{Re}\left\{ \frac{\underline{\varepsilon}_p^* - \underline{\varepsilon}_m^*}{\underline{\varepsilon}_p^* + 2\underline{\varepsilon}_m^*} \right\} \qquad (3.7)$$

where $\underline{\varepsilon}_p^* = \varepsilon_p - j\sigma_p/\omega$ is the complex permittivity of the particle, $\underline{\varepsilon}_m^* = \varepsilon_m - j\sigma_m/\omega$ is the complex permittivity of the medium, and 'Re { }' denotes the real part of the frequency dependent Clausius-Mossotti function, f_{CM}. It is assumed the particle lies in a homogenous

external electric field. Unless otherwise stated the permittivity and conductivity parameters, ε and σ, are implicitly assumed to be frequency independent.

Water, for example, exhibits ε and σ that are practically frequency independent up to 17 GHz. As before, the angular frequency is $\omega = 2\pi f$ where f is frequency (Hz) and $E =$ magnitude (peak) of the electric field. Substituting the relations for the complex permittivities,

$$\mathrm{Re}\{f_{CM}(\omega)\} = \left[\frac{(\sigma_p - \sigma_m)(\sigma_p + 2\sigma_m) + \omega^2(\sigma_p - \sigma_m)(\sigma_p + 2\sigma_m)}{(\sigma_p + 2\sigma_m)^2 + \omega^2(\sigma_p + 2\sigma_m)^2} \right] \tag{3.8}$$

By considering the conditions $\sigma_p \gg \sigma_m$, $\sigma_p \ll \sigma_m$ for the limiting case $\omega \to 0$, and $\varepsilon_p \gg \varepsilon_m$, $\varepsilon_p \ll \varepsilon_m$ for $\omega \to \infty$, it is evident, $-0.5 \le \mathrm{Re}\{f_{CM}(\omega)\} \le 1$.

Analysis of the transient response of the sphere to an electric field reveals a MW relaxation time constant τ_{MW} associated with free charge storage at the spherical interface (Jones, 1995),

$$\tau_{MW} = \frac{\varepsilon_p + 2\varepsilon_m}{\sigma_p + 2\sigma_m} \tag{3.9}$$

The relaxation time constant enables (3.8) to be cast (Benguigui and Lin, 1982; Jones, 1995),

$$\mathrm{Re}\{f_{CM}(\omega)\} = \left[\frac{\varepsilon_p - \varepsilon_m}{\varepsilon_p + 2\varepsilon_m} + \frac{3(\varepsilon_m \sigma_p - \varepsilon_p \sigma_m)}{\tau_{MW}(\sigma_p + 2\sigma_m)^2(1 + \omega^2 \tau_{MW}^2)} \right] \tag{3.10}$$

and reveals two interesting features. First, it shows the conductivity parameters dominate at low frequencies, and the permittivities at high frequencies,

$$\mathrm{Re}\{f_{CM}(\omega)\} = \begin{cases} (\sigma_p - \sigma_m)/(\sigma_p + 2\sigma_m), & \tau_{MW}\omega \ll 1 \\ \\ (\sigma_p - \sigma_m)/(\sigma_p + 2\sigma_m), & \tau_{MW}\omega \gg 1 \end{cases} \tag{3.11}$$

Second, in the case $\varepsilon_m \sigma_p = \varepsilon_p \sigma_m$, the real part of the Clausius-Mossotti function is shown to be frequency independent.

Combining (3.6) – (3.8), the small-time averaged DEP force resulting from Maxwell-Wagner polarisation for a sphere with radius, r, and volume, $V = 4\pi r^3/3$ is

$$F_{DEP}(\underline{x}) = \frac{1}{4}\alpha V \frac{d|E|^2}{dx} = \pi r^3 \varepsilon_m \operatorname{Re}\{f_{CM}(\omega)\}\frac{d|E|^2}{dx}$$

$$= \pi r^3 \varepsilon_m \frac{d|E|^2}{dx}\left[\frac{(\sigma_p - \sigma_m)(\sigma_p + 2\sigma_m) + \omega^2(\varepsilon_p - \varepsilon_m)(\varepsilon_p + 2\varepsilon_m)}{(\sigma_p + 2\sigma_m)^2 + \omega^2(\varepsilon_p + 2\varepsilon_m)^2}\right]$$

(3.12)

In (3.12), positive DEP occurs when $\operatorname{Re}\{f_{CM}(\omega)\}>0$, the direction of the force F is governed by $d|E|^2/dx$, so the particle moves towards the region of maximum electric field intensity. Conversely, negative DEP occurs when $\operatorname{Re}\{f_{CM}(\omega)\}<0$, and the direction of the force is towards electric field minima. The conditions for positive and negative DEP also apply to non-spherical geometry (Jones, 1995).

The transition from positive to negative DEP occurs when $\vec{F}_{DEP} = 0$ and means that the direction of a DEP driven transport process can be reversed. The *positive/negative* transition may, theoretically, involve any suitable combinations of σ, ε and ω values that force the numerator of (3.8) to be zero. In practice the parameters controlled in DEP experiments are ω, σ_m, and sometimes ε_m. The other parameters remain constant.

Applying the condition $\operatorname{Re}\{f_{CM}\}=0$ in (3.8), establishes the relationship between cross-over frequency $f = f_c$ and medium conductivity for these bioparticles,

$$f_c = \frac{1}{2\pi}\sqrt{\frac{(\sigma_p - \sigma_m)(\sigma_p + 2\sigma_m)}{(\varepsilon_m - \varepsilon_p)(\varepsilon_p + 2\varepsilon_m)}}$$

(3.13)

The conductivity of the particle (bioparticle) σ_p, of radius r, consists of the bulk conductivity σ_b of the polystyrene and from ion movement shunted around, tangential, to the surface of the particle (O'Konski, 1960) with surface conductance, K_s (S). K_s includes ion movement in both parts of the double layer described in section 2.3.4 (Hughes *et al.*, 1999).

$$\sigma_p = \sigma_b + 2K_s/r$$

(3.14)

Example: Typical values for the permittivities of water and 282 nm diameter latex bead as an example bioparticle are $\varepsilon_m = 78.4\varepsilon_o$ and $\varepsilon_p = 2.55\varepsilon_o$ (Green and Morgan, 1997a) where the permittivity of free space is $\varepsilon_o = 8.854\times10^{-12}$ F/m. Selecting a low conductivity 1 mM potassium phosphate suspension, $\sigma_m = 0.018$ S/m with bioparticle parameters, $r = 141$ nm, $\sigma_b \cong 0$ and $K_s = 2.2$ nS, equation (3.14) yields $\sigma_p = 0.0312$ S/m, and (3.13) predicts $f_c = 5.23$ MHz – which is close to the experimentally observed crossover frequency (Green and Morgan, 1997a). Also the above values in (3.9) predict $f_{MW} = 1/(2\pi\tau_{MW}) = 3.93$ MHz. It is anticipated the DEP crossover frequency will be in the vicinity of the relaxation frequency

The real and imaginary parts of the Clausius-Mossotti function for a 216 nm diameter bead is plotted in Fig. 3-6 for $10^3 \leq f \leq 10^9$ Hz with ε_m and ε_p as in the previous calculation but $r = 108$ nm, and slightly different values for $\sigma_m = 1.7$ mS/m and $\sigma_p = 18.5$ mS/m calculated from (3.14) with $\sigma_b = 0$ and $K_s = 1.0$ nS. It yields a cross-over frequency slightly above 3 MHz as shown. There are several points to be highlighted

- the transition from positive to negative DEP force, as the applied frequency f or conductivity σ_m are varied, means these parameters can be varied to explore subsequent changes in DEP collection rates.

- the region of the crossover frequency can be estimated from the M-W relaxation time.

- experiments exhibiting a large deviation of crossover frequency, compared with predicted relaxation frequency, may indicate another polarisation mechanism is operating.
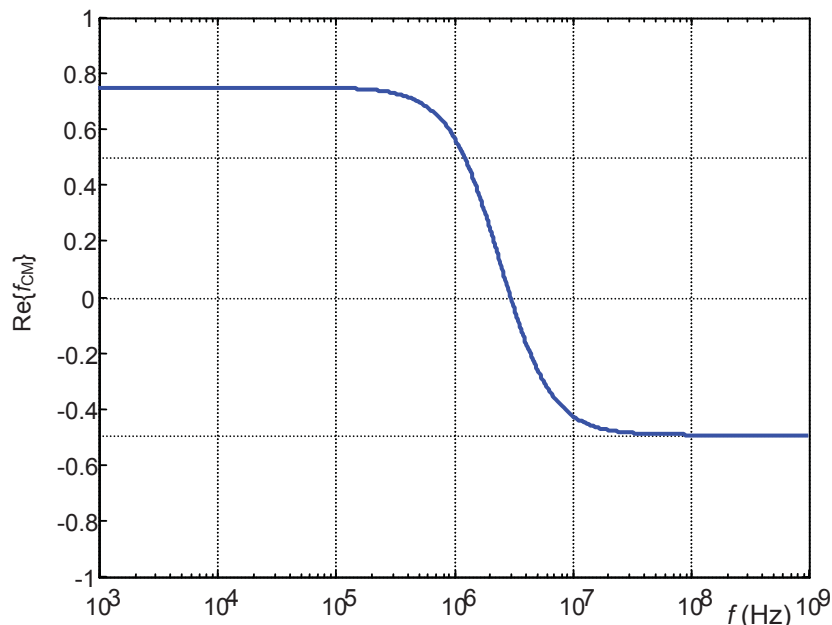

Fig. 3-6 Real component of the frequency dependent Clausius-Mossotti function, Re{f_{CM}}

3.2.4 Maxwell-Wagner polarisation for DNA

Maxwell-Wagner polarisation models for DNA suspensions have been undertaken by a number of researchers, e.g. Grosse (1989) and Saif *et al.* (1991). MW interfacial polarisation models tend to predict high relaxation frequencies in the order of 100's of MHz and therefore appears to be a less successful model for explaining the dielectric behaviour of DNA than it is for bioparticles. This is perhaps because relatively dilute suspensions of DNA exist as worm-like entanglements with a poorly defined interface compared with the well defined spherical or rod-like boundaries of bioparticles (Nagasawa, 1974; Bonincontro *et al.*, 1984; Mandel and Odijk, 1984).

A brief account of MW polarisation is given. The DNA macromolecule is modelled as a long cylindrical insulating core surrounded by a highly conducting 'sheath', immersed in an electrolyte of low conductivity. The model of the DNA is shown in Fig. 3-7; the amino acid, sugar phosphate, double helix that constitutes DNA with a diameter of 2 nm is represented by an insulator (light yellow). The high conductivity sheath (light green) represents the bound counterions on the negatively charged sugar phosphate backbone. The low conductivity electrolyte is shown as light blue medium.
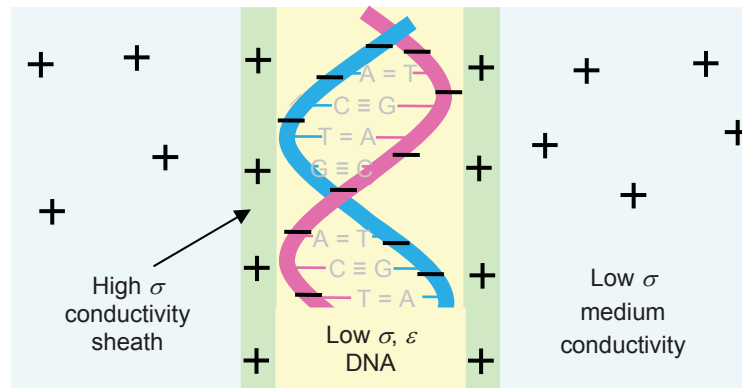

Fig. 3-7 dsDNA as a negatively charged polyelectrolyte in solution attracts positive ions. Counterions form a cylindrical sheath (light green) around the double helix of the DNA

The dielectric decrement for Maxwell-Wagner dispersion for DNA is predicted to be

$$\Delta\varepsilon' \cong 8\varepsilon_m \nu_f / 3\varepsilon_0 \qquad\qquad (3.15)$$

where ε_m is the permittivity of the bulk electrolyte medium and ε_o is the permittivity of free space, Grosse (1989). Similarly, the high frequency relaxation is approximated in terms of the DNA *suspension* conductivity σ_s (or conductivity of the electrolyte medium, σ_m) and fraction of condensed counterions, ϕ_c ,

$$f_R = \sigma_m \phi_c / (4\pi\varepsilon_o \varepsilon_{rm} \nu_f) \qquad\qquad (3.16)$$

where $\sigma_m = (1 - \nu_f)\sigma_s / (1 - \phi_c)$.

Example: using $\sigma_s = 8.5 \times 10^{-3}$ S/m at 25 ^{o}C, $\nu_f = 0.20$ %, $\varepsilon_{rm} = 78.4$ and the fraction of condensed counterions, $\phi_c = 0.25$, equations (3.15) and (3.16) yield $\Delta\varepsilon' \cong 0.42$ and $f_R \cong 162$ MHz.

An alternative approach mimics the rod-shaped DNA macromolecule with conducting sheath by a randomly oriented shelled, prolate ellipsoid with a very short minor axis, and an extremely long major axis (Asami *et al.,* 1980). Again this approach predicts a very high relaxation frequency of hundreds of MHz (Bone *et al.*, 1995). Polarisation due to charge movement along, or across, a poorly defined boundary, such as, a double-layer is probably better explained with the counterion fluctuation model.

3.2.5   Counterion fluctuation polarisation

It is the response of the counterions to an externally applied AC electric field that results in counterion polarisation. Since there is Coulombic attraction between the charged body and the counterion layer, the counterions attempt to pull the charged body along with them as they follow the electric field. The double layer introduced in section 2.3.4 plays a key role in the movement of counterions and there are subtle differences in the two models between bioparticles and DNA, (Eisenberg, 1976).

3.2.6   Counterion fluctuation polarisation for bioparticles

Investigations of the low frequency dispersion of bioparticles have been undertaken by a number of groups, and was given impetus by Schwarz (1962) who derived expressions for the dielectric increment and relaxation frequency for a spherical particle. In the model proposed by Schwarz, the counterions were so strongly attracted to the surface, they could only move along the surface but not perpendicular to it. The effect of the diffuse layer was included in subsequent refinements of the model (Dukhin, 1971; Fixman 1980a; Lyklema *et al.*, 1983; O'Brien, 1986) and accommodated radial and tangential ion movement, Fig. 3-8.
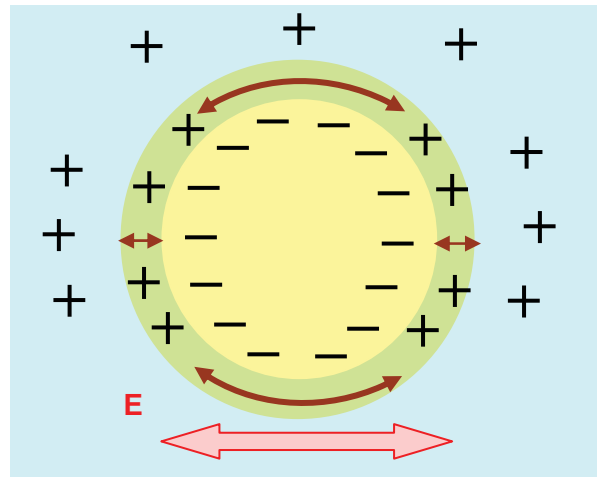
Fig. 3-8 Counterion polarisation: a negatively charged latex bead attracts ions of opposite (positive) charge, or counterions. Application of an AC electric field (red bi-directional arrow) causes charge movement tangential to the surface (brown, curved bi-directional arrows) within the double-layer (light green) surrounding the bead. It also causes radial counterion movement within the double-layer (shown by short, horizontal, brown bi-directional arrows).

There has been much progress in understanding counterion polarisation mechanisms but further investigations are needed to resolve differences between theoretical predictions of dielectric dispersions and experimental data. The dielectric increment and relaxation frequency are predicted by the following formulae that show the influence of the double layer. The thickness of the diffuse

layer, illustrated in Fig. 3-8, is described by the reciprocal of the Debye screening length, given by κ_s (m^{-1}),

$$\kappa_s = \frac{1}{\lambda_D} = \left(\frac{2c_0 N_{Av} z^2 q^2}{\varepsilon_m k_B T} \right)^{0.5} \tag{3.17}$$

where c_o (mol m^{-3}) is the equilibrium concentration of counterions in the medium, N_{Av} is Avogadro constant (6.022×10^{23} mol^{-1}), the electronic charge is $q = 1.602 \times 10^{-19}$ (C), Boltzmann's constant is $k_B = 1.381 \times 10^{-23}$ (JK^{-1}) (Lide, 1994), absolute temperature T is nominally 298 (K), and all other symbols have been previously defined.

Expressions for the static dielectric increment and relaxation time arising from the movement of bound charges are given in works by Lyklema (Lyklema *et al*., 1983 and Lyklema *et al*., 1986),

$$\Delta \varepsilon(0) = \frac{9 r v_f q \rho_b}{4 \varepsilon_o k_B T} \frac{1}{M} \tag{3.18}$$

and

$$\tau = \frac{r^2 q}{2 \mu k_B T} \frac{1}{M} = \frac{r^2}{2 D_b} \frac{1}{M} \tag{3.19}$$

where ρ_b is the bound layer charge density of the sphere, μ (m^2 V^{-1} s^{-1}) is the counterion mobility in the double layer, D_b is diffusion coefficient of bound counterions. The dimensionless factor, M, is

$$M = 1 + \frac{q \rho_b}{k_B T \underbrace{\varepsilon_m \kappa_s \cosh(q \Phi_d / 2 k_B T)}_{C_d}} \tag{3.20}$$

where Φ_d is the diffuse double layer potential, or outer Helmholtz plane potential (Pohl, 1978, p. 275-8, Lyklema *et al*., 1986) and can be approximated by the zeta potential, $\Phi_d \approx \Phi_\zeta$ (Green *et al*., 1997a).

Comment: the effect of the diffuse layer is shown by the reciprocal Debye length, κ_s, in (3.17), and includes in the differential capacitance, C_d, parameter. Thus, the diffuse layer influences both the increment, $\Delta\varepsilon(0)$, and relaxation time, τ, through the dimensionless factor M in equations (3.18) and (3.19). Excluding the effects of the diffuse layer is achieved by allowing $\lambda_D \to 0$ so $M \to 1$ in both equations.

3.2.7   Counterion fluctuation polarisation for DNA

The counterion polarisation mechanism is due to solution counterions (such as Na^+, Mg^{2+}, etc.) interacting with negatively charged phosphate groups along the DNA polyion backbone. The counterions move freely along lengths of DNA in response to the component of the external electric field parallel to the major axis or 'backbone', Fig. 3-9. Their migration results in an induced dipole moment, and hence, an identifiable polarisability. To reiterate: dispersions arise when the oscillating cloud of counterions can no longer follow the alternating electric field (Oosawa, 1971), and this effect is observed in both real and imaginary parts of the complex permittivity.
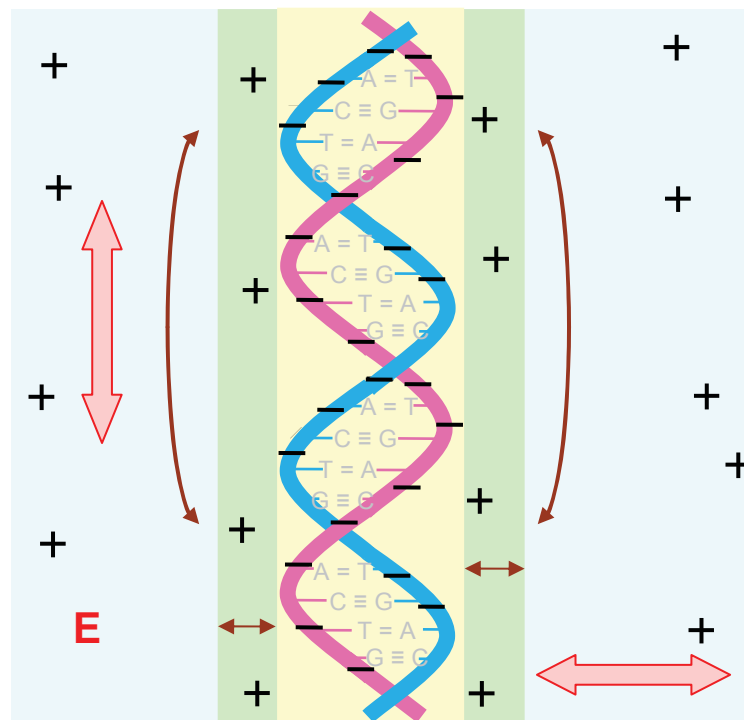

Fig. 3-9 Counterion polarisation on a short segment of DNA: a negatively charged sugar phosphate double helix attracts counterions. Components of an applied AC electric field (red bi-directional arrows) causes counterion movement in the longitudinal direction - along the DNA backbone, and transverse direction (brown bi-directional arrows). The counterion movement tends to be within the 'cylindrical' double-layer (light green).

A popular model of counterion polarisation is the Mandel-Manning-Oosawa model developed in various stages by these authors (Mandel, 1961; Manning, 1969, 1978a, 1978b; Oosawa, 1970). In this model, the counterions move freely along macromolecular "subunit lengths" and are permitted to cross from one subunit to a neighbouring subunit only by overcoming "potential barriers" (van der Touw and Mandel, 1974: Part I, p. 223-4; Mandel, 1977). The *subunit length L_s* is described as the length along the average macromolecular conformation between "breaks", or "potential barriers" resulting from perturbations in the equipotentials (due to conformational processes, folding, etc.), Fig. .   Counterions moving along these *subunit* lengths, under the influence of an external electric field, manifest *high* frequency dispersion – which is of major interest to DEP investigations. The dispersion is also molecular weight independent.

This polarisation scenario contrasts with molecular weight dependent counterion movement along the entire macromolecular contour length that results in *low* frequency dispersion and accounts for the static permittivity (van der Touw and Mandel, 1974: Part II). It is also proposed (Manning 1969, 1978a, 1978b) that a proportion of the counterions are so strongly attracted to the polyelectrolyte that they are said to 'condense' onto the DNA backbone.

Essentially there are three distinct phases: (Saif *et al.*, 1991)

(i) *condensed* counterions – these are sufficiently, but non-locally, bound (or 'delocalised') to the phosphate groups of the DNA, and thereby neutralise a fraction of the DNA charge.

(ii) *diffuse* counterions which are responsible for neutralising the remainder of the DNA charge, with a density which decreases exponentially with distance from the axis.

(iii) *bulk* ions or 'added salt' ordinary aqueous solution ions.
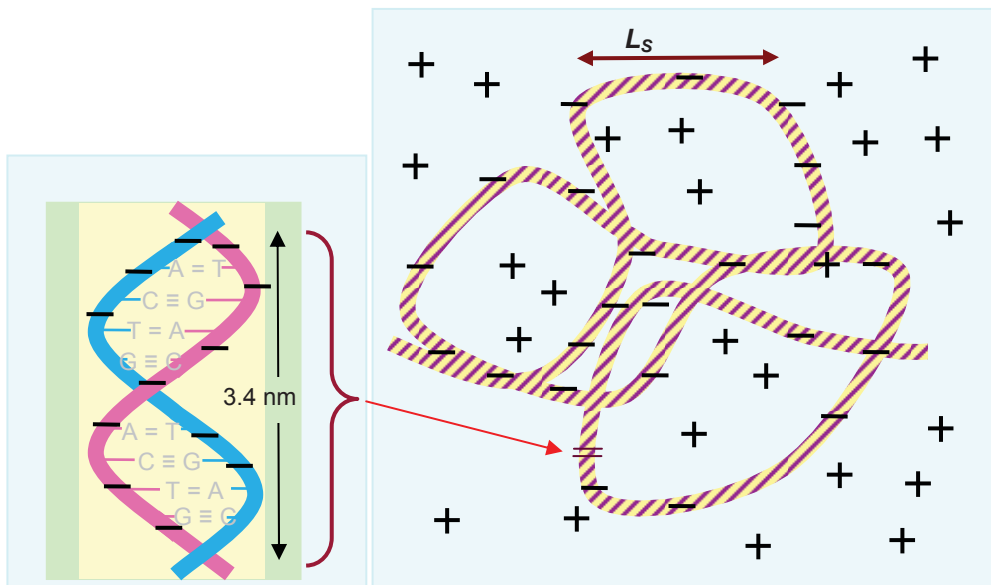
Fig. 3-10 Worm-like chain model (and close-up) of dsDNA with double-layer is divided into sub-unit lengths, L_S, based on the distance between equipotentials. Not to scale.

In terms of their contribution to polarisability, the condensed counterion phase is the most important. A feature of the condensed state is that the local concentration of counterions around the DNA does not tend to zero when the bulk electrolyte concentration does (Anderson and Record, 1982). Condensation occurs when the condition $\xi \geq 1/|z|$ is satisfied (Manning, 1978a; Bone and Small, 1995) where z is the valence of each counterion and the charge density parameter, ξ, is given by

$$\xi = q^2 / 4\pi\varepsilon_m k_B Tb \tag{3.21}$$

47

where b is the average distance between charged sites, and for the B-DNA double helix, $b = 1.73$ Å. The fraction of condensed counterions is ϕ_c

$$\phi_c = 1 - \left|z^{-1}\right|\left|\xi^{-1}\right| = 1 - 4\pi\varepsilon_m k_B T b / q^2 |z| \tag{3.22}$$

Example: using $\varepsilon_m = 78.4\varepsilon_o$ and $z = 1.00$, the charge density parameter at 25°C is evaluated to be $\xi = 4.132$, and hence for monovalent cations, $\phi_c = 0.7580 \cong 0.76$.

The 'Manning-Mandel-Oosawa' model yields a generalised expression for scalar longitudinal polarisability α_s per subunit length L_s,

$$\alpha_s = \frac{z^2 q^2 L_s^2 n_{cc} A_{st}}{12 k_B T} \tag{3.23}$$

where n_{cc} is the number of condensed counterions that can be predicted theoretically (Manning, 1978a; Bone and Small, 1995),

$$n_{cc} = \phi_c L_s / |z| b \tag{3.24}$$

A_{st} is the stability factor of the ionic phase and includes mutual repulsion between fixed charges on the backbone and the effect of Debye screening,

$$A_{st} = [1 - 2(|z|\xi - 1)\ln(\kappa_s b)]^{-1}$$ (3.25)

and the reciprocal Debye screening length κ_s^{-1} (m) is given by Penafiel and Litovitz (1992)

$$\kappa_s = \left[\left(\frac{N_{Av} 4\pi q^2}{4\pi\varepsilon_m k_B T} \right) \left(\sum_i C_i z^2 + \frac{C_p}{\xi} \right) \right]^{0.5}$$ (3.26)

where and C_i and C_p are the molar concentrations of ions in the bulk and diffuse phase, and phosphate groups, respectively.

Combining equations (3.21) to (3.26), (3.23) can be rewritten

$$\alpha_s = \frac{\pi \varepsilon_o \varepsilon_{rm} L_s^3 A_{st}(|z|\xi - 1)}{3}$$ (3.27)

Equating the predicted α_s for counterion fluctuation (3.27) with α_s determined using the experimentally measured dielectric decrement $\Delta\varepsilon'$

$$\alpha_s = \frac{3\varepsilon_o \Delta\varepsilon'}{C_s} = \frac{3\varepsilon_o \Delta\varepsilon'}{N_{Av} C_p (b/L_s)}$$ (3.28)

yields an expression for L_s,

$$L_s = \sqrt{\frac{9\Delta\varepsilon'}{\pi\varepsilon_{rm}(|z|\xi - 1)A_{st} N_{Av} C_p b}}$$ (3.29)

This is the general expression for the subunit length based on the dielectric decrement $\Delta\varepsilon'$. The polarisability can be also derived an expression for the relaxation time Mandel (1961)

$$\tau = \frac{L_s^2 q}{\pi^2 \mu k_B T}$$ (3.30)

Comment: comparing (3.17) with (3.26) for bioparticles (excluding the phosphate ions), and (3.19) with (3.30), the algebraic form of the expressions for κ_s and τ are similar.

Example calculation: Selecting the temperature, $T = 298.2$ K (25.0 °C) and using $C_p = 2.72$ mol/m³, $C_i = 1.10$ mol/m³ and previous values for the other parameters, (3.21), (3.25) and (3.26) simplify, $\xi\big|_{25\,°C} = 4.132$, $\kappa_s\big|_{25\,°C} = 9.754 \times 10^7$ and $A_{st}\big|_{25\,°C} = 3.764 \times 10^{-2} \cong 0.038$ Thus, at 25.0°C (3.29) simplifies,

$$L_s = 3.308 \times 10^{-8} \sqrt{\Delta\varepsilon'} \tag{3.31}$$

Selecting again 25°C temperature, and assuming the mobility value $\mu = 8.00 \times 10^{-8}$, (3.30) simplifies,

$$L_s = 1.424 \times 10^{-4} \sqrt{\tau} \tag{3.2}$$

> *Question*: Suppose a sample of dsDNA is found to have dispersion with $\Delta\varepsilon' = 9$ and a relaxation time $\tau = 500$ ns. What are the predicted subunit lengths?
>
> *Answer*: Equation (3.31) gives $L_s = 100$ nm and (3.32) gives $L_s = 101$ nm. Physically, this is is very close to the worm-like chain Kuhn length for dsDNA. In the framework of the counterion model, the result would support the notion that equipotentials arise from natural curvature of the dsDNA suspended in solution.

3.2.8   Other polarisation mechanisms

A variety of other polarisation mechanisms include counterion polarisation transverse to the DNA axis (Xammara Oro and Grigera, 1984), rotation of water bound molecules along and across the grooves of the DNA (Mashimo *et al.,* 1989) and relaxation of DNA polar groups (Takashima *et al.,* 1984) - although some re-interpretations of the latter have favoured the "bound water" molecule approach (Takashima *et al.,* 1986).   These polarisation mechanisms tend to predict very high frequency dispersions of the order of 100's of MHz. Also the relaxation times have temperature dependence that predicts much high activation energies than measured.   Consequently they have received less significance in the literature (Bone and Small, 1995).

3.3 Micro-environments for biomolecule transport

Micro-environments can be either naturally evolved (e.g. the interior cytoplasm of cell, cell membrane pumps) or artificial (e.g. made using photolithographic techniques).   It is the latter of focus in this e-book and photolithographic techniques have been advanced for making semiconductor electronic devices (Pacansky and Lyerla, 1979).   An example use of biomolecule transport lies in separation of biomolecules based on their size, dielectric constants, etc.
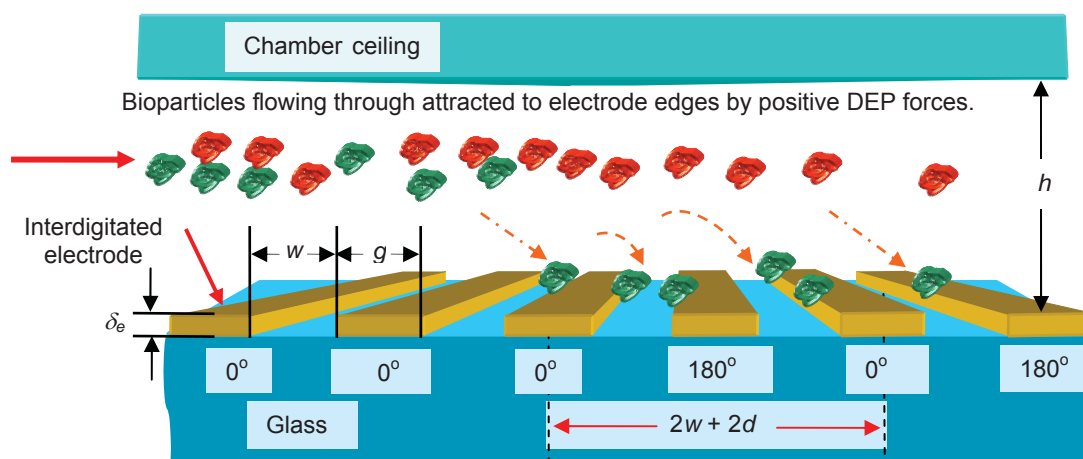
Fig. 3-11 Diagram flow-through DEP collection experiment (using interdigitated electrodes fabricated on glass with width *w*, interelectrode space *g*, and thickness δ_e) *not* to scale.

A chromatography microdevice is shown in Fig. 3-11 where red and green bioparticles are introduced on the left; the green are attracted to the planar electrode array by DEP forces generated by nonuniform field flux stemming from the array, whereas the red pass through.   The array is energized with AC signals with phases as shown.   Note that the first three electrodes on the left have the same phase so that there is little electric field flux created by them and so little DEP. Elsewhere the 180$^\text{o}$ phases difference gives rise to a nonuniform electric fields and hence, positive DEP (pDEP).   Details of the electric fields are given in Chapter 5.   Electrode widths, *w*, and inter-electrode gaps, *g*, can vary considerably.   Those on the order of 10 microns (μm) are capable of

generating fields of 10^6 V/m using low signal amplitudes of 10's of volts. This is sufficient to create DEP forces for technological application.

The four main steps involved with standard photolithographic fabrication of the gold electrode array are described and illustrated in Fig. 3-12: resist (polymer) exposure, resist development, metal evaporation and lift-off. The reason for using a titanium (Ti) under-layer of the gold (Au) is that it does not adhere to glass very well; so Ti acts to bond the Au to the glass.
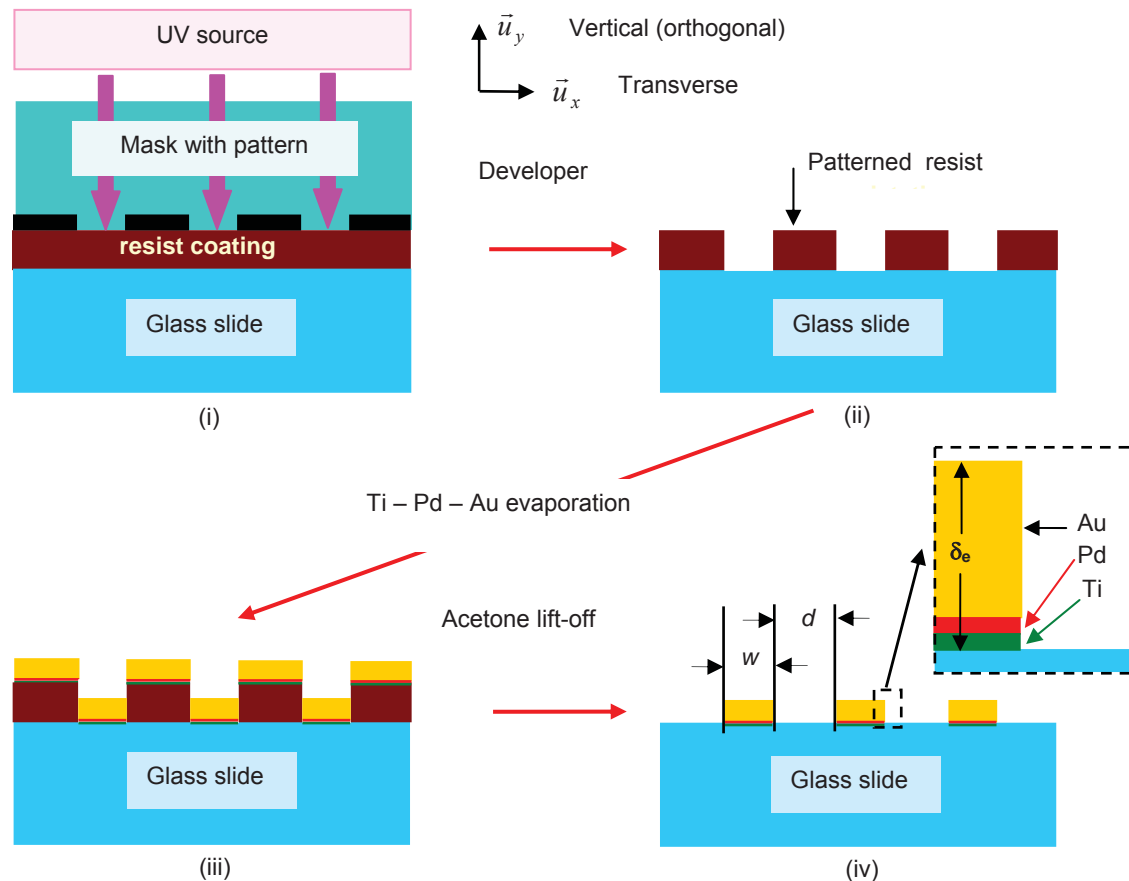
Fig. 3-12 Key steps in electrode micro-fabrication (cross-section or transverse plane view): (i) UV pattern exposure through mask onto resist coated glass microscope slide, (ii) application of developer removes irradiated (positive) resist, (iii) Ti – Pd – Au consecutively evaporated on to patterned resist/slide, and (iv) application of acetone lifts off metal layers leaving electrodes firmly bonded onto glass. Drawn *not* to scale

3.4 Concluding remarks

Biomolecule transport in water using electric fields has been discussed in this chapter with the focus on movement on nonuniform electric fields called dielectrophoresis (DEP). DEP operates whether or not the biomolecule is electrically neutral or charged. The electric field can be said to

52

act twice: first, to induce a dipole, and second to interact on that dipole in an uneven way so as to cause movement.

Inducable polarisability is fundamental to DEP and two key dielectric polarization mechanisms apply for motion in nonuniform fields. The two mechanisms are Maxwell-Wagner interfacial polarization and counterion polarisation. Interfacial polarisation arises from electric charge accumulation at well defined interfaces whereas counterion ploarisation arises from a condensed sheath of ions along the major axes of biomolecules, surrounded by a more diffuse layer. The counterions attempt to move in accordance with the externally applied electric field and since they are also hydrodynamically coupled to the biomolecule by Coulombic attraction, also drag the biomolecule. Micro-environments for creating electric fields use standard photolithographic techniques pioneered by semiconductor technology.

4 Basic micro- and nano-transport

There are a number of computational approaches for predicting the transport of biomolecules in water and other fluids, such as, air. The most straightforward method to model the transport of biomolecules in low to moderate concentrated suspensions is to consider the biomolecules as spherical or oblate spheroids and assume that they do not interact. Most are not spheres or even rods. DNA and double stranded RNA, for example, are considered as a freely jointed chain with straight segments corresponding to twice the persistence length (100 nm for double stranded DNA). The motion of each bioparticle is governed by four kinds of Newtonian force: inertial, external, friction and thermal.

4.1 Inertial, friction and sedimentation forces on single biomolecules

As an initial approximation, it is reasonable to introduce the concept of a *bioparticle* as a sphere with effective hydrodynamic radius r moving through a fluid. The inertial force is given by product of bioparticle mass m and acceleration,

$$F_{Inert}(x,t) = m\frac{d^2x}{dt^2}$$

(4.1)

The mass of a bioparticle with radius r (and volume V) is values of its density $\rho_p = 1.05$ g/cm^3 = 1.05×10^3 kg/m^3.

A bioparticle moving though a liquid medium with velocity v experiences Stokes' drag, or friction, force F_{Drag}, in a direction opposite to its movement,

$$F_{Drag} = -\zeta v = -\zeta\, dx/dt$$

(4.2)

where ζ (kg s^{-1}) is the friction, or Stokes' drag, coefficient. The friction coefficient for a sphere is

$$\zeta = 6\pi\eta\, r$$

(4.3)

where the dynamic viscosity, η (kg m^{-1} s^{-1}) for evaluating viscous drag. A consequence of the biomolecular density being near water is that the inertial force is small compared with viscous drag and the acceleration is quickly dampened to terminal velocity. The ratio m/ζ is an important parameter for understanding how quickly a bioparticle approaches, or 'relaxes' to, steady state terminal velocity. For a simple sphere, the relaxation time τ (s)

$$\tau = m/\zeta = \rho V/\zeta = \rho 4\pi r^3/(18\pi\eta r) = 2\rho r^2/(9\eta)$$

(4.4)

The relaxation time for a 200 nm bioparticle will be about a nanosecond, $\tau = 1$ ns. Biomolecules in their native environment (i.e. at standard temperature and pressure), being organic, have a density that varies but is generally on a par with surrounding water. Biomolecules do not sink in water as quickly as metals do or resurface like air; unless moved by external forces, they tend remain evenly suspended in water for quite long periods.

The force due to gravity F_g, acting in the vertical direction (adopting the convention upwards as positive), can be written as the product of bioparticle mass m and gravitational acceleration g (that is assumed to have a constant value, $g = 9.8$ m s^{-2}),

$$F_g = -mg = -\rho_p V g$$

(4.5)

The bioparticle mass m, in turn, can be expressed as the density ρ_p and volume of the bioparticle, V.

The fluid displaced by the bioparticle, exerts an buoyancy force (upwards),

$$F_b = \rho_m V g$$

(4.6)

where ρ_m is the density of fluid medium (1.00×10^3 kg/m^3). Both gravitational and buoyancy forces can be combined into a sedimentation force that is constant,

$$F_{Const} = F_b + F_g = (\rho_m - \rho_p)V g$$

(4.7)

The constant force due to gravity and buoyancy, for example, on a 216 nm diameter spherical polystyrene bioparticle with $\rho_p = 1.05 \times 10^3$ kg/m^3 submerged in water $\rho_m = 1.00 \times 10^3$ kg/m^3 is, $F_{Const} \cong -2.6 \times 10^{-18}$ (N). The minus sign indicates the direction of the net force is downwards.

A centrifuge is an example of standard laboratory equipment that can be viewed as creating a large inertial 'fictitious' force arising from high speed rotary motion. It results in sufficiently high bioparticle terminal velocities so that suspensions of biomolecules can be separated from water in minutes. Combining (4.2) and (4.7) and replacing g by the angular acceleration $\dot{\theta}^2 R$ gives

$$\zeta \frac{dR}{dt} = (\rho_m - \rho_p)V \dot{\theta}^2 R$$

(4.8)

where R is the circular path radius and $\dot{\theta}$ is the angular velocity (rads/s).

4.2 Electromagnetic forces acting on single biomolecules

The constituents of biomolecules, such as nucleic acids, proteins, lipids, and fats mean often they are susceptible to electromagnetic (EM) forces. The influence on the biomolecule of the externally applied electric and magnetic components of EM radiation is discussed separately.

4.2.1 Electric fields and electrophoresis

Electric fields are generated often by applying electrical potentials to electrodes immersed in electrolyte solution. Dissociated ions mean there are there are free charges in solution and subsequently a considerable amount of electrostatic screening. In the general case the potential, Φ, is solved from Poisson's equation

$$\nabla^2 \Phi = -\frac{\rho}{\varepsilon_0} \qquad\qquad (4.9)$$

where ρ is the free charge density and the del operator is $\dfrac{\partial^2}{\partial x^2} + \dfrac{\partial^2}{\partial y^2} + \dfrac{\partial^2}{\partial z^2}$. For a rapidly oscillating AC electric field, equation (4.9) is solved by applying the quasi-static approximation that effectively decouples space and time so that the problem becomes similar to the DC case. The location of the screened free charges mean that Poisson's equation is complex to model so to a first

approximation the screened free charge is assumed to be practically negligible. Hence, Poisson's equation is replaced by Laplace's equation,

$$\nabla^2 \Phi = 0 \qquad (4.10)$$

The electric field is found from

$$\vec{E} = -\vec{\nabla}\Phi \qquad (4.11)$$

where $\rightarrow$ denotes vector quantity and $\vec{\nabla}$ is the gradient operator,

$$\vec{\nabla} = \vec{u}_x \frac{\partial}{\partial x} + \vec{u}_y \frac{\partial}{\partial y} + \vec{u}_z \frac{\partial}{\partial z} \equiv \vec{u}_x \partial_x + \vec{u}_y \partial_y + \vec{u}_z \partial_y \qquad (4.12)$$

The last term in (4.12) introduces a slightly more compact notation for partial derivatives. Poisson's and Laplace's equations are solved by applying Boundary Conditions (BCs) for the potential and the electric field. There are two types of BCs, Dirichlet and Neumann, and these are described with examples in the next chapter.

As discussed in previous chapters many biomolecules, such nucleic acids or proteins, are responsive to electric fields and laboratory *electrophoresis* equipment used today testifies to this property. It is a technique commonly used to separate biomolecules according to charge, and the *electrophoretic* (EP) force was expressed in equation (3.1). It is easily generalised to 3D and to include time,

$$\vec{F}_{EP}(\underline{x},t) = \mu\,\zeta\,\vec{E}(\underline{x},t) \qquad (4.13)$$

where $\underline{x} \equiv (x,y,z)$ and all other symbols are as previously defined. If the electric field is very slowly oscillating (0 – 10 Hz), the then the biomolecule or bioparticle moves in accordance with the field. Applying safe voltages across between the two wire electrodes immersed in a droplet of water (less than 30V, preferably platinum) a simple experiment can be set-up to show a sample of bioparticles oscillating in the suspension. Note that bubbles arising electrolysis at the wires need to be channeled to avoid interference. As the frequency is increased beyond 100 Hz, the bioparticles have less time to move with the field and eventually their movement is barely detectable. Mathematically, one can say that their small-time average is zero.

4.2.2 Inhomogenous electric fields and dielectrophoresis

As discussed in Chapter 3, using DC signals can cause problematic hydrolysis. Consequently, using more applicable AC signals, the small-time averaged DEP force is just half the DC value (shown next page)

The non-maths oriented reader can skip this page and go onto the next.

The simple case represented by equation (3.3) is generalised to a 3D case in a time varying electric field. The DEP force acting on a small neutral bioparticle at position $\underline{x} = (x, y, z)$ and time t approximated to first order is

$$\vec{F}_{DEP}(\underline{x}, t) = (\vec{p}(\underline{x}, t) \cdot \vec{\nabla}) \vec{E}(\underline{x}, t) \tag{4.14}$$

E is the externally applied electric field (peak value), and the symbol $\bullet$ denotes inner product. The generalised induced dipole moment, $\vec{p}$, for the case where the dielectric bioparticle of volume V, is homogeneously, linearly and isotropically polarisable, is

$$\vec{p}(\underline{x}, t) = \alpha V \vec{E}(\underline{x}, t) \tag{4.1}$$

As described in Chapters 2 and 3, the induced polarisability, α, or effective dipole moment per unit volume in unit electric field has dimensions Farad per metre (Fm^{-1}). It is assumed, for the force to be proportional to the gradient of E in (4.15), that the dimension of the dipole p is small compared with the characteristic length of the electric field non-uniformity. Any spatial electric field phase variation is considered to be negligible.

As in the 1D case in Chapter 3, our interest lies in the in-phase component of the DEP force since the experiments supply electrodes with potentials of 180° phase difference. The polarisability is considered to be a real, scalar, quantity. Writing the electric field is written in terms of angular frequency ω and arbitrary phase, θ,

$$\vec{E}(\underline{x}, t) = \vec{E}(\underline{x}) \cos(\omega t + \theta) \tag{4.2}$$

The effects of magnetism in the entire system - bioparticle, medium, and electrodes - can be ignored. Hence, the magnetic field vector, $\vec{B} = 0$, and the differential form of Faraday's Law simplifies, $\Rightarrow \vec{\nabla} \times \vec{E} = 0$ where '$\times$' denotes outer or cross product. Combining (4.14) to (4.16),

$$\vec{F}_{DEP}(\underline{x}, t) = \frac{1}{2} \alpha V \vec{\nabla} |\vec{E}(\underline{x})|^2 \cos^2(\omega t + \theta) = \underbrace{\frac{1}{4} \alpha V \vec{\nabla} |\vec{E}(\underline{x})|^2}_{\vec{F}_{DEP}(\underline{x})} (1 + \cos(2\omega t + 2\theta)) \tag{4.17}$$
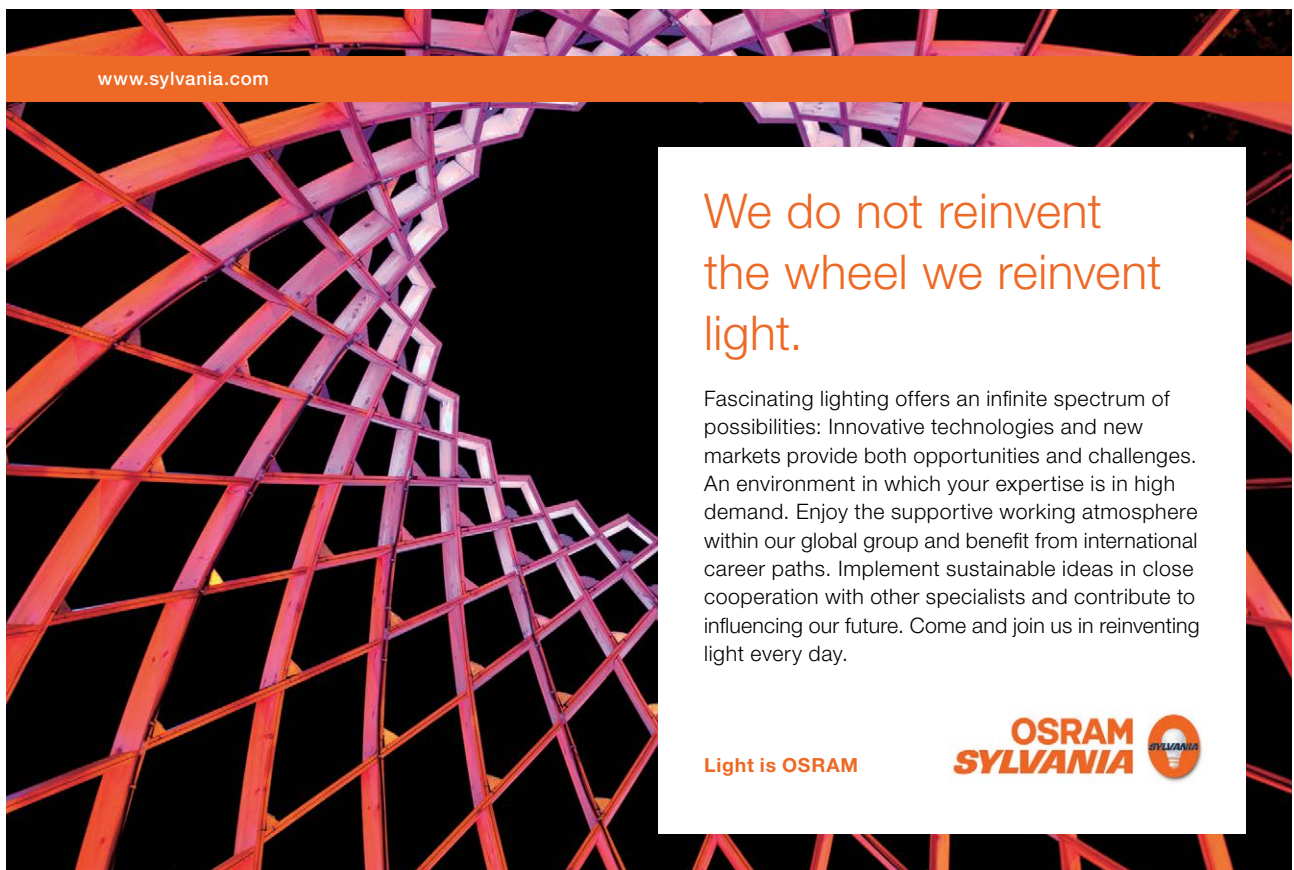
The spatial component of the DEP force is segregated from the time varying part, and is labelled as shown. In practice, for electric field frequencies above 20 kHz, the contribution of the co-sinusoidal oscillatory term to the motion of the bioparticle is negligible. Thus, the force is given in

terms of a 'small-time' average, denoted by $\langle \ \ \rangle_t$, over an oscillation period. Equation (4.17) simplifies

$$\left\langle \vec{F}_{DEP}(\underline{x},t)\right\rangle_t = \vec{F}_{DEP}(\underline{x}) = \frac{1}{4}\alpha V\vec{\nabla}\left|\vec{E}(\underline{x})\right|^2 = \frac{1}{2}\alpha V\vec{\nabla}\left|\vec{E}_{rms}(\underline{x})\right|^2$$

(4.18)

and can be expressed in terms of the electric field root-mean-square (rms), E_{rms}. The DEP force is understood to be 'almost instantaneous'. Repeating some of the keys points in previous chapters, equation (4.18) underlines important properties of DEP,

- the direction of the force is *invariant* to the electric field direction (or sign of the electrode potentials)

- AC signals can be used rather than DC signals that tend to cause hydrolysis

- the frequency dependent polarisability is a governing parameter of the magnitude and direction of the DEP force

- the frequency dependent polarisability α can in many instances be calculated or measured from dielectric spectroscopy as shown in the previous chapter.

4.2.3 Electroosmosis

Electroosmosis (EO) arises from an electric field being applied that is tangential to a surface where there is a double layer, described in section 2.3.4. The electric field acts on the charges in the double layer causing them to move. In this way the surface of electrodes, for example, with an electrical potential difference between them and immersed in an electrolyte will be surrounded by double layers that provide a source of electroosmotic flow. The double layer around an electrode surface will be similar manner to the surface of a bioparticle illustrated in Fig. 2-7.

There are two types of EO: DC and AC. DC EO is well known and finding application in microfluidics. The EO fluid velocity is proportional to the electric field and can be predicted using an electroosmotic mobility relation in a similar manner to EP. AC is less well-known at present but important in non-uniform electric fields (Morgan and Green, 2003). Like DEP AC EO does not arise in a uniform electric field because the small-time averaged movement would be zero – as it is for electrophoresis. Instead it arises in a non-uniform electric field because there is time averaged movement.

To understand this mechanism, consider an AC electric voltage applied to an electrode. At an instant in time during the cycle (electrode is say, positive) a double layer of counterions (predominantly negative) will form. A tangential electric field generated by the electrode will act on the negative double layer charges surrounding the surface by Coulombic forces and the charges will move. Conversely, during the part of the cycle when the electrode is *negative*, a *positive* counterion double layer will form and the direction of the tangential electric field will be *opposite* compared with before. Therefore, the Coulombic forces on the charges will be in the *same* direction. It can be said that, like DEP, there is a 'double action': the electric field sets up the double layer then acts on it, so small time-averaged flow results.

4.2.4 Magnetic fields

Biomolecules are not usually susceptible to magnetic fields, unless they are exceedingly strong. Again standard laboratory equipment demonstrates this property. A magnetic stirrer consists of a beaker with a magnetic stirring element at the bottom. Motion is transferred to the element from the base plate by a rotating magnetic field. The magnetic stirring element is able to do its job because it transfers only viscous forces to suspensions, and the magnetism does not attract biomolecules. Magnetic forces can be used, however, if the biomolecules are attached to para-magnetic nanospheres or other tiny biocompatible magnetically susceptible particles. This is the basis for a number of new laboratory techniques and has been facilitated by the emergence new high-magnetic flux materials.

Conceptually, magnetophoresis (MAP) is the 'magnetic equivalent' of dielectrophoresis (i.e. not electrophoresis). The relations developed in the preceding section can be easily converted for MAP. Unfortunately, in practice MAP is more difficult to currently achieve for micro-device applications as illustrated in Fig. 1-2 due to complexity of fabricating micro-coils. Developments may change this situation; for the time being our interest lies more in DEP than MAP.

4.3 Thermal fluctuations

Nano-sized bioparticles in a liquid medium, at room temperature, incur incessant collisions from neighbouring molecules. The collisions of the thermally agitated molecules with each bioparticle, are random in direction and time, and cause the bioparticle to move in a haphazard way. This random movement is called Brownian motion, named after the botanist, Robert Brown, who in 1827 observed the irregular motion of pollen grains suspended in water (Gardiner, 1985).

To fully describe the irregular motion of the nano-scale bioparticle would require knowledge about the motion of all the colliding molecules. This is practically impossible, therefore the motion of the bioparticle is described probabilistically. At least two assumptions have been made about the nature of this probabilistic movement (Einstein, 1905):

- the movement of each bioparticle is *independent* of the movement of all other bioparticles,

- the movements of a particular bioparticle in successive time intervals are *independent* processes, as long as the time intervals are chosen 'not too small'.

There have been many experimental and theoretical studies of Brownian motion that indicate the two assumptions are essentially correct provided the suspension of bioparticles is dilute. The force exerted on the nano-scale bioparticle, from each thermal collision (Gardiner, 1985) is

$$F_{Therm}(t) = \sqrt{2\zeta\, k_B T}\, \xi(t)$$

(4.19)

where all symbols have been previously defined and the collisions are assumed to be spatially invariant, hence $F_{Therm}(t)$ is written without x dependence. The statistical term, $\xi(t)$, is called a *random variable* (RV) that describes the time of the 'impact' (Papoulis, 1984).

The idea of a RV may seem foreign to some readers but it is helpful to think of examples in daily life. Examples include the side of a coin, that shows heads or tails; or the sides of a dice that reveals numbers, 1, …, 6. The RV has units of time in seconds ($s^{-1/2}$) which may also appear strange to readers; the dimensions of F_{Therm} are easily confirmed to be Newtons (N). The impact of the nth bioparticle, out of a population of N, is written as, $\xi_n(t)$. The first important property is that it has a population (or ensemble) average, or mean, of zero.

The not-so-maths keen reader can skip this page and go to the next page at the next check-box

---

61

$$\langle \xi(t) \rangle = \lim_{N \to \infty} \left\{ \frac{1}{N} \sum_{n=1}^{N} \xi_n(t) \right\}$$

$$\cong \frac{1}{N} \sum_{n=1}^{N} \xi_n(t) = \sum_n \xi_n(t) = 0$$

(4.20)

On the second line of the above equation N is assumed to be sufficiently large and the middle term is convenient short-hand notation. Physically, this means that the total force for a population of bioparticles is zero, $\langle F_{Therm}(t) \rangle = 0$. A consequence of this that the 'centroid' of Brownian thermal motion that drives diffusion remains motionless, $\langle x(t) \rangle = 0$. This is observed experimentally and is often seen in a lab cup of tea or coffee when milk is dropped in (assuming no convection or stirring)!

The second parameter is the autocorrelation,

$$\langle \xi(t')\xi(t) \rangle = \sum_i \sum_j \xi(t_i')\xi(t_j) = \delta(t' - t)$$

(4.21)

where $\delta(t' - t)$ is the Dirac delta function (or functional) and can be defined (Haken, 1978)

$$\int_{t_0 - \varepsilon}^{t_0 + \varepsilon} \delta(t - t_0)\, dt = 1 \text{ for any } \varepsilon > 0$$

and

$$\delta(t - t_0) = 0 \text{ for } t \neq t_0$$

(4.22)

This says that the peak of the delta function at $t = t_0$ can be any value provided the area under it remains unity. As the peak approaches infinity, it becomes infinitesimally narrow. Elsewhere, $t \neq t_0$ the function is zero. The mathematics dealing with delta functions is not trivial. A simple and important result is obtained by integrating the velocity with respect to time, the variance of displacement can be found

$$\text{var}\{x(t)\} = \left\langle \left[x(t) - \langle x(t) \rangle \right]^2 \right\rangle = \left\langle x(t)^2 \right\rangle = 2k_B T(t - t_1)/\zeta = 2Dt$$

(4.23)

where the diffusion process is assumed to start at $t_1 = 0$ and D is the Einstein diffusion coefficient.

The relationship $<x(t)^2> = 2Dt$ or writing $<x(t)^2> = l^2$ in terms of characteristic length l of a micro-device chamber gives a simple law

$$t_{diff} \propto l^2 \qquad (4.24)$$

and has important implications for transport processes where *diffusion* is dominant (diffusion limited). For example, reducing length l by a factor of 10 results in time reduction of 100. The equation says that the effect of entirely randomizing the transport of bioparticles by *stochastic* thermal motion makes the average transport time dependent on the square of the length.

This contrasts with controlled or *deterministic* unidirectional motion where the time duration between start and end points is linearly proportional to the length traversed, i.e. $t \propto l$.

4.4 Combining forces for predicting single bioparticle trajectory

Applying the Second Law of Motion, the inertial force on a bioparticle is expressed as the sum of external, friction and thermal forces,

$$F_{Inert}(x,t) = F_{Ext}(x,t) + F_{Drag}(x,t) + F_{Therm}(t)$$

(4.25)

where the external force is sum of deterministic components

$$F_{Ext}(x,t) = F_{DEP}(x,t) + F_{EP}(x,t) + F_{Const}$$

(4.26)

4.5 Langevin equation for a single bioparticle (biomolecule)

Substituting (4.1) and (4.2) into (4.25) yields a second order stochastic differential equation (SDE),

$$m\frac{d^2x}{dt^2} = F_{Ext}(x,t) - \zeta\frac{dx}{dt} + F_{Therm}(t)$$

(4.27)

Equation (4.27) can solved by partitioning into two equations,

$$\frac{dx}{dt} = v$$

$$m\frac{dv}{dt} = F_{Ext}(x,t) - \zeta v + F_{Therm}(t)$$

(4.28)

and use adiabatic elimination methods that allow the fast variable $v = dx/dt$ to be controlled, or 'slaved', to the slow variable x (Haken, 1983). The second equation then becomes a first order SDE and is solved for the bioparticle velocity, v. An alternative, approximate approach is to recognise the bioparticle mass m is very small, so the inertial force term in (4.28) can be neglected, and the left hand side (*lhs*) is set to zero. This yields the *Langevin equation*,

$$v(x,t) = \frac{dx}{dt} = \underbrace{\frac{F_{Ext}(x)}{\zeta}}_{\text{deterministic}} + \underbrace{\sqrt{\frac{2k_BT}{\zeta}}\,\xi(t)}_{\text{stochastic}}$$

(4.29)

In the case where the electric field is AC and given by (4.16), combining (4.13), (4.17), and (4.26) with (4.29) yields

$$v(x,t) = \frac{F_{DEP}(x)}{\zeta}[1 + \cos(2\omega t + 2\theta)] + \frac{F_{EP}(x)\cos(\omega t + \theta)}{\zeta} + \frac{F_{Const}}{\zeta} + \sqrt{\frac{2k_BT}{\zeta}}\xi(t)$$

(4.30)

64

Integration of (4.30) over a small-time period yields displacements the excursions of the oscillatory electrophoretic and AC component of the DEP forces can be ignored for radio frequencies above 20 kHz. Thus, (4.30) can be simplified to the Langevin equation for moderate to high radio frequencies

$$\frac{dx}{dt} = \underbrace{\frac{F_{DEP}(x) + F_{Const}}{\zeta}}_{\text{deterministic}} + \underbrace{\sqrt{\frac{2k_BT}{\zeta}}\,\xi(t)}_{\text{stochastic}} \tag{4.31}$$

4.6 Langevin equation stochastic integration and the modified diffusion equation (MDE)

To describe the behaviour of a population of bioparticles, an ensemble average of (4.31) is taken – similar to equation (4.20),
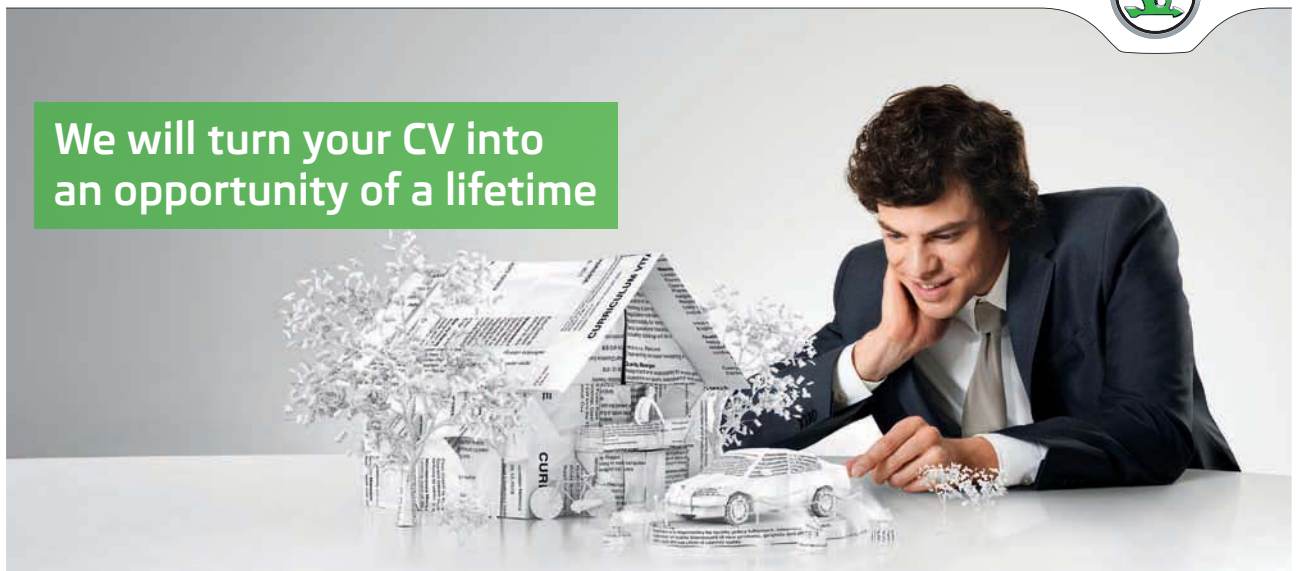
$$\langle v \rangle = \frac{1}{\zeta}[F_{DEP}(x) + F_{Const} + \sqrt{2k_BT\zeta}\,\langle \xi(t) \rangle] = \frac{1}{\zeta}[F_{DEP}(x) + F_{Const}] \tag{4.32}$$

Equation (4.32) says that the mean velocity is given by the DEP and constant forces (usually fluidic drift). To determine spread of the particles requires either numerical, stochastic algebraic integration of the Langevin equation (4.29) or other approaches (Haken, 1978). Stochastic integration is beyond the scope of this book. Therefore, the result is simply given and it is called the *Fokker-Planck equation* (FPE), also Smoluchowski, Kolmogorov, modified diffusion equation (MDE), or continuity equation (van Holde, 1971; Risken, 1989; Doi and Edwards, 1986; Gardiner, 1985). The latter title is not surprising since the expression can be developed from continuity considerations in a similar manner as Fick's Second Law (Hiemenz, 1986), so the mathematical structure form can be verified.

The bioparticle position, as the dependent variable in (4.28), is replaced by the spatial-temporal probability density $p(x, t)$ of an ensemble (or population) of particles. By definition for a 1D system,

$$\int_a^b p(x,t)dy = 1 \ \forall \ t, \ p(x,t) \geq 0 \tag{4.33}$$

The concept of probability density may sound rather strange to some readers but it becomes much more tangible when probability density is related to bioparticle concentration $c(x, t)$, simply by the total number of particles in the system, N. The probability density has the same units as concentration, and for a 1D system (m^{-1}).

The 'chances' of finding a particle at a position, x, and moment, t, is

$$p(x,t) = c(x,t)/N \tag{4.34}$$

The evolution of probability density (or concentration) over time therefore is written

$$\frac{\partial p}{\partial t} = -\frac{\partial(pv)}{\partial x} + \frac{k_B T}{\zeta} \frac{\partial^2 p}{\partial x^2} = -\frac{\partial}{\partial x}\left(pv - D\frac{\partial p}{\partial x} \right) = -\frac{\partial J(x,t)}{\partial x} \tag{4.35}$$

where the diffusion coefficient is $D = k_B T/\zeta$ and it is understood $p = p(x, t)$ and $v = v_{dtm}(x)$ is deterministic. It is also useful to render the equation in terms of the "probability flux", $J(x, t)$.

Again the notion of "probability flux" may be odd to some readers. A simple way of thinking about it, leaving diffusion aside for the moment, in a 1D system it is the number of bioparticles passing by a point per unit time (or bioparticle flux) divided by the total number of bioparticles

$$J = cv/N \tag{4.36}$$

with units (s^{-1}). Why use probability? One pragmatic reason is that it's convenient and easy to keep track of during computer simulations, since (4.33) implies that the spatial integral should sum to unity at all times.

66

4.6.1 Example of one-dimensional (1D) MDE transport

Boundary Conditions (BCs) and Initial Condition (IC) are needed to solve the partial differential equation (PDE). A simple and important situation refers to bioparticles inside a chamber being drawn down to the array and where both the array and boundaries are impenetrable or reflect, i.e. bioparticle flux is zero. An example of bioparticle collection under the action of a deterministic downwards force and then release after it is switched off is illustrated in Fig. 4-1.
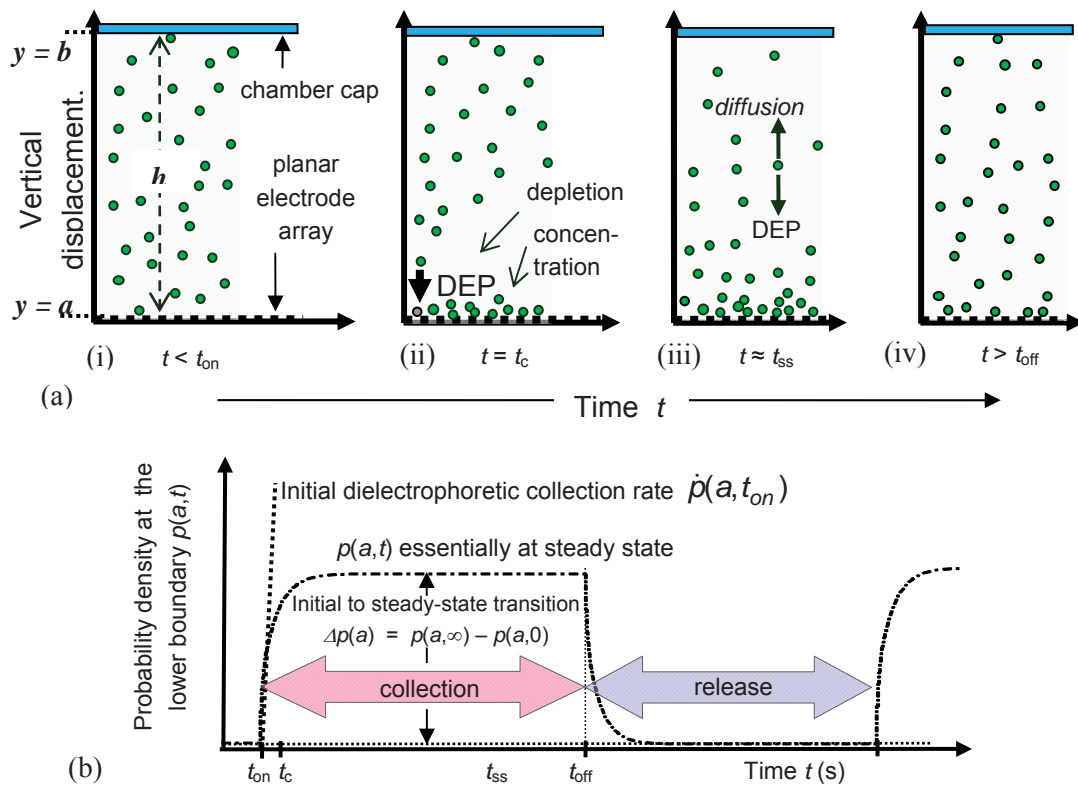

Fig. 4-1 Particle collection under the action of DEP force and release after the DEP force is switched off. (a) Cartoon - side view (i) initially uniform (ii) soon after force is switched on ($t = t_{on}$) DEP force attacts bioparticles downwards causing a depletion layer above (iii) depletion layer widens and system reaches steady state ($t \approx t_{ss}$) where fluxes balance (iv) after the DEP force is switched off (t_{off}) bioparticles diffuse away from array. (b) Probability density at the array as a function of time, $p(a, t)$, showing particle collection and release with times corresponding to Fig.(a). Repitition can form continuous 'on/off' cycle.

A cartoon showing particle distribution (side view) is shown in Fig. 4-1(a) Initially, the bioparticle distribution is uniform (i), soon after the electrodes are energised ($t = t_{on}$) the dielectrophoretic force on nearby particles attracts them towards the lower boundary (array) causing a localised concentration increase and leaving a depletion layer above (ii). The depletion layer widens and travels towards the upper boundary, and reaches steady state ($t \approx t_{ss}$) where the DEP particle flux is balanced by diffusion (iii). After the DEP force is switched off (t_{off}) the particles diffuse away from the array into the bulk, and the distribution returns to the initial state (iv).

4.6.2 1D MDE transport parameters

The probability density at the array as a function of time, $p(a, t)$, corresponding to Fig. 4-1(a) is shown in Fig. 4-1(b). It shows the bioparticle collection and release with times and two useful parameters that characterise transport from bulk solution into a confined volume with impenetrable boundaries. These two summary parameters are

- the initial rate of change of probability density, is represented as the slope of the line in Fig. 4-1(b), referred to as the *initial collection rate*, $\dot{p}(a, t_{on})$ (Pohl, 1978; Gascoyne *et al.*, 1994)

- the *initial to steady-state transition* $\Delta p(a)$ as shown in Fig. 4-1(b)

The DEP collection and release process can be repeated – forming a continuous 'on/off' cycle.

4.6.3 3D MDE transport and parameters

The MDE (4.34) can be generalised for three-dimensions with a probability density (m^{-3})

$$\frac{\partial p(\underline{x}, t)}{\partial t} = -\vec{\nabla} \cdot \vec{J}(\underline{x}, t) = -\vec{\nabla} \cdot [p(\underline{x}, t)\vec{v}(\underline{x})] + D \ \vec{\nabla} \cdot (\vec{\nabla} p(\underline{x}, t)) \qquad (4.37)$$

where the velocity vector is given by $\vec{v}(\underline{x}) = v_x(\underline{x})\vec{u}_x + v_y(\underline{x})\vec{u}_y + v_z(\underline{x})\vec{u}_z$. As with the 1D system, one can view the 3D probability flux, leaving diffusion aside, as the number of bioparticles passing through per unit boundary area per unit time, or bioparticle flux, divided by the total number of bioparticles

$$J = cv / N \qquad (4.38)$$

with units ($\mathrm{m^{-2}s^{-1}}$).

When the probability density no longer changes with time and the *lhs* = 0, $p(\underline{x}, t)$ is said to have reached *steady state*, or become *stationary*, and the system of particles remains at equilibrium. The probability flux arising from DEP is balanced by diffusion and the divergence of the flux $J(\underline{x},t)$ is zero,

$$\vec{\nabla} \cdot \vec{J}(\underline{x},t) = 0 \qquad (4.39)$$

Other parameters for 1D can be easily generalised to 3D, for example the initial collection rate and initial to steady-state transition introduced in section 4.6.2 as 1D parameters. In 3D these point parameters are $\dot{p}(\underline{x},t_{on})$ and $\Delta p(\underline{x})$ and related physically to concentration by generalizing (4.34),

$$p(\underline{x},t) = c(\underline{x},t) / N \qquad (4.40)$$

Point parameters such as probability density or concentration tend to be convenient for simulations but they are often not directly measured experimentally. Instead, the initial collection rate and initial to steady-state transition are measured in terms of numbers of bioparticles or biomolecules at observed using a microscope at an instant in time, $n(t)$, counted within a designated volume, V_{desig}, or an observable indicator, such as, their emitted fluorescence, $F(t)$. For moderately low concentrations they are related,

$$n(t) = kF(t) \qquad (4.41)$$

where k is a proportionality constant determined by counting a sample of collected bioparticles and mapping their fluorescence. The volumetric (n, F) and point (p, c) parameters are all concisely related in the expression below,

$$F(t) = \frac{n(t)}{k} = \frac{1}{k}\iiint\limits_{V_{desig}} c(\underline{x},t)dV = \frac{N}{k}\iiint\limits_{V_{desig}} p(x,y,z,t)dxdydz \qquad (4.42)$$

So experiments and simulations can be directly compared. Counting and fluorescence measures are practical for experiments and examples are given in the next chapter.

4.7 Concluding remarks

The primary forces are introduced with emphasis on electrokinetic mechanisms, and in particular on motion arising from non-uniform electric fields (DEP). The forces are categorised as *deterministic* - that are known, such as, gravity or an ideal, noiseless electric signal; and *stochastic* – that are uncertain, for example, motions that arise from thermal random motion and give rise to diffusion. Newton's laws of motion are applied to develop a quantitative description of transport applicable for the micro- and nano-scales. The single bioparticle motion is described by the Langevin equation that combines both deterministic and stochastic forces. The motion of a population (or suspended solute) of bioparticles can be derived from the Langevin equation and is described by the Fokker Planck, or modified diffusion, equation. Alternatively it can be derived by quite simple continuity arguments.

5 Observing, quantifying and simulating electrically driven biomolecule micro-transport

This final chapter describes example computer simulations and real time recordings of bioparticle and biomolecule (dsDNA) transport under the action of nonuniform AC electric fields (DEP). The transport process occurs in a micro-chamber and includes a diffusive component.

5.1 Micro-device and experimental arrangement

An experimental arrangement for observing biomolecule transport in a microdevice setup is shown in Fig. 5-1. Fig. 5-1(a) is simplified from the general microdevice platform shown in Fig. 1-2 in that it is a non-motility arrangement transporting for biomolecules i.e. devices A and B. The
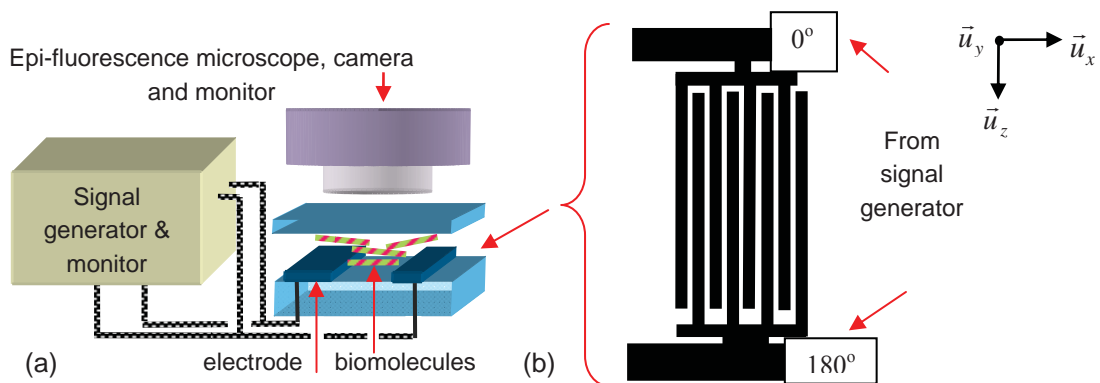

Fig. 5-1 (a) Scheme of DEP experimental apparatus showing AC signal source (including amplifier and monitoring oscilloscope), epi-fluorescence microscope and camera, video recorder and television monitor. (b) Plan (above) view detail of interdigitated of electrodes.

tracking of biomolecules as they move in real time is achieved by tagging or labeling them with a fluorescent dye and observing their microscopic movement with a epi-fluorescence microscope (Piller, 1977; Ploem and Tanke, 1987) with typically 200× or above magnification. Usually a camera is used to record display biomolecule movement on a PC/TV screen - since the experimentalist often needs to perform other tasks away from the microscope, e.g. change controls on the signal generator.

A plan view detail of the microelectrode 'fingers' that are responsible for generating electric fields that drive DEP biomolecule transport is shown in Fig. 5-1(b). The interdigitated electrodes were microfabricated according to standard procedures described section 3.3. Fig. 5-1(b) shows the signal supplies at 0^0 and 180^0. A photograph of eight individually addressable planar interdigitated arrays mounted on Printed Circuit Board (PCB) is shown in Fig. 5-2. In this example picture, the electrode widths and gaps are both 10 μm so they are individually too small to be seen by naked eye - a magnified view of these is represented in Fig. 5-1(b) – and each of the eight arrays appears

71

as a small millimeter rectangular blur. The photograph shows a common electrical path or bus that is usually neutral (earth) and eight individual, active, supply rails that connect to a signal generator.

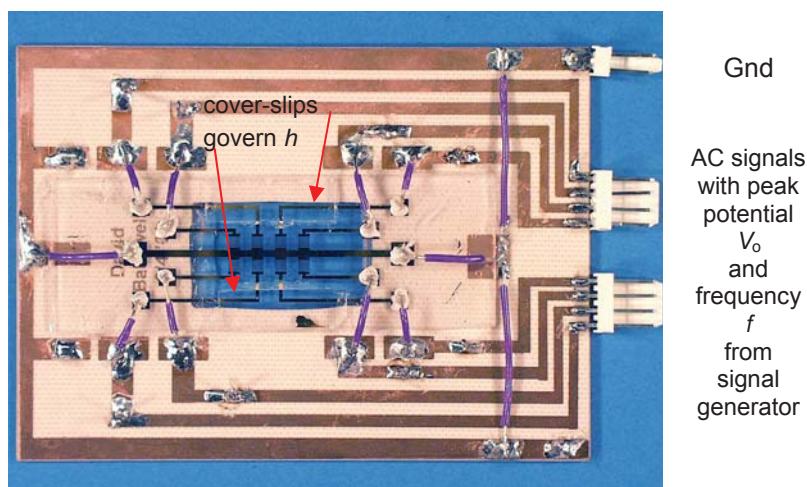**Fig. 5-2** Separately addressable 8 array interdigitated electrodes fabricated on a glass slide and mounted onto a PCB with supply buses. The ~150 μm thickness of two narrow cover-slips, adhered to the slide as shown, governs the minimum possible height h between the surface of the array and the 18×18 mm cover-slip (not shown) used to reduce evaporation.
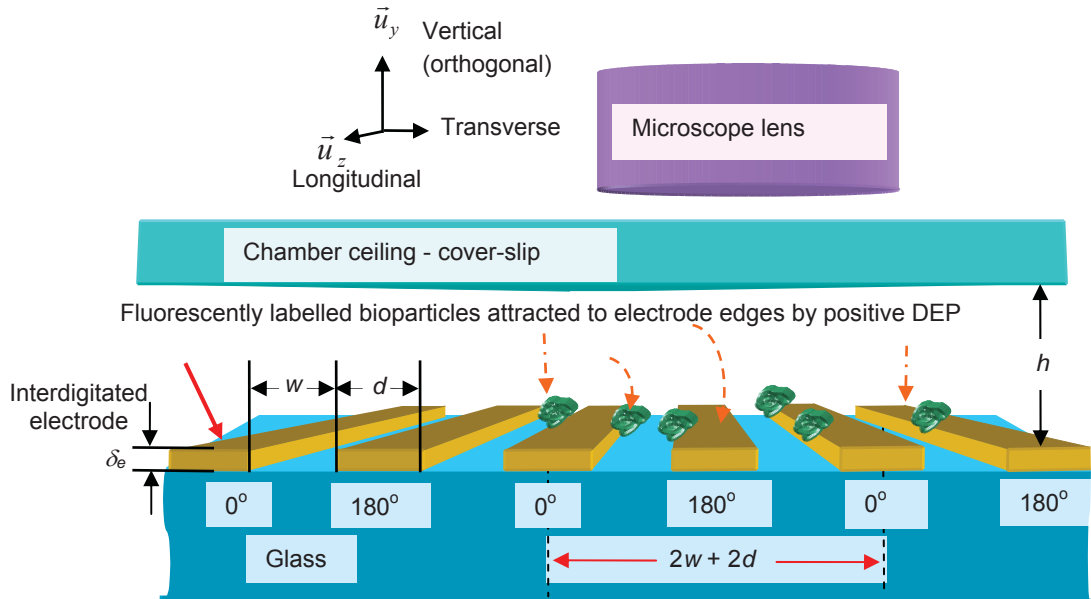
Fig. 5-3 Diagram of a DEP experiment (interdigitated electrodes fabricated on glass with width w, interelectrode gap g, and thickness δ_e) *not* to scale. The movement of the fluorescently labelled bioparticles, suspended in aqueous medium, is monitored with a epi-fluorescence microscope.

The experimental aims and apparatus is for a first stage characterization of a flow-through microdevice described in section 3.3, Fig. 3-11. This means that our interest lies mainly in the vertical movement of bioparticles rather than horizontal flow-through. Therefore, in the arrangement microdevice chamber does not require a comprehensive microfluidic arrangement with, say, flow-pumps and a screw-down sealed chamber. Rather a simpler apparatus is sufficient at this stage and is shown in Fig. 5-3. Referring to the photograph, Fig. 5-3, usually a 10 – 20 μl droplet of fluorescently labeled - and if needed, agent to reduce photobleaching - is micro-pipetted over the planar array and capped with a cover-slip to allow microscopic viewing and reduce evaporation. In the photograph, narrow coverslips act as the chamber walls, as shown, so in Fig. 5-3 the chamber height in the vertical y-direction is about $h = 160$ μm and the chamber ceiling is a coverslip. The length of each 'finger' is the longitudinal z-direction is so long that edge effects can be ignored.
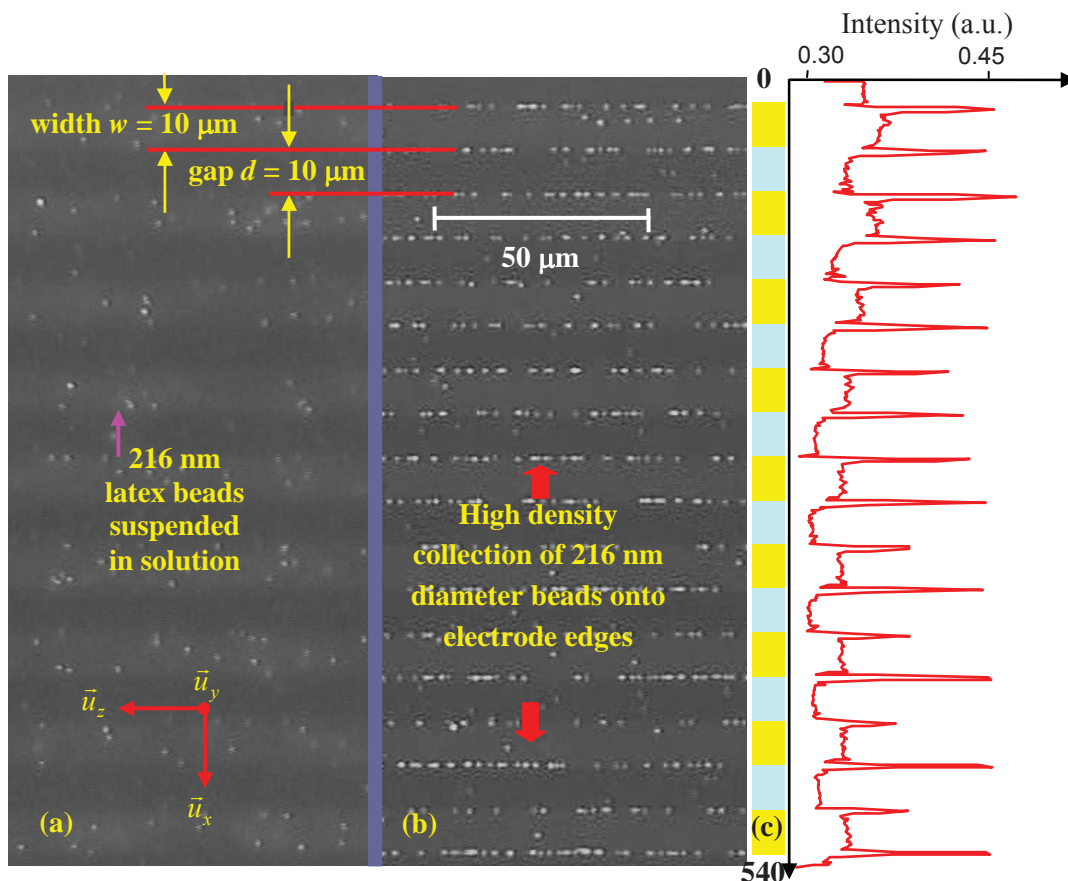

Fig. 5-4 Positive DEP collection of 216 nm polystyrene microspheres (a) 1 second before DEP started (electrodes were energised) (b) nearly 37 seconds after the DEP force was applied (c) longitudinal average greyscale light intensity for each of 540 transverse pixels.

5.2 Observations and quantitative measurements

When the electrode array is energized or switched on bioparticles randomly distributed in solution are attracted by DEP forces onto the electrode edges near where the electric field nonuniformity, and hence the DEP force, is the greatest. The arrival and settling of bioparticles at the electrodes is called DEP *collection*, and camera images at different times are shown in Fig. 5-3.

Microscope images of a DEP collection experiment of a sample of 216 nm diameter beads suspended in water inside a chamber is shown in Fig. 5-4. A slice of the camera image is shown in (a) initially, about one second before DEP force was applied (or electrodes energized with signal) with the beads are exhibiting random Brownian motion; (b) about 37 seconds after DEP was applied; and (c) average fluorescence intensity, $I(x)$ along the longitudinal z-direction as a function of the pixel count in the transverse x-direction. Note that images (a) and (b) shown are strips one-third of the original 720 pixel width and cropped for illustrative purposes. Since the dimensions of the electrodes are small compared with their length, electrode end effects are ignored.

5.2.1 Using geometry of DEP force aids quantification

Quantification of the camera images was achieved by recognizing that for fairly low bead concentrations, the optical fluorescence in a given volume was proportional the number of beads. The volume was assumed a vertical thickness corresponding to the microscope depth-of-focus. Software coded in Matlab (MathWorks, USA) and the mathematics and image processing details can be found (Bakewell and Morgan, 2001; Bakewell and Morgan, 2004). The geometry of the array governs the gradient of electric field-squared, which in turn governs the DEP force. It is shown in the simulations comprising next section that solution for the components of DEP force, in the transverse direction, show the array is periodic every electrode width and associated inter-electrode gap, i.e. $w + g$.
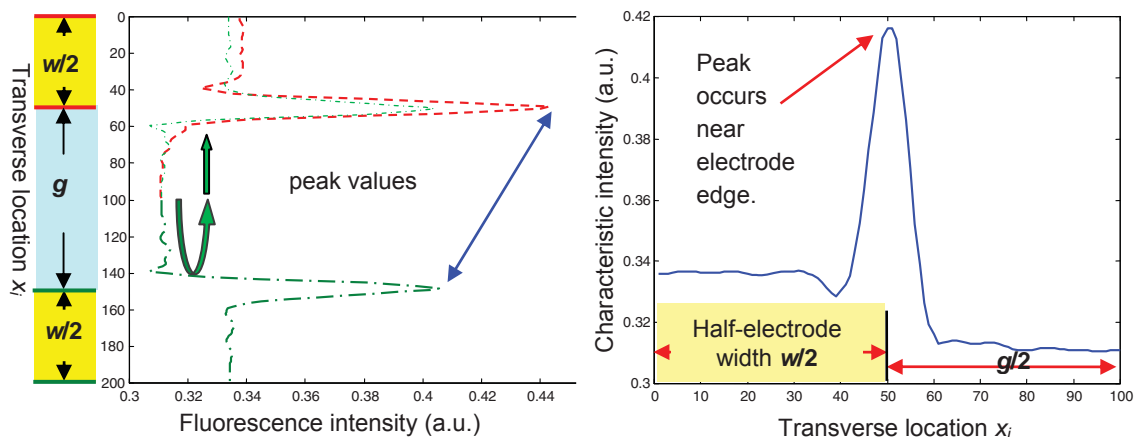

Fig. 5-5 DEP bioparticle collection quantification (a) fluoresence intensity - periodic average (b) fluoresence intensity – further symmetric average yields characteristic.

The periodic properties are exploited so that pairs of peaks of the intensity plotted in Fig. 5-4(c) can be summed and averaged to yield a second periodic average. In addition, within the period there is

75

symmetry at the mid-width or mid-gap interval, as shown in Fig. 5-5. This means that by rotating one of the peaks (shown as green) at the edge point, it can be averaged with the other (red) peak to give a characteristic intensity spanning half-width and half-gap, $w/2 + g/2$.

The resultant average intensity profile, rotated for conventional viewing, is shown in Fig. 5-6. It spans one-half electrode width and one-half inter-electrode gap $w/2 + g/2$ and characterizes the bead collection on the entire array at that moment in time (t = 37 s); thus, it is called a *characteristic*. Applying the same procedure to a series of video frames yields a collection
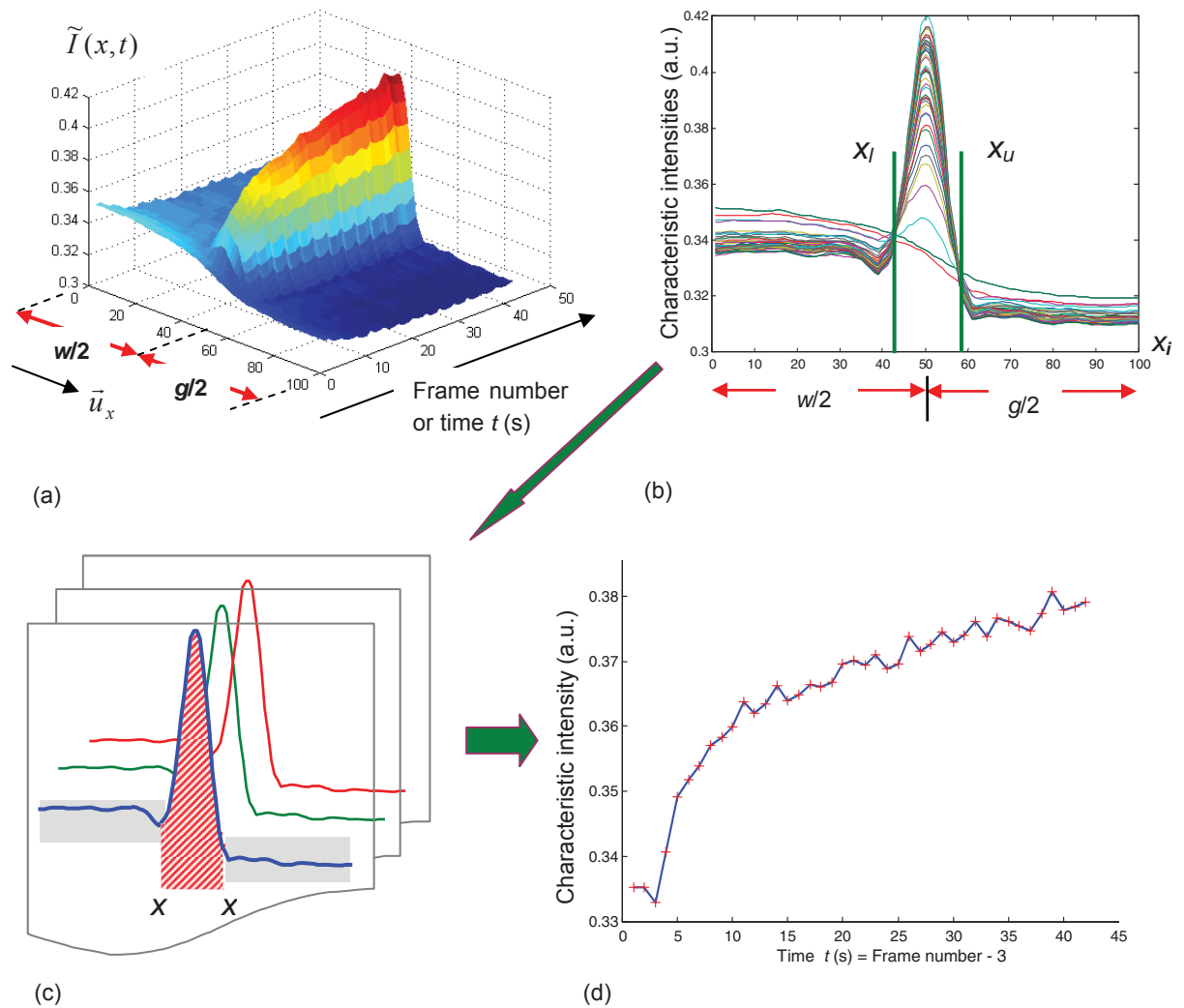
Fig. 5-6 DEP bioparticle collection characteristics (a) orthographic view (b) spatial view and set limits (c) determine fluorescence by integration between limits for each video frame (d) resulting time profile.

characteristic over time. A 3D orthographic view of the fluorescence intensity as a function of space (x-direction) and time (or frame number) is shown in Fig. 5-6(a). This surface encapsulates the fluorescence over the entire array versus time. A 2D projection along the time axis is shown in Fig. 5-6(b) where the fluorescence peaks are shown to correspond to the bead accumulation about the edge of the electrode.

The 3D surface contains much useful information. However, 3D surfaces are not so convenient when many collection experiments are being compared. Instead, a 2D summary time profile is more useful. This is obtained by integrating the fluorescence over a interval between a lower and an upper limit, x_l and x_u, as shown in Fig. 5-6(b), or by finding either the value of each peak. The former tends to be more robust against mechanical vibrations and sources of noise. Integrating over x_l and x_u, for each fluorescence characteristic generated each frame, as represented in Fig. 5-6(c) yields a collection time profile, Fig. 5-6(d).

The profile shows that the greatest increase in fluorescence, and therefore bead collection occurs almost immediately after the array is electrically energized (DEP force switched on). This is attributed to DEP flux solely acting and can be quantified by the collection rate transport parameter $\dot{p}(a,t_{on})$ – introduced in the previous chapter. Thereafter the flux arising from diffusion acts against the increasing concentration near the electrodes edges so the collection rate decreases and eventually levels to steady-state. The second quantification parameter, also introduced in section is the initial to steady-state transition $\Delta p(a)$ initial rate of change of probability density, or concentration. The system characteristic shown in Fig. 5-6(d) indicates it is not yet at steady-state; an approximate extrapolation indicates $\Delta p \leq 0.05$.

The fluorescence profile also shows time fluctuations on the scale of a few seconds. These can arise from a number noise sources including mechanical vibrations and variations in the light source of the epi-fluorescence microscope. Fluctuations are smoothed out by integrating the

fluorescence of the entire arrays and normalizing the fluorescence about the edges with respect to it (for brevity, not shown). Thus, the normalized fluorescence is typically around unity before the DEP is switched on and the collections start.

5.2.2 DEP collections exhibit frequency and voltage dependence

The time profile shown in Fig. 5-6(d) represents one collection experiment for an electrical signal with fixed radio frequency, 10 kHz to 20 MHz and amplitude. Generally a sine waveform is used and is specified in terms of peak voltage, V_o or root-of mean of sum of the squares (RMS). One of the electrode buses is generally ground (0V) so the peak electrode voltage difference is simply represented as the potential, Φ_p or more conventionally, V_o (volt). Repeating DEP collection experiments for a range of radio frequencies and voltages of 216 nm latex beads yields varying collection profiles; typical ones are shown in Fig. 5-7.
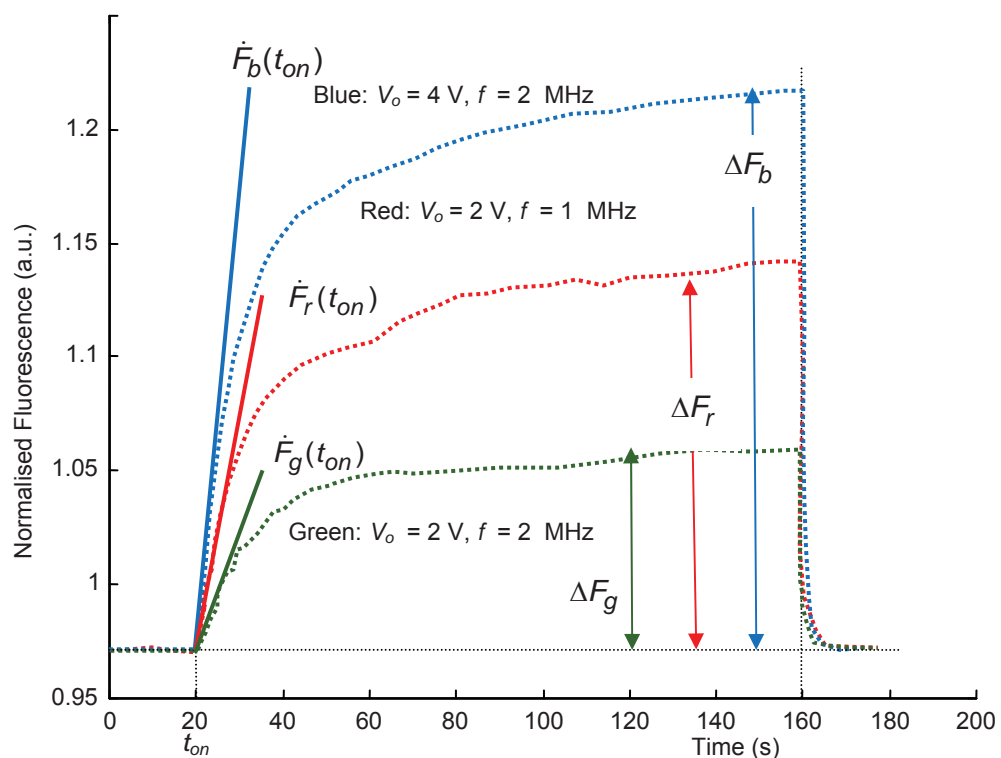

Fig. 5-7 Experimental DEP frequency and voltage dependent collection and release by diffusion

All red, blue and green profiles show normalized fluorescence, each measured and evaluated using the averaging procedures for a planar interdigitated array described above. Experimental parameters for the green profile were V_o = 2V and f = 2 MHz as indicated in Fig. 5-7. The red profile was measured and evaluated with one experimental parameter the same V_o = 2V but the other signal frequency parameter had been halved to f = 1 MHz as indicated. The blue profile was measured and evaluated with the potential doubled V_o = 4V but the signal frequency was the same as the green f = 2 MHz as indicated. No collections were observed at 3 MHz.

Question: How can we account for these profiles evaluated from experiments given (i) the known V_o and f parameter values, and (ii) the conceptual and factual material in the previous chapters ?
Clues/hints: start by asking what type of entity are we dealing with? Bioparticle or biomolecule? Think of the process: it is DEP driven transport with beads small enough so that Brownian motion plays a role. What parameters does the DEP transport depend on?
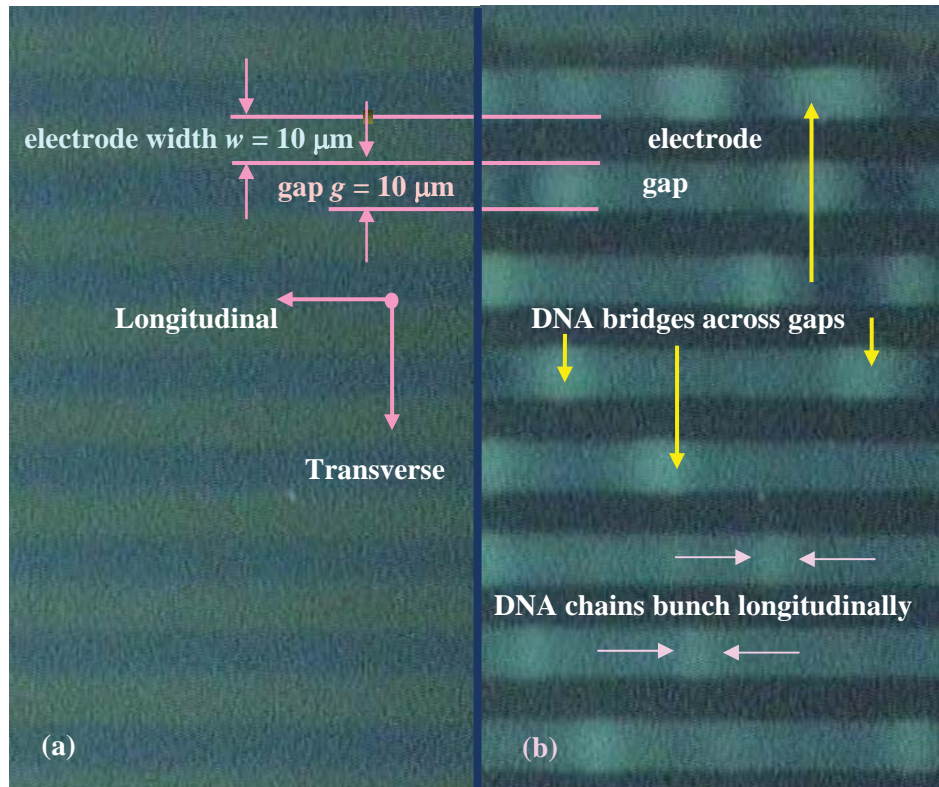More clues and answers towards the end of the chapter!

Fig. 5-8 Positive DEP collection of fluorescently labeled DNA suspension: half-frame width images: (a) before DEP, and (b) ~ 0.1 s after DEP switched on with V_o = 4.5 V, f = 100 kHz

DEP collections of DNA and RNA biomolecules have also been performed, advancing the early pioneering work by Washizu (see refs). The DNA was 12 kilobase pair (kbp) plasmid which means that the strands are joined together so they can be circular. They are twisted – superficially like an elastic band that has been rolled between our fingers. Dielectric studies on this DNA, purified using standard methods (Maniatis *et al.*, 1982) revealed three dispersions at 140 kHz, 2 MHz and 12 MHz (Bakewell *et al.*, 2000).

Photos of fluorescently stained DNA are shown in Fig. 5-8; (a) before the DEP was switched on and (b) several seconds after the electrode were energized with V_o = 4.5 V and f = 100 kHz. Time profiles for frequencies up to 2 MHz are detailed in Bakewell and Morgan (2006), they are qualitatively similar to those with beads in that the collections decreased with frequency. Note that in Fig. 5-8(b) the DNA strands appear to span the inter-electrode 10 μm gaps. This prompts *questions*: How long would be a 12 kbp (12,000 base pair) DNA biomolecule? *Hint*: see section

79

2.2.1 on nucleic acids. Is it possible for one biomolecule to span the 10 μm gap? - even if the strands were cut so the DNA was no longer circular but linear?

5.3 Simulations of electrically driven biomolecule micro-transport

Prediction of biomolecule or bioparticle transport between locations in a microfluidic-type chamber is achieved by solving the modified diffusion equation (MDE) described in Chapter 4. It includes deterministic (known) and stochastic (uncertain) terms and is solved so that transport is determined for spatial and temporal areas of interest. This means there are two steps for simulating the transport of biomolecules or bioparticles in microfabricated structures. These are

- solving Laplace's equation for the electric field and hence the deterministic biomolecule or bioparticle DEP force and flux

- solution of the diffusion equation modified to include DEP flux (MDE) thus predicting the biomolecule concentration over the spatial and temporal areas of interest.

5.3.1 Determining the dielectrophoretic force throughout the chamber.

The DEP force is computed from (4.18) by first evaluating the electric field. As described in the previous chapter, the electric field is determined by solving Laplace's equation (4.9) as an approximation to Poisson's equation.

Again, the length of each 'finger' of the interdigitated electrode array in the longitudinal *z*-direction is so long that edge effects can be ignored. This enables the solution space of Laplace's equation to be reduced from 3D to 2D, thus, considerably saving computation resources (memory, speed, time, etc).
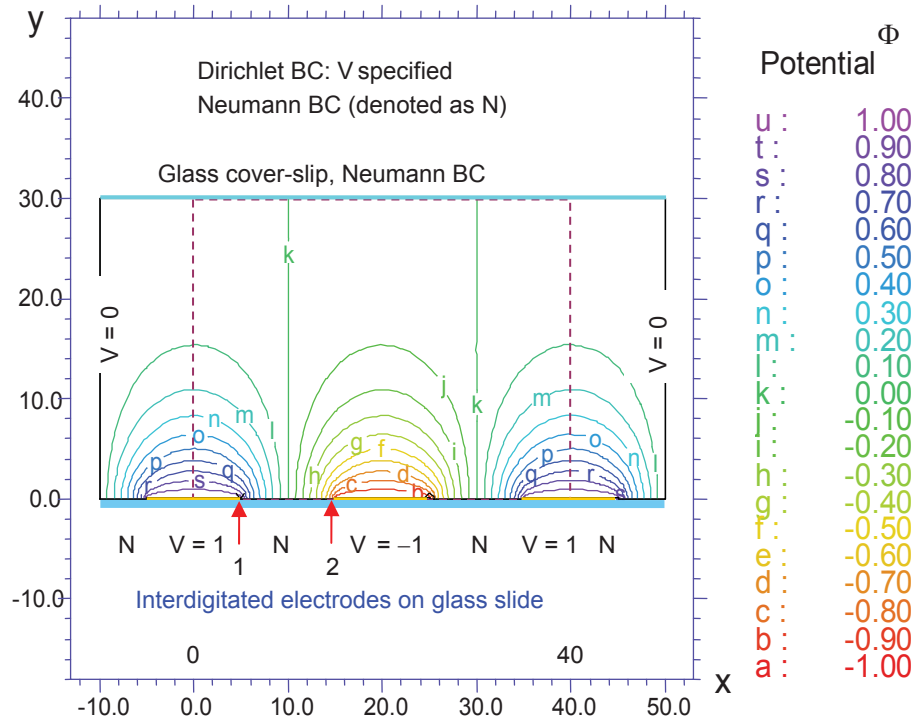

Fig. 5-9 Electric potential contour plot obtained by numerically solving Laplace's equation with δ = 0.1, *w* = *g* = 10, *h* = 30 and V_o = ±1 (a.u.). The BCs are as shown, see text for details.

Fig. 5-9 shows a contour plot of the solution for the electric potential, with normalized parameters and BCs as indicated:

- Dirichlet BC at known potentials (V) along the electrodes (gold), as shown, and at solution space boundaries

- Neumann BC, denoted 'N' at electrolyte solution glass interfaces and to preserve electric field symmetry, where the electric field component normal to the boundary is set to zero.

The values used in the numerical finite element integration (FlexPDE, PDE Solutions, USA) of Laplace's equation, *w, g, h*, and V_o are normalized for illustrative purposes, hence, arbitrary units (a.u.). The contours of potentials are repeated (periodic) and exhibit symmety, therefore the width of the solution space for the DEP force is reduced to $w/2 + g/2 = 10$ a.u. This further reduction in simulation space enables finer mesh resolutions, and hence accuracy, for given computation resources.

Contours of the electric field are plotted in Fig. 5-10 for the reduced space, and for illustrative purposes, the height of the chamber cap is shortened to 10 a.u. Most of the contours are localized
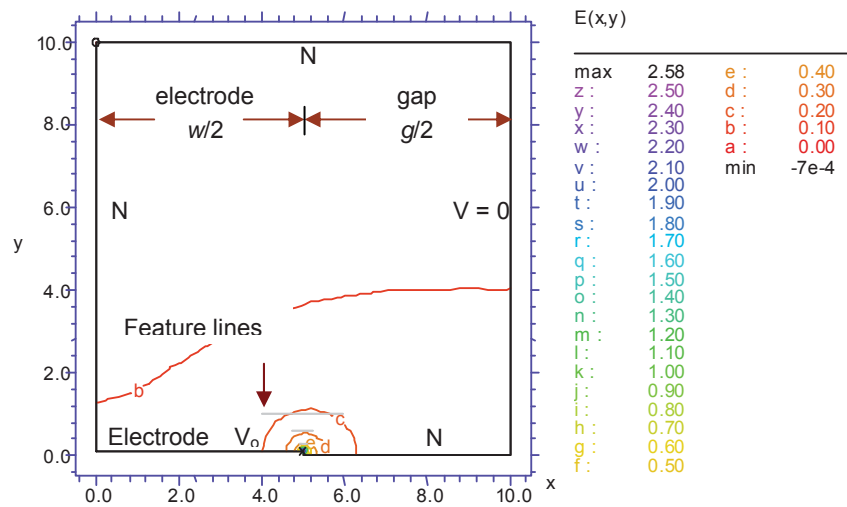
Fig. 5-10 Contour plot of the electric field magnitude $\left|\vec{E}(x, y)\right|$ obtained by numerically solving Laplace's equation using the same parameters as Fig. except h = 10 (a.u.). Dirichlet BCs have potential (V) as specified, the Neumann BCs are denoted 'N'.

Fig. 5-11 Plots of normalized DEP force or electric field magnitude-squared gradients: $\partial_x\left|\vec{E}\right|^2$ acting sideways and $\partial_y\left|\vec{E}\right|^2$ acting vertically. Profiles numerically evaluated at y = 0.2 cross-section for x = 0 to 10 using values δ_e = 0.1, w = g = 10, h = 10 and V_o = 1 (a.u.).

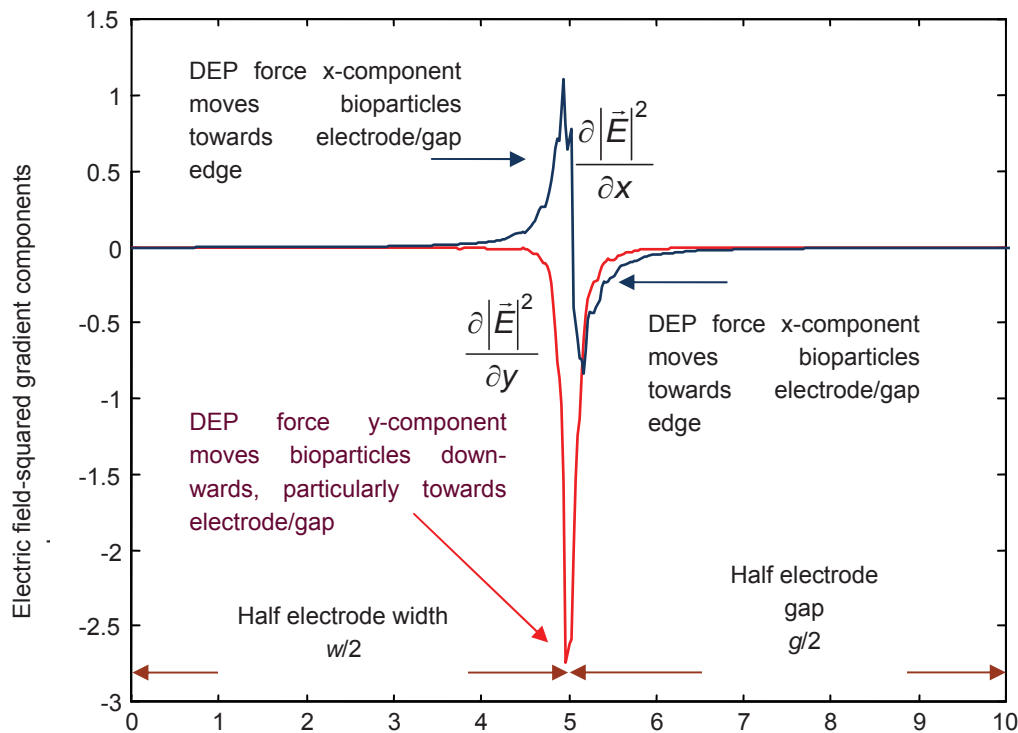around the electrode edge with the glass, so that the mesh size was refined in this region by coding 'feature lines' into the FlexPDE software to achieve accurate prediction of the electric field.   Note that the left vertical BC above the electrode is Neumann since the potential cannot be specified above the electrode, only the gradient of the potential is zero - as the simulation shows in Fig. 5-9.

The electric field was evaluated using (4.11) and Contour plots of the field magnitude squared accentuate localization of contours at the edge. Consequently contour plots for *x* and *y* components of the *gradient* of the electric field magnitude squared, $\nabla \left| \vec{E} \right|^2$, are not very insightful! Instead they are plotted for a *y* cross-section just above the planar array, in Fig. 5-11. Recall that the DEP force is proportional to this quantity, $F_{DEP} \propto \vec{\nabla} \left| \vec{E} \right|^2$ so the figure is actually the DEP force normalized for illustrative purposes.

The positive force *x*-component over the half-electrode indicates that particles will be attracted towards the electrode/gap edge. The negative force *x*-component over the half-gap indicates that bioparticles will be attracted in the reverse direction, resulting in them moving also towards the edge. The negative force *y*-component over the edge indicates that bioparticles in suspension above the planar array are attracted downwards towards the edge. The profiles decrease in their magnitude further away from the array with a behavior that stays much the same. In summary, the positive DEP force is shown to act towards electrode edge thus confirming the experimental observations of bioparticles collecting on array edges in the previous sections.

5.3.2 Solutions of the MDE for predicting bioparticle collections

The MDE partial differential equation (4.37) also requires BCs and an initial condition (IC) for a particular solution to exist. This *second* set of BCs concern bioparticle flux and are not to be confused with the *first* set of BCs used to solve Laplace's equation! The BCs in this example are that the bioparticle flux, J given by (4.38) is zero meaning that bioparticles cannot pass through. This is obvious for the lower and upper boundaries, shown in Fig. 5-12, since their glass and gold material properties mean they are reflective or impenetrable. For the vertical boundaries, the zero flux BC may be less obvious. One way to think of this is in terms of symmetry - that is, processes on each side of each boundary are the same so that the bioparticle movement that happens on one side mirrors, or reflects, the events on the other side. This means that the net flux of bioparticles passing through each of these boundaries at any moment in time is zero.
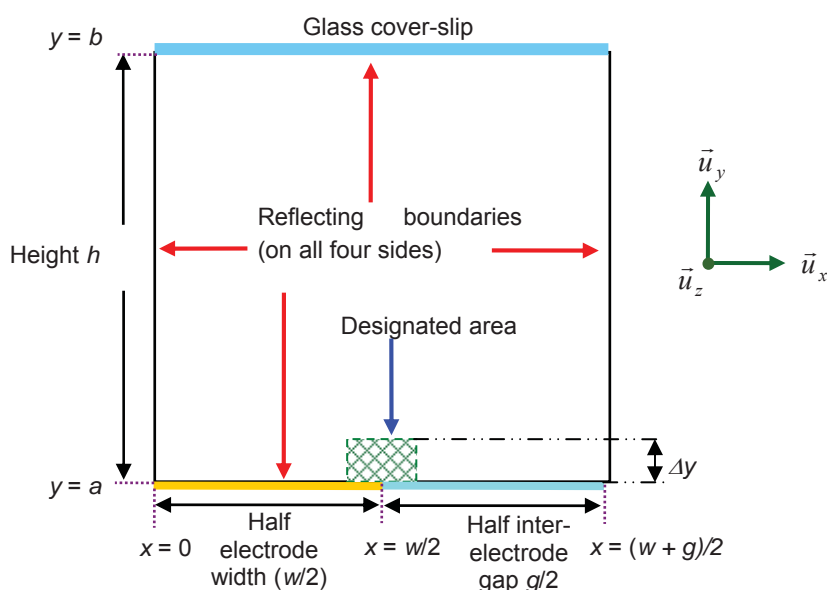

Fig. 5-12 MDE solution space with reflecting BCs and showing designated collection area.

A realistic IC used for bioparticles is that they are uniformly distributed in the chamber. Having established the BCs and IC, particle collections are simulated by specifying a designated region that mimics a realistic collection volume. In the previous section 5.2 the collection area was defined by the depth of focus in the vertical *y*-direction. The transverse *x*-direction chosen depends on properties of the collection:

- for bioparticles (beads), the collections occurred about the electrode edges

- for DNA, the biomolecules collected in between the electrodes

The MDE, BCs and IC are coded in application software, FlexPDE, that integrates (4.37) by finite elements (Zienkiewicz and Taylor, 1989). Simulation results for bioparticles (216 nm diameter

84

latex beads) with parameter values that enable comparisons with experiments are shown in Fig. 5-13. The simulations were performed using the above methods with realistic values for parameters, e.g. $h = 200$ μm.
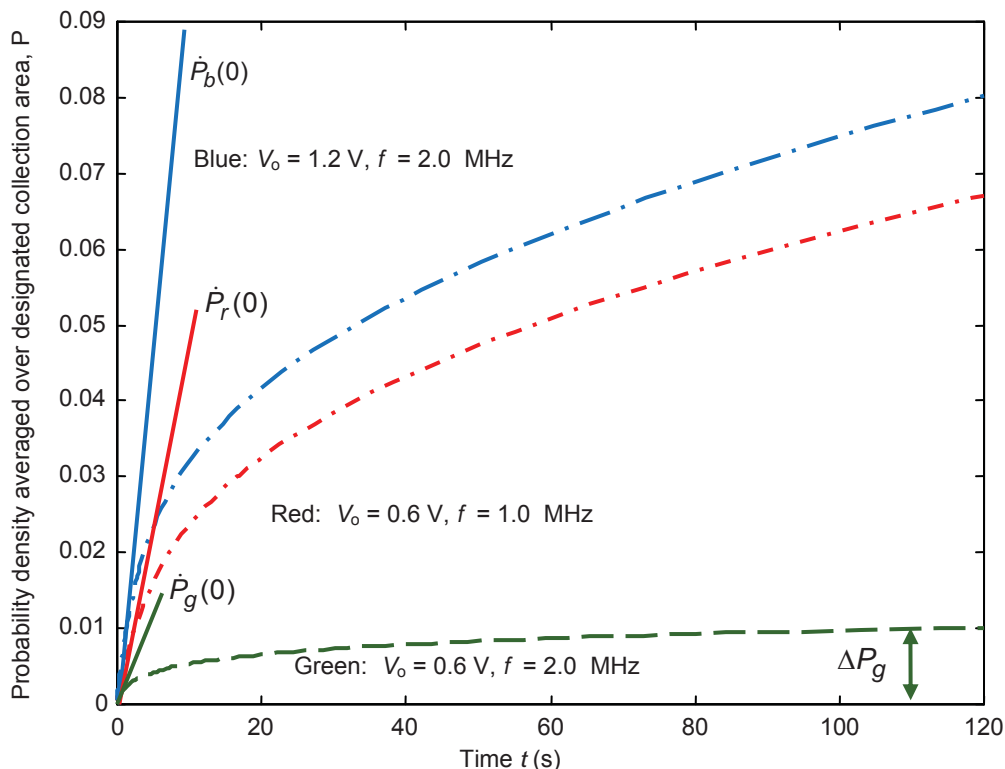

Fig. 5-13 Simulated DEP frequency and voltage dependent bioparticle collection profiles.

5.4 Brief discussion of experiments and theory

As a general observation the values for voltages are set lower than those used in the experiments. Compare the experimental 2 MHz green profile in Fig. 5-7 that used 2 volts with the comparable simulated 2 MHz green profile in Fig. 5-13 that used 0.6 volts. Anomalous results were obtained when a value of 2 volts or more were attempted in the simulations, indicating the theoretical model is too sensitive and predicts DEP transport that is far stronger than occurs experimentally. In fact a steady state solution (for brevity, not described) predicted that all beads would be attracted out of solution by DEP onto the array leaving none in the suspension. That is, a concentration or probability density in the bulk of zero. Such an affect has never been observed to our knowledge.

Comparisons of the trends of the initial collection rates of experiments, however, concurred with trends in the simulations. Using the 2 MHz green profile as a 'baseline', consider the effect of doubling the applied voltage in Fig. 5-7 from 2 V to 4 V shown by the blue profile. The initial fluorescence rate, given by the slope of the tangent, $\dot{F}_b(0)$, is about four times (or four fold) more than the green, $\dot{F}_g(0)$. This agrees with the simulated collection rates; compare slopes of blue and

85

green tangents, $\dot{P}_b(0)$ and $\dot{P}_g(0)$ in Fig. 5-13 – there is a four-fold change. The simulations confirm the square-law dependence of the DEP bioparticle force on electric field (and hence electrode voltage) depicted in equation (4.18). It is easy to image that a four-fold increase of force, and hence, velocity or flux, of bioparticles into a tiny volume would lead to the same four-fold bioparticle number increase within that volume! Formal mathematical expressions can be derived using equation (4.42). So the simulations confirm the trend one intuitively expects.

The same argument applies to comparing the effect of changing the signal frequency. Again using the 2 MHz green profile as baseline, consider the effect of reducing the applied frequency in Fig. 5-7 from 2 MHz to 1 MHz as indicated by the red profile. The initial fluorescence rate $\dot{F}_r(0)$, given by the slope of the tangent, is about twice more than the green. This agrees with the simulated collection rates; compare slopes of red, $\dot{P}_r(0)$, and green tangents in Fig. 5-13, there is a two-fold increase. The simulations confirm the frequency dependence of the DEP bioparticle force on the inducible polarisability via the real part of the Claussius-Mossotti factor, $\text{Re}\{f_{CM}\}$, section 3.2.3 equation (3.12). Inspecting the plot in Fig. 3-6, as the frequency *decreases* from 2 MHz to 1 MHz, the $\text{Re}\{f_{CM}\}$ *increases* from about 0.3 to 0.6, or doubles. So the simulations and experiments concur and confirm the trends predicted by theory. Thus one can encapsulate these results by suggesting that the bioparticle collection rates behave as,

$$\dot{n}(0) \propto \text{Re}\{f_{CM}\}V_o^2 \tag{5.1}$$

Comparisons of the initial to steady-state transition for the experimental versus simulation are quite different. The three experiments in Fig. 5-7 show steady state after two minutes. However, only the green profile in the simulations, Fig. 5-13, could be considered to be quasi-steady state at two minutes; the red and blue are clearly not at this time point. Extrapolations of the blue and red profiles indicate the steady-state values are at least order of magnitude greater than the green profile! Clearly, experiments do not concur with simulations for the initial to steady-state transition parameter despite being based on the same theoretical models as the collection rates.

A rough summary of Fig. 5-7 is that the experimental transitions are *nearly proportional* to the real part of the Claussius-Mossotti factor and the voltage-squared. In contrast, integration of (4.37) with (4.39) imposed predicts a theoretical *exponential* (Boltzmann) dependence on the DEP energy! Again the discrepancy appears to lie in sensitivity of values and the physical reasons are not entirely clear. It appears one factor is fluid motion arising from hydrodynamic effects and electroosmosis that disrupts steady state conditions. These additional effects are not included in the theory, nor is the fact the polarisability could saturate more than expected. An alternative approach is to use a DEP mobility relation (Asbury and Van Den Engh, 1998) in a similar way to electrophoresis and methods for inferring model parameters from data are being developed (Bakewell, 2008).

DEP of DNA studies have also exhibited close agreement of experiments and simulations with the initial collection rate parameter in contrast to the initial to steady state transition. Nonetheless, biomolecules themselves bring in further questions. We leave the reader to think about another question. For example, why are the DNA biomolecules bridged across the inter-electrode gaps in Fig. 5-8 when DEP force in Fig. 5-11 is shown to be localized around the electrode edges? One of the answers could be that the presence of DNA biomolecule itself alters the electric field surrounding it in a way as to attract more DNA towards it. In fact bioparticles are known to form perl-chains that can bridge across the inter-electrode gaps for this reason (e.g. Llamas *et al.*, 1998).

5.5 Concluding remarks

Laboratory apparatus, experiments and simulations of dielectrophoretic driven biomolecule and bioparticle transport over the micron and submicron scale has been described in this chapter. The chapter draws on concepts and theory developed in previous chapters and describes how geometrical properties of the sample chamber can be exploited to enable experimental quantification biomolecule and bioparticle transport in space and time. The geometrical properties of the sample chamber have also been used to simulate transport using Laplace's equation and the modified diffusion equation. Comparisons between experiments and simulations using the initial collection rate parameter show agreement in trends that depend on signal frequency and voltage. However, there are differences in terms of sensitivity and this is observed in the initial to steady-state transition parameter. In summary, experiments and simulations confirm the basic theoretical framework of DEP driven transport but also raises a need for further modeling of other electrokinetic phenomena supported by experimental investigations.

6 References

6.1 General – selected books

ALBERTS, B., JOHNSON, A., LEWIS, J., RAFF, M., ROBERTS, K and WALTER, K. (2008) *Molecular Biology of The Cell*, 5th Edit., Garland Science, New York, USA.

BERG, H. C. (1983) *Random walks in biology*. Princeton University Press, Princeton, USA.

BLOOMFIELD, V. A., CROTHERS, D. M., and TINOCO Jr, I. (1974) *Physical chemistry of nucleic acids*. Harper and Row, New York, USA.

CALLADINE, C. R. and DREW, H. R. (1997) *Understanding DNA*. 2nd Ed., Academic Press, London, UK.

DOI, M. and EDWARDS, S. F. (1986) *The theory of polymer dynamics*. Clarendon Press, Oxford, UK.

GARDINER, C. W. (1985) *Handbook of stochastic methods for physics, chemistry, and the natural sciences*. Springer-Verlag, Berlin, Germany.

GRANT, E. H., SHEPPARD, R. J., and SOUTH, G. P. (1978) Dielectric behaviour of biological molecules in solution. **In**: *Monographs on physical biochemistry*. Eds. Harrington, W. F. and Peacocke, A. R., OUP.

JACKSON, J. D. (1975) *Classical Electrodynamics*. 2nd Ed., John Wiley, New York, USA.

JONES, T. B. (1995) *Electromechanics of particles*. Cambridge University Press, Cambridge, UK.

MORGAN, H. and GREEN, N. (2003) *AC Electrokinetics*, Research Studies Press (IoP Publishing), England, UK.

NELSON, D. L. and COX, M. M. (2008) *Lehninger Principles of Biochemistry*, 5th Edit., W. H. Freeman, New York, USA

OOSAWA, F. (1971) *Polyelectrolytes*. Marcel Dekker, New York, USA.

PAPOULIS, A. (1984) *Probability, random variables, and stochastic processes*. McGraw-Hill (ISE), New York, USA.

PETHIG, R. (1979) *Dielectric and electronic properties of biological materials*. John Wiley, New York, USA.

POHL, H. A. (1978) *Dielectrophoresis*. Cambridge University Press, Cambridge, UK.

POLLARD, T. D. and EARNSHAW, W. C. (2008) *Cell Biology*, 2nd Edit., Saunders-Elsevier, Philadelphia, USA.

RUSSEL, W. B., SAVILLE., D. A., and SCHOWALTER., W. R. (1999) *Colloidal dispersions*. Cambridge University Press, Cambridge, UK.

RUSSELL, P. J. (1994) *Fundamentals of genetics*. Harper-Collins College Publishers, New York, USA.

TAKASHIMA, S. (1989) *Electrical properties of biopolymers and membranes*. Adam Hilger, Philadelphia, USA.

VON HIPPEL, A. R. (1954) *Dielectrics and waves*. John Wiley, London, UK.

6.2 Research articles and other reading

ANDERSON, C. F. and RECORD, M. T. Jr. (1982) Polyelectrolyte theories and their applications to DNA. *Ann. Rev. Phys. Chem.,* **33**, p. 191-222.

APPELS, R. and DVORÁK, J. (1982) The wheat ribosomal DNA spacer region: its structure and variation in populations and among species. *Theor. Appl. Genet.*, **63**, p. 337-348.

ARMSTRONG, R. W. and STRAUSS, U. P. (1969) Polyelectrolytes. **In**: *Encyclopedia of polymer science and engineering*. Vol. 10. John Wiley, New York, USA, p. 781-861.

ARNOLD, W. M., GESSNER, A. G. and ZIMMERMANN, U. (1993) Dielectric measurements on electro-manipulation media. *Biochem. Biophys. Acta,* **1157**, p. 32-44.

ASAMI, K., HANAI, T., and KOIZUMI, N. (1980) Dielectric approach to suspensions of ellipsoidal particles covered with a shell in particular reference to biological cells. *Jap. J. Appl. Phys.*, **19**, 2, p. 359-365.

ASBURY, C. L. and VAN DEN ENGH, G (1998) Trapping of DNA in nonuniform oscillating electric fields. *Biophys. J.*, **74**, 2, p. 1024-1030.

BAKEWELL, D., ERMOLINA, I., MORGAN, H., MILNER, J. and FELDMAN Y. (2000) Dielectric relaxation measurements of 12 kbp plasmid DNA. *Biochem. Biophys. Acta.,* **1493**, p. 151-158.

BAKEWELL, D. J. and MORGAN, H. (2001) Measuring the frequency dependent polarisability of colloidal particles from dielectrophoretic collection data. *IEEE Trans. Dielect. and Elec. Ins.*, **8**, p. 566-571.

BAKEWELL, D. J. and MORGAN, H. (2004) Quantifying dielectrophoretic collections of sub-micron particles on microelectrodes. *Meas. Sci. Technol.*, 15, 254-266.

BAKEWELL, D. J. and MORGAN, H.. (2006) Dielectrophoresis of DNA: time and frequency dependent collections on microelectrodes, *IEEE Trans. Nanobioscience*, 5(1), 1-8.

BAKEWELL, D. J. G. and NICOLAU, D. V. (2007) Linear protein molecular motors and associated hybrid devices (review), *Australian J. Chemistry*, **60**, pp314–332.

CONCEIÇÃO, R. C., BAKEWELL D. J. G and NICOLAU, D. V. (2008) Statistical analysis of the motility of nano-objects propelled by molecular motors. *Proceedings of SPIE Volume 6865*. SPIE, Bellingham, USA pp 1-8

BAKEWELL, D. J. G. (2008) Nanosize particle movement in time-modulated nonuniform electric fields: a Fourier-Bessel series solution. *Proceedings of SPIE 6799*. SPIE, Bellingham, USA pp 1-12.

BENGUIGUI, L. and LIN., I. J. (1982) More about the dielectrophoretic force. *J. Appl. Phys.*, **53**, 2, p. 1141-1143.

BONE, S., and SMALL, C. A. (1995) Dielectric studies of ion fluctuation and chain bending in native DNA. *Biochim. Biophys. Acta,* **1260**, p. 85-93.

BONE, S., LEE, R. S. and HODGSON, C. E. (1996) Dielectric studies of intermolecular interactions in native DNA. *Biochim. Biophys. Acta*, **1306**, p. 93-97.

BONINCONTRO, A., CAMETTI, C., DI BIASIO, A. and PEDONE, F. (1984) Effect of ions on counterion fluctuation in low-molecular weight DNA dielectric dispersions. *Biophys. J.,* **45**, p. 495-501.

DELACEY, E. H. B. and WHITE, L. R. (1981) Dielectric response and conductivity of dilute suspensions of colloidal particles. *J. Chem. Soc. Faraday Trans. 2*, **77**, p. 2007-2039.

DUKHIN, S. S. (1971) Dielectric properties of disperse systems. **In**: *Surface and colloid science*, **3**. Ed. E. Matijevic, John Wiley, New York, USA, p. 83-165.

EINSTEIN, A. (1905) *Investigations on the theory of Brownian movement*. Ed. R. Fürth, Translated by A. D. Cowper (1956), Dover Publications, New York, USA.

EISENBERG, H. (1976) *Biological macromolecules and polyelectrolytes in solution*. Clarendon Press, Oxford, UK.

FELDMAN, Yu. and KOZLOVICH, N. (1995) Time-domain dielectric spectroscopy studies of macromolecular solutions. *Trends in Polymer Sci*., **3**, p. 53-60.

FELDMAN, Yu. D, ANDRIANOV, A., POLYGALOV, E., ERMOLINA, I., ROMANYCHEV, G., ZUEV, Y., MILGOTIN B. (1996) Time domain dielectric spectroscopy: an advanced measuring system. *Rev. Sci. Instrum*.**, 67**, p. 3208-3216.

FIXMAN, M. (1980a) Charged macromolecules in external fields. 1. The sphere. *J. Chem, Phys*. **72**, 9, p. 5177-5186.

FIXMAN, M. (1980b) Charged macromolecules in external fields. 2. Preliminary remarks on the cylinder. *Macromolecules,* **13**, p. 711-716.

GASCOYNE, P. R. C., NOSHARI, J., BECKER, F. F. and PETHIG, R. (1994) Use of dielectrophoretic collection spectra for characterising differences between normal and cancerous cells. *IEEE Trans. Ind. Appl*., **30**, no. 4, p. 829-833.

GRATTAROLA, M. and MASSOBRIO, G. (1998) *Bioelectronics handbook*. McGraw-Hill, New York, USA.

GREEN, N. G. and MORGAN, H. (1997a) Dielectrophoretic investigations of sub-micrometre latex spheres. *J. Phys. D: Appl. Phys*. **30**, p. 2626-2633.

GREEN, N. G. and MORGAN, H. (1997b) Dielectrophoretic separation of nano-particles. *J. Phys. D: Appl. Phys*. **30**, p. L41-44.

GREEN, N. G. and MORGAN, H. (1998) Separation of submicrometre particles using a combination of dielectrophoretic and electrohydrodynamic forces. *J. Phys. D: Appl. Phys*. **31**, p. L25-30.

GREEN, N. G., RAMOS, A., GONZALEZ, A., MORGAN, H. and CASTELLANOS, A. (2000a) Fluid flow induced by non-uniform AC electric fields in electrolytic solutions on micro-electrodes. Part I: Experimental measurements. *Phys. Rev. E*, **61**, p. 4011-4018.

GREEN, N. G., RAMOS, A. and MORGAN, H. (2000b) AC electrokinetics: a survey of sub-micrometre particle dynamics. *J. Phys. D: Appl. Phys.*, **33**, p. 632-641.

GROSSE, C., (1989) Microwave absorption of suspensions of DNA type particles in electrolyte solution. *Alta Frequenza,* **58**, p. 365-8.

HAGERMANN, P. J. (1998) Flexibility of DNA. *Ann. Rev. Biophys. Biophys. Chem.*, **17**, p. 265-286.

HAKEN, H. (1978) *Synergetics – an introduction*. 2nd Ed., Springer-Verlag, Berlin, Germany.

HAKEN, H. (1983) *Advanced synergetics*. Springer-Verlag, Berlin, Germany.

HIEMENZ, P. C. (1986) *Principles of colloid chemistry*. 2nd Ed., Marcel Dekker, New York, USA.

HILFER, R., NØST, B., HASLUND, E., KAUTZSCH, VIRGIN, B. and HANSEN, B. D. (1994) Local porosity theory for the frequency dependent dielectric function of porous rocks and polymer blends. *Physica A*, **207**, p. 19-27.

HUGHES, M. P., MORGAN, H. and FLYNN, M. F. (1999) The dielectrophoretic behaviour of sub-micrometre latex spheres: influence of surface conductance. *J. Colloid and Interface Sci.*, **220**, p. 454-457.

KAMYSHNY, A., ERMOLINA, I., MAGDASSI, S., FELDMAN Yu. (2000) Study of the dynamic structure of native and hydrophobized glucose oxidase by time-domain dielectric spectroscopy. *J. Phys. Chem. B*, **104**, p. 7588-7594.

KAPUSCINSKI, J. (1995) DAPI: a DNA-specific fluorescent probe. *Biotechnic and Histochemistry*, **70**, 5, p. 220-233.

LEE, R. S. and BONE, S. (1998) Dielectric studies of chain melting and denaturation in native DNA. *Biochim. Biophys. Acta*, **1397**, p. 316-324.

LIDE, D. R. (Ed.) (1994) *CRC handbook of chemistry and physics*. CRC Press, Ann Arbor, USA.

LLAMAS, M., GINER, V. and SANCHO, M. (1998) The dynamic evolution of cell chaining in a biological suspension induced by an electric field. *J. Phys. D: Appl. Phys.*, **31**, p. 3160-3167.

LYKLEMA, J., DUKHIN, S. S., and SHILOV, V. N. (1983) The relaxation of the double layer around colloidal particles and the low-frequency dielectric dispersion: Part I. Theoretical considerations. *J. Electroanal. Chem.*, **143**, p. 1-21.

LYKLEMA, J., SPRINGER, M. M., SHILOV, V. N. and DUKHIN, S. S. (1986) The relaxation of the double layer around colloid particles and the low-frequency dielectric dispersion: Part III. Application of theory to experiments. *J. Electroanal. Chem.*, **198**, p. 19-26.

MANDEL, M. (1961) The electric polarisation of rod-like, charged macromolecules. *Mol. Phys.* **4**, p. 489-496.

MANDEL, M. (1977) Dielectric properties of charged linear macromolecules with particular reference to DNA. *Ann. N. Y. Ac. Sci.,* **303**, p. 74-87.

MANDEL, M. and ODIJK, T. (1984) Dielectric properties of polyelectrolyte solutions. *Ann. Rev. Phys. Chem.,* **35**, p. 75-108.

MANDEL, M. (1988) Polyelectrolytes. **In**: *Encyclopedia of polymer science and engineering*. Vol. 11. John Wiley, New York, USA, p. 739-829.

MANIATIS, T., FRITSCH, E. F., and SAMBROOK, J. (1982) *Molecular cloning - a laboratory manual*. Cold Spring Harbour Laboratory.

MANNING, G. S. (1969) Limiting laws and counterion condensation in polyelectrolyte solutions I. colligative properties. *J. Chem. Phys.,* **51**, p. 924-933.

MANNING, G. S. (1978a) The molecular theory of polyelectrolyte solutions with applications to the electrostatic properties of polynucleotides. *Q. Rev. Biophys.,* **11**, 2, 1978, p. 179-246.

MANNING, G. S. (1978b) Limiting laws and counterion condensation in polyelectrolyte solutions V. Further development of the chemical model. *Biophys. Chem.,* **9**, 1978, p. 65-70.

MANNING, G. S. (1993) A condensed counterion theory for polarization of polyelectrolyte solutions in high fields. *J. Chem. Phys.,* **99**, 1, p. 477-486.

MASHIMO, S., UMEHARA, T. and KUWABURA, S. (1989) Dielectric study on dynamics and structure of water bound to DNA using a frequency range 10 MHz - 10 GHz. *J. Phys. Chem.,* **93**, p. 4963-4967.

MOHANTY, U. and ZHAO, Y. (1996) Polarisation of counterions in polyelectrolytes. *Biopolymers*, **38**, p. 377-388.

NEWMAN, J. SWINNEY, H. L., BERKOWITZ, S. A., and DAY, L. A. (1974) Hydrodynamic properties and molecular weight of fd bacteriophage DNA. *Biochem.* **13**, 23, p. 4832-4838.

NAGASAWA, M. (1974) Ion-binding phenomena of polyelectrolytes. **In**: *Polyelectrolytes*. Vol. 1 Eds. E. Sélégny, M. Mandel, and U. P. Strauss, NATO Adv. Stud. Inst., France, 1972, D. Reidel Publishing, Holland, p. 57-77.

O'BRIEN, R. W. (1986) The high-frequency dielectric dispersion of a colloid. *J. Colloid and Interface Sci*., **113**, 1, p. 81-93.

O'BRIEN, R. W. and WHITE, L. R. (1978) Electrophoretic mobility of a spherical colloidal particle, *J. Chem. Soc. Faraday Trans. 2,* **74**, p. 1607-1626.

ODIJK, T. (1979) Possible scaling relations for semidilute polyelectrolyte solutions. *Macromolecules,* **12**, p. 688-693.

OHSHIMA, H. (1997) Electrophoretic mobility of spherical colloidal particles in concentrated suspensions. *J. Colloid and Interface Sci*., **188**, p. 481-485.

O'KONSKI, C. T. (1960) Electric properties of macromolecules. V. Theory of ionic polarisation in polyelectrolytes. *J. Phys. Chem*., **64**, p. 605-619.

OOSAWA, F. (1970) Counterion fluctuation and dielectric dispersion in linear polyelectrolytes. *Biopolymers*, **9**, p. 677-688.

PACANSKY, J. and LYERLA, J. R. (1979) Photochemical decomposition mechanisms for AZ-type photoresists. *IBM. Res. Develop.*, **23**, 1, p. 42-55.

PENAFIEL, L. M. and LITOVITZ, T. A. (1992) High frequency dielectric dispersion of polyelectrolyte solutions and its relation to counterion condensation. *J. Chem. Phys*. **97**, p. 559-567.

PILLER, H. (1977) *Microscope photometry*. Springer-Verlag, Berlin, Germany.

PLOEM, J. S. and TANKE, H. J. (1987) *Introduction to fluorescence microscopy*. Oxford University Press, Oxford, UK.

PRICE, J. A. R., BURT, J. P. H., and PETHIG, R. (1988) Applications of a new optical technique for measuring the dielectrophoretic behaviour of micro-organisms. *Biochem. Biophys. Acta*, **964**, p. 221-230.

REESE, H. R. (1994) Effects of DNA charge and length on the electrophoretic mobility of intercalated DNA. *Biopolymers*, **34**, p. 1349 - 1358.

RISKEN, H. (1989) *The Fokker-Planck equation*. 2nd Ed., Springer-Verlag, Berlin, Germany.

SAIF, B., MOHR, R. K., MONTROSE, C. J., and LITOVITZ, T. A. (1991) On the mechanism of dielectric relaxation in aqueous DNA solutions. *Biopolymers*, **31**, p. 1171 - 1180.

SAUER, F. A. (1985) Interaction-forces between microscopic particles in an external electromagnetic field. **In**: *Interactions between electromagnetic fields and cells*. Eds. A. Chiabrera, C. Nicolini and H. P. Schwan, NATO Adv. Sci. Inst. Series, Plenum, New York, USA, p. 181-202.

SASAKI, S., ISHIKAWA, A. and HANAI, T. (1981) Dielectric properties of spherical macroion suspensions. I: Study on monodisperse polystyrene latex. *Biophys. Chem.*, **14**, p. 45-53.

SCHWAN, H. P., SCHWARTZ, G., MACZUK, J., and PAULY, H. (1962) On the low-frequency dielectric dispersion of colloidal particles in electrolyte solution. *J. Chem.*, **66**, p. 2626-2635.

SCHWARZ, G. (1962) A theory of the low-frequency dielectric dispersion of colloidal particles in electrolyte solution. *J. Phys. Chem.*, **66**, p. 2636-2642.

SCHWARZ, G. (1963) General equation for the mean electrical energy of a dielectric body in an alternating electrical field. *J. Chem. Phys.*, **39**, p. 2387-2388.

SPRINGER, M. M., KORTEWEG, A., and LYKLEMA, J. (1983) The relaxation of the double layer around colloid particles and the low-frequency dielectric dispersion: Part II. Experiments. *J. Electroanal. Chem.*, **153**, p. 55-66.

STRANG, G. (1986) *Introduction to applied mathematics*. Wellesley-Cambridge Press, Massachusetts, USA.

STRYER, L. (1995) *Biochemistry*. 4th Ed., W. H. Freeman, New York, USA.

TAKASHIMA, S., GABRIEL, C., SHEPPARD, R. J., and GRANT, E. H. (1984) Dielectric behaviour of DNA solution at radio and microwave frequencies (at $20^{o}C$). *Biophys. J.,* **46**, p. 29-34.

TAKASHIMA, S., CASALEGGIO, A., GIULIANO, F., MORANDO, M., ARRIGO, P. and RIDELLA, S. (1986) Study of bound water of poly-adenine using high frequency dielectric measurements. *Biophys. J.,* **49**, p. 1003-1008.

TANFORD, C. (1961) *Physical chemistry of macromolecules*. John Wiley, USA.

TRITTON, D. J. (1988) *Physical fluid dynamics*. Oxford University Press, Oxford, UK.

VAN DER TOUW, F. and MANDEL, M. (1974) Dielectric increment and dielectric dispersion of solutions containing simple charged linear macromolecules. *Biophys. Chem.*, **2**, Parts I and II, p. 218-241.

VAN HOLDE, K. E. (1971) *Physical Biochemistry*. Prentice-Hall, Englewood Cliffs, USA.

VIOVY, J.-L. and DUKE, T. (1993) DNA electrophoresis in polymer solutions. *Electrophoresis*, **14**, p. 322-329.

WASHIZU, M. (1990) Electrostatic manipulation of biological objects. *J. Electrostatics,* **25**, p. 109-123.

WASHIZU, M. and KUROSAWA, O. (1990) Electrostatic manipulation of DNA in microfabricated structures. *IEEE Trans. Industry Appl.,* **26**, no. 6, p. 1165-1172.

WASHIZU, M., SHIKIDA, M., AIZAWA, S. and HOTANI, H. (1992) Orientation and transformation of flagella in electrostatic field. *IEEE Trans. Ind. Appl.,* **28**, no. 5, p. 1194-1202.

WASHIZU, M., SUZUKI, S., KUROSAWA, O., NISHIZAKA, T. and SHINOHARA, T. (1994) Molecular dielectrophoresis of biopolymers. *IEEE Trans. Ind. Appl.,* **30**, no. 4, p. 835-843.

WASHIZU, M., KUROSAWA, O, ICHIRO, A., SUZUKI, S. and SHIMAMOTO, N. (1995) Applications of electrostatic stretch-and-positioning of DNA. *IEEE Trans. Ind. Appl.,* **31**, no. 3, p. 447-456.

XAMMAR ORO, J. R. DE and GRIGERA, J. R. (1984) Dielectric properties of aqueous solutions of sonicated DNA above 40 MHz. *Biopolymers*, **23**, p. 1457-1463.

ZIENKIEWICZ, O. C. and TAYLOR, R. L. (1989) *The finite element method.* 4th Ed., McGraw-Hill, London, UK.